

EN

Volume IX

Enhanced Night Visibility Series: Phase II—Characterization of Experimental Objects

PUBLICATION NO. FHWA-HRT-04-140

DECEMBER 2005



U.S. Department of Transportation
Federal Highway Administration

Research, Development, and Technology
Turner-Fairbank Highway Research Center
6300 Georgetown Pike
McLean, VA 22101-2296

FOREWORD

The overall goal of the Federal Highway Administration's (FHWA) Visibility Research Program is to enhance the safety of road users through near-term improvements of the visibility on and along the roadway. The program also promotes the advancement of new practices and technologies to improve visibility on a cost-effective basis.

The following document provides a characterization of the experimental objects used in the evaluation of the visual performance of drivers during nighttime driving in various weather conditions. The experimental objects were used in the Phase II efforts of the Enhanced Night Visibility (ENV) project, a comprehensive evaluation of evolving and proposed headlamp technologies. The individual studies within the overall project are documented in an 18-volume series of FHWA reports, of which this is Volume IX. It is anticipated that the reader will select those volumes that provide information of specific interest.

This report will be of interest to headlamp designers, automobile manufacturers and consumers, third-party headlamp manufacturers, human factors engineers, and people involved in headlamp and roadway specifications.

Michael F. Trentacoste
Director, Office of Safety
Research and Development

Notice

This document is disseminated under the sponsorship of the U.S. Department of Transportation in the interest of information exchange. The U.S. Government assumes no liability for the use of the information contained in this document.

The U.S. Government does not endorse products or manufacturers. Trademarks or manufacturers' names appear in this report only because they are considered essential to the objective of the document.

Quality Assurance Statement

The Federal Highway Administration (FHWA) provides high-quality information to serve Government, industry, and the public in a manner that promotes public understanding. Standards and policies are used to ensure and maximize the quality, objectivity, utility, and integrity of its information. FHWA periodically reviews quality issues and adjusts its programs and processes to ensure continuous quality improvement.

TECHNICAL REPORT DOCUMENTATION PAGE

1. Report No. FHWA-HRT-04-140	2. Government Accession No.		3. Recipient's Catalog No.	
4. Title and Subtitle Enhanced Night Visibility Series, Volume IX: Phase II—Characterization of Experimental Objects		5. Report Date December 2005		
		6. Performing Organization Code:		
7. Author(s) Ronald B. Gibbons, Jonathan M. Hankey		8. Performing Organization Report No.		
9. Performing Organization Name and Address Virginia Tech Transportation Institute 3500 Transportation Research Plaza Blacksburg, VA 24061		10. Work Unit No.		
		11. Contract or Grant No. DTFH61-98-C-00049		
12. Sponsoring Agency Name and Address Office of Safety Research and Development Federal Highway Administration 6300 Georgetown Pike McLean, VA 22101-2296		13. Type of Report and Period Covered Final Report		
		14. Sponsoring Agency Code HRDS-05		
15. Supplementary Notes Contracting Officer's Technical Representative (COTR): Carl Andersen, HRDS-05				
<p>16. Abstract</p> <p>The Enhanced Night Visibility (ENV) project is a series of experiments undertaken to investigate different visual enhancement systems (VES) for the nighttime driving task. The purpose of this portion of the ENV project is to establish the photometric nature of the objects presented to the observer. The photometric measurements of interest are the headlamp illuminance, object luminance, and the background luminance. Other calculated parameters were established such as object contrast with the background, reflectance of the objects, and object visibility level. The measurements were taken and calculated for 11 VESs and 8 object types.</p> <p>The correlation of the measurement results to those of the ENV visual performance studies was calculated. It was found that all the calculated metrics were fairly highly correlated to the participant results. The visibility level was the least correlated, and the Weber contrast ratio was the most highly correlated.</p> <p>The transmittance of the atmosphere was also calculated for each of the weather conditions used in the ENV visual performance studies. The correlations calculated for these conditions showed that the Weber contrast was again the most highly correlated metric.</p>				
17. Key Words Halogen, Headlamps, High Intensity Discharge, Liquid System, Nighttime, Photometry, Luminance, Contrast, Visibility Level, Ultraviolet, Visibility, Vision Enhancement System		18. Distribution Statement No restrictions. This document is available through the National Technical Information Service, Springfield, VA 22161.		
19. Security Classif. (of this report) Unclassified		20. Security Classif. (of this page) Unclassified	21. No. of Pages 113	22. Price

SI* (MODERN METRIC) CONVERSION FACTORS				
APPROXIMATE CONVERSIONS TO SI UNITS				
Symbol	When You Know	Multiply By	To Find	Symbol
		LENGTH		
in	inches	25.4	millimeters	mm
ft	feet	0.305	meters	m
yd	yards	0.914	meters	m
mi	miles	1.61	kilometers	km
		AREA		
in ²	square inches	645.2	square millimeters	mm ²
ft ²	square feet	0.093	square meters	m ²
yd ²	square yard	0.836	square meters	m ²
ac	acres	0.405	hectares	ha
mi ²	square miles	2.59	square kilometers	km ²
		VOLUME		
fl oz	fluid ounces	29.57	milliliters	mL
gal	gallons	3.785	liters	L
ft ³	cubic feet	0.028	cubic meters	m ³
yd ³	cubic yards	0.765	cubic meters	m ³
NOTE: volumes greater than 1000 L shall be shown in m ³				
		MASS		
oz	ounces	28.35	grams	g
lb	pounds	0.454	kilograms	kg
T	short tons (2000 lb)	0.907	megagrams (or "metric ton")	Mg (or "t")
		TEMPERATURE (exact degrees)		
°F	Fahrenheit	5 (F-32)/9 or (F-32)/1.8	Celsius	°C
		ILLUMINATION		
fc	foot-candles	10.76	lux	lx
fl	foot-Lamberts	3.426	candela/m ²	cd/m ²
		FORCE and PRESSURE or STRESS		
lbf	poundforce	4.45	newtons	N
lbf/in ²	poundforce per square inch	6.89	kilopascals	kPa
APPROXIMATE CONVERSIONS FROM SI UNITS				
Symbol	When You Know	Multiply By	To Find	Symbol
		LENGTH		
mm	millimeters	0.039	inches	in
m	meters	3.28	feet	ft
m	meters	1.09	yards	yd
km	kilometers	0.621	miles	mi
		AREA		
mm ²	square millimeters	0.0016	square inches	in ²
m ²	square meters	10.764	square feet	ft ²
m ²	square meters	1.195	square yards	yd ²
ha	hectares	2.47	acres	ac
km ²	square kilometers	0.386	square miles	mi ²
		VOLUME		
mL	milliliters	0.034	fluid ounces	fl oz
L	liters	0.264	gallons	gal
m ³	cubic meters	35.314	cubic feet	ft ³
m ³	cubic meters	1.307	cubic yards	yd ³
		MASS		
g	grams	0.035	ounces	oz
kg	kilograms	2.202	pounds	lb
Mg (or "t")	megagrams (or "metric ton")	1.103	short tons (2000 lb)	T
		TEMPERATURE (exact degrees)		
°C	Celsius	1.8C+32	Fahrenheit	°F
		ILLUMINATION		
lx	lux	0.0929	foot-candles	fc
cd/m ²	candela/m ²	0.2919	foot-Lamberts	fl
		FORCE and PRESSURE or STRESS		
N	newtons	0.225	poundforce	lbf
kPa	kilopascals	0.145	poundforce per square inch	lbf/in ²

*SI is the symbol for the International System of Units. Appropriate rounding should be made to comply with Section 4 of ASTM E380.
(Revised March 2003)

ENHANCED NIGHT VISIBILITY PROJECT REPORT SERIES

This volume is the ninth of 18 volumes in this research report series. Each volume is a different study or summary, and any reference to a report volume in this series will be referenced in the text as “ENV Volume I,” “ENV Volume II,” and so forth. A list of the report volumes follows:

Volume	Title	Report Number
I	Enhanced Night Visibility Series: Executive Summary	FHWA-HRT-04-132
II	Enhanced Night Visibility Series: Overview of Phase I and Development of Phase II Experimental Plan	FHWA-HRT-04-133
III	Enhanced Night Visibility Series: Phase II—Study 1: Visual Performance During Nighttime Driving in Clear Weather	FHWA-HRT-04-134
IV	Enhanced Night Visibility Series: Phase II—Study 2: Visual Performance During Nighttime Driving in Rain	FHWA-HRT-04-135
V	Enhanced Night Visibility Series: Phase II—Study 3: Visual Performance During Nighttime Driving in Snow	FHWA-HRT-04-136
VI	Enhanced Night Visibility Series: Phase II—Study 4: Visual Performance During Nighttime Driving in Fog	FHWA-HRT-04-137
VII	Enhanced Night Visibility Series: Phase II—Study 5: Evaluation of Discomfort Glare During Nighttime Driving in Clear Weather	FHWA-HRT-04-138
VIII	Enhanced Night Visibility Series: Phase II—Study 6: Detection of Pavement Markings During Nighttime Driving in Clear Weather	FHWA-HRT-04-139
IX	Enhanced Night Visibility Series: Phase II—Characterization of Experimental Objects	FHWA-HRT-04-140
X	Enhanced Night Visibility Series: Phase II—Visual Performance Simulation Software for Objects and Traffic Control Devices	FHWA-HRT-04-141
XI	Enhanced Night Visibility Series: Phase II—Cost-Benefit Analysis	FHWA-HRT-04-142
XII	Enhanced Night Visibility Series: Overview of Phase II and Development of Phase III Experimental Plan	FHWA-HRT-04-143
XIII	Enhanced Night Visibility Series: Phase III—Study 1: Comparison of Near Infrared, Far Infrared, High Intensity Discharge, and Halogen Headlamps on Object Detection in Nighttime Clear Weather	FHWA-HRT-04-144
XIV	Enhanced Night Visibility Series: Phase III—Study 2: Comparison of Near Infrared, Far Infrared, and Halogen Headlamps on Object Detection in Nighttime Rain	FHWA-HRT-04-145
XV	Enhanced Night Visibility Series: Phase III—Study 3: Influence of Beam Characteristics on Discomfort and Disability Glare	FHWA-HRT-04-146
XVI	Enhanced Night Visibility Series: Phase III—Characterization of Experimental Objects	FHWA-HRT-04-147
XVII	Enhanced Night Visibility Series: Phases II and III—Characterization of Experimental Vision Enhancement Systems	FHWA-HRT-04-148
XVIII	Enhanced Night Visibility Series: Overview of Phase III	FHWA-HRT-04-149

TABLE OF CONTENTS

CHAPTER 1—INTRODUCTION.....	1
CHAPTER 2—METHODS.....	3
EXPERIMENTAL DESIGN.....	3
Independent Variables.....	3
Dependent Variables.....	8
APPARATUS	11
TESTING PROCEDURE	12
DATA ANALYSIS	16
Reflectivity	16
Fluorescence	17
Contrast	17
Visibility Level.....	18
CHAPTER 3—RESULTS.....	21
ILLUMINANCE FROM THE HEADLAMPS	21
UV-A Illuminance	21
Pedestrian and Cyclist Objects	22
Child's Bicycle and Tire Tread Objects.....	26
OBJECT LUMINANCE	26
Pedestrian and Cyclist Objects	27
Child's Bicycle	34
Tire Tread.....	35
Cyclist Bicycles	36
OBJECT BACKGROUND LUMINANCE	37
Pedestrian and Cyclist Objects	39
Child's Bicycle.....	44
Tire Tread.....	45
OBJECT REFLECTANCE	47
OBJECT FLUORESCENCE.....	49
LUMINANCE DIFFERENCE	52
Pedestrian and Cyclist Objects	53
Child's Bicycle.....	59

Tire Tread.....	60
VISIBILITY LEVEL.....	60
Pedestrian and Cyclist Objects	61
Child's Bicycle.....	66
Tire Tread.....	67
CHAPTER 4—DISCUSSION.....	69
CHAPTER 5—EFFECT OF ADVERSE WEATHER.....	83
RAIN	83
SNOW	86
FOG.....	88
Calibration Procedure	91
Mathematical Model.....	93
VISUAL PERFORMANCE EXPERIMENT CORRELATION	96
Correlation Analysis	96
Threshold Analysis.....	97
REFERENCES.....	101

LIST OF FIGURES

1. Diagram. Object stations (locations) on the Virginia Smart Road.	6
2. Illustration. Parallel pedestrian measurement points.	9
3. Illustration. Perpendicular pedestrian measurement points.	9
4. Illustration. Cyclist measurement points.	10
5. Illustration. Child's bicycle measurement points.	10
6. Illustration. Tire tread measurement points.	11
7. Bar graph. Comparison of the mean of background object luminance for HLB combined with different UV-A levels when the photometer operator is in the back seat or the driver's seat.	14
8. Bar graph. Comparison of object luminance for HLB combined with different UV-A levels when the photometer operator is in the back seat or the driver's seat.	15
9. Equation. Lambertian reflection.	16
10. Equation. Specular reflection.	16
11. Equation. Object fluorescence.	17
12. Equation. Contrast ratio.	17
13. Equation. Basic ΔL_{th} model.	18
14. Equation. Time factor for the ΔL_{th} model.	19
15. Equation. Age factor for the ΔL_{th} model.	19
16. Equation. Complete ΔL_{th} model.	19
17. Equation. Visibility level.	20
18. Bar graph. Object illuminance by UV-A level.	22
19. Bar graph. Illuminance from each VES by measurement height for the pedestrian object types.	23
20. Bar graph. Illuminance from each VES by object position for the pedestrian object types.	24
21. Bar graph. Illuminance and distance relationship by lamp and measurement location with the inverse square law trends for the pedestrian object types.	25
22. Bar graph. Illuminance on the child's bicycle and the tire tread for each VES type.	26
23. Bar graph. Object luminance by VES for white- and black-clothed pedestrians.	27
24. Bar graph. Object luminance by VES for black-clothed pedestrians and cyclist by object position.	28
25. Bar graph. Object luminance by VES for black-clothed perpendicular pedestrians by measurement height.	29

26. Bar graph. Object luminance by VES for white-clothed pedestrians by object position.....	31
27. Bar graph. Object luminance by VES for white-clothed perpendicular pedestrian by measurement height.....	32
28. Bar graph. Object luminance by VES for white-clothed pedestrians by measurement distance.	33
29. Bar graph. Object luminance by VES for the child's bicycle.	34
30. Bar graph. Object luminance by VES for the tire tread.	35
31. Bar graph. Object luminance by VES for the cyclists' bicycles.	37
32. Bar graph. Background luminance for white- and black-clothed pedestrians by UV-A-based VES.....	38
33. Bar graph. Influence of VES on background luminance by pedestrian position.	39
34. Bar graph. Influence of VES on background luminance by measurement height.	40
35. Bar graph. Influence of VES on background luminance by pedestrian type and measurement height.....	41
36. Bar graph. Influence of VES on background luminance by measurement distance.....	42
37. Bar graph. Influence of station on background luminance for pedestrians by VES.....	43
38. Bar graph. Influence of measurement height on background luminance of child's bicycle by VES.....	44
39. Bar graph. Influence of station on background luminance for the child's bicycle by VES.....	45
40. Bar graph. Influence of measurement height on background luminance for the tire tread by VES.	46
41. Bar graph. Influence of station on background luminance for the tire tread by VES....	46
42. Bar graph. Reflectance of all objects both dry and wet.	47
43. Bar graph. Specular reflection of all bicycle objects for both black-clothed and white-clothed cyclist.....	48
44. Bar graph. Fluorescence for the black-clothed and white-clothed pedestrians by roadway position.	49
45. Bar graph. Fluorescence for the black-clothed and white-clothed objects by VES type.	50
46. Bar graph. Fluorescence for the white-clothed objects by VES type and position on the roadway.	51
47. Bar graph. Fluorescence of the child's bicycle by VES type.....	52
48. Bar graph. Luminance difference by VES for black-clothed pedestrians by object position.....	54

49. Bar graph. Luminance difference by VES for black-clothed pedestrians by measurement height.....	55
50. Bar graph. Luminance difference by VES for black-clothed pedestrians by measurement distance.	56
51. Bar graph. Luminance difference by VES for white-clothed pedestrians by object position.....	57
52. Bar graph. Luminance difference by VES for white-clothed pedestrians by measurement distance.	58
53. Bar graph. Luminance difference by VES for the child's bicycle.....	59
54. Bar graph. Luminance difference by VES for the tire tread.....	60
55. Bar graph. Visibility level by age and VES for the pedestrian objects.....	61
56. Bar graph. Visibility level by VES for the black-clothed pedestrian objects by position.....	62
57. Bar graph. Visibility level by VES for the black-clothed pedestrian objects by distance.....	63
58. Bar graph. Visibility level by VES for the white-clothed pedestrian objects by position.	64
59. Bar graph. Visibility level for the white-clothed pedestrians by distance and VES.....	65
60. Bar graph. Visibility level for the child's bicycle by age and VES.....	66
61. Bar graph. Visibility level for the tire tread by age and VES.....	67
62. Equation. Weber ratio contrast equation.	69
63. Bar graph. Threshold Weber ratio for black-clothed pedestrian objects.	76
64. Bar graph. Threshold Weber ratio for white-clothed pedestrian objects.	76
65. Bar graph. Threshold visibility level for black-clothed pedestrian objects.....	78
66. Bar graph. Threshold visibility level for white-clothed pedestrian objects.....	79
67. Bar graph. Threshold dosage factor for black-clothed pedestrian objects.	80
68. Bar graph. Threshold dosage factor for white-clothed pedestrian objects.	81
69. Equation. Transmittance of illuminance based on the ratio of the clear measurements.....	84
70. Equation. Transmittance of luminance based on the ratio of the clear measurements.....	84
71. Bar graph. Transmittance of the atmosphere for the illuminance, object luminance, and background luminance in the rain.....	85
72. Line graph. Illuminance for both clear and snow conditions.	87
73. Line graph. Transmittance of the atmosphere for the illuminance through snow.....	88
74. Diagram. Possible reaction of light after collision with a water particle in a fog bank...89	

75. Equation. Intensity of light based on the scattering coefficient and incident illuminance.....	90
76. Diagram. Depiction of the incident beam broken into small lamina.	90
77. Equation. Differential change in illuminance for each portion of a light beam.....	90
78. Equation. Total attenuation according to Bouguer's law.	91
79. Equation. Reduction caused by the fog attenuation.	91
80. Scatter plot. Measured backscatter versus the $\beta(\theta)$ function.	92
81. Scatter plot. Measured backscatter versus the extinction factor.	93
82. Equation. $\beta(\theta)$ function based on the adjusted backscatter.....	94
83. Equation. Extinction factor based on the adjusted backscatter.....	94
84. Scatter plot. Backscatter versus β by model.....	95
85. Scatter plot. Backscatter versus extinction with model.....	95
86. Bar graph. Threshold Weber ratio for white-clothed pedestrian objects in rain condition.....	98
87. Bar graph. Threshold visibility level for white-clothed pedestrian objects in rain condition.....	99
88. Bar graph. Threshold dosage for white-clothed pedestrian objects in rain condition. .	100

LIST OF TABLES

1. Experimental design	3
2. List of object types.	4
3. List of VES configurations.	5
4. Station and object relationship.....	7
5. Components in the measurement process.....	8
6. Object dimension summarization.....	20
7. Object reflectance summary.....	47
8. Pearson correlation coefficients between detection and recognition distances and measured and calculated values for all age, VES, and object types.....	70
9. Pearson correlation coefficients between detection distance and measured and calculated values for all VES and object types by age.....	70
10. Pearson correlation coefficients between detection distance and measured and calculated values for all ages and VESs by object types.....	71
11. Pearson correlation coefficients between detection distance and measured and calculated values for all age and object types by VES.....	73
12. Critical distance calculation for the objects based on a 6 minute of arc Ricco area.	75
13. Fog modeling calibration measurement.....	92
14. Backscatter measurements in the clear condition.....	94
15. Correlation results between participant detection distance and photometric metrics for all weather conditions.....	96
16. Correlation results between participant recognition distance and photometric metrics for all weather conditions.	97

LIST OF ACRONYMS AND ABBREVIATIONS

General Terms

ENV	Enhanced Night Visibility
IR.....	infrared
VES	vision enhancement system
SUV.....	sport utility vehicle
UV-A.....	ultraviolet A (wavelength 315 to 400 nanometers)

Vision Enhancement Systems

HLB.....	halogen (i.e., tungsten-halogen) low beam
hybrid UV-A + HLB	hybrid UV-A/visible output together with halogen low beam
three UV-A + HLB.....	three UV-A headlamps together with halogen low beam
five UV-A + HLB	five UV-A headlamps together with halogen low beam
HLB-LP.....	halogen low beam at a lower profile
HHB	halogen high beam
HOH.....	high output halogen
HID	high intensity discharge
hybrid UV-A + HID	hybrid UV-A/visible output together with high intensity discharge
three UV-A + HID.....	three UV-A headlamps together with high intensity discharge
five UV-A + HID	five UV-A headlamps together with high intensity discharge
IR-TIS.....	infrared thermal imaging system

Objects

BC	black-clothed cyclist
BPL	black-clothed pedestrian, parallel configuration
BPP	black-clothed pedestrian, perpendicular configuration
CB	child's bicycle
TT.....	tire tread
WC	white-clothed cyclist
WPL	white-clothed pedestrian, parallel configuration
WPP	white-clothed pedestrian, perpendicular configuration

Statistical Terms

ANOVA	analysis of variance
DF	degrees of freedom
F value.....	F-ratio
MS.....	mean square
N.....	number of measurements
P value.....	statistical significance
SS	sums of squares

Measurements

ΔL	luminance difference
ΔL_{th}	threshold luminance difference
C	contrast
cd/m^2	candela per square meter
ft	feet
kPa	kilopascals
L	luminance
lx	lux
m	meters
nm	nanometers
psi	pounds per square inch
s	seconds
VL	visibility level
μm	micrometers

Calculated Variables

AF	age factor
F_{CP}	negative contrast factor
t	observation time
TF	time factor
ρ	reflectivity
E	illuminance
$\beta(\theta)$	angular scattering coefficient
θ	angle of observation
dx	length of lamina
β	total scattering per unit length

CHAPTER 1—INTRODUCTION

To travel safely during darkness, the human visual system must adapt from daylight sensitivity to darkness sensitivity. For the task of driving in the dark, the detectability of objects on the roadway becomes critical, and a vehicular vision enhancement system (VES) is required. Traditionally, a VES has been considered to be vehicle headlamps only, but with the development of new technologies, a VES can be headlamps in conjunction with ultraviolet (UV-A) sources, infrared (IR) technology, or camera-dependent systems. Their effectiveness and effect on the driver vary based on the type of technology used.

The Enhanced Night Visibility (ENV) project is a series of experiments undertaken to investigate different VESs for the nighttime driving task. The execution of this project was conducted in three phases, one as a preliminary study and the other two at the contractor's facility. This report is particularly concerned with the experiments conducted in Phase II, the first performed at the contractor's facility. In this set of visual performance experiments, detection and recognition distances of 12 different VESs were measured. Detection distance was defined as the distance in front of the vehicle at which an object can just be seen. Recognition distance was defined as the distance at which the object can be clearly identified. For these experiments, the objects represented real hazards on the roadway such as pedestrians, cyclists, tire treads, and bicycles. In total, nine objects differing in size and shape were used for the experiments.

The purpose of this portion of the ENV project was to establish the photometric nature of the objects presented to the observer. The photometric measurements of interest were the headlamp illuminance, object luminance, and the object background luminance. Other calculated parameters were established such as object contrast with the background, reflectance of the objects, luminance of the object background, and object visibility.

Even though the Phase II visual performance experiments used up to nine objects and 12 VESs, this activity characterized only eight object types and 11 VESs. Two of the Phase II objects were similar in appearance, so they were characterized as one object. The visible light produced by the Phase II IR VES came from a headlamp system shared by another VES, so the IR VES was excluded from characterization.

This investigation sought to answer the following research questions:

1. What is the correlation between the photometric performance of the VES and visual detection and recognition performance from the Phase II ENV visibility studies (ENV Volumes III, IV, V, and VI)?
2. Of the visibility metrics analyzed, what threshold values are required for detection and recognition of the objects tested?
3. What is the effect of different weather conditions on the visibility of the tested objects?

This report presents an indepth analysis of the visibility of the objects in clear weather to answer the first and second questions. The effect of the weather is then considered based on the results from the clear investigation.

CHAPTER 2—METHODS

The method in this experiment was used primarily for the investigation of the objects that were used in the ENV clear-condition visual performance study, which are fully documented in Volume III of this series. The effects of rain, snow, and fog conditions were also assessed, and these results are included after the analysis of the results for the clear weather condition.

EXPERIMENTAL DESIGN

The experiment used a full-factorial design for the measurement process for both the object and VES data. In total, 8 of the objects and 11 of the VESs compared in the ENV clear-condition study were also used in this experiment.

The factorial format in this experiment was an 8 (Object Type) by 11 (VES Configuration) by 6 (Station) by 4 (Measurement Distances) design with the conditions shown in table 1.

Table 1. Experimental design.

Independent Variable	Levels
Object type	8 objects
VES	11 VES configurations (The infrared thermal imaging system, or IR-TIS, VES from the Phase II ENV visual performance studies was not evaluated.)
Station	6 stations
Distance	4 measurement distances

Within each of these variables, the levels were selected to match those of the ENV Phase II visual performance experiments.

Independent Variables

Object Type

The objects varied in both color and position relative to the roadway. Table 2 outlines the objects used in this study and the objects they represented from the ENV clear-condition study. It should be noted that the objects used for this investigation were all static, but most of the objects in the ENV clear-condition study were dynamic. The characterization used static objects because the measurement process was lengthy, requiring that the objects be still during the process. This also

meant that the white-clothed static pedestrian and white-clothed parallel pedestrian from the ENV clear-condition study were characterized as the same object in this investigation.

Table 2. List of object types.

Abbreviation	Object Type	Object Description	ENV Visual Performance Study Condition
WPL	White-clothed pedestrian—parallel configuration	Pedestrian dressed in white clothing standing at the right edgeline of the road and facing the approaching vehicle. This represents the white-clothed parallel and static conditions from the ENV clear-condition study.	Clear, Rain, Snow
BPL	Black-clothed pedestrian—parallel configuration	Pedestrian dressed in black clothing standing on the right edgeline of the road and facing the approaching vehicle. This represents the black-clothed parallel condition from the ENV clear-condition study.	Clear, Rain
WPP	White-clothed pedestrian—perpendicular configuration	Pedestrian dressed in white clothing standing in the center of the driving lane and facing the edge of the road. This represents the white-clothed perpendicular pedestrian condition from the ENV clear-condition study.	Clear, Rain, Snow, Fog
BPP	Black-clothed pedestrian—perpendicular configuration	Pedestrian dressed in black clothing standing at the center of the driving lane and facing the edge of the road. This represents the black-clothed perpendicular pedestrian condition from the ENV clear-condition study.	Clear, Rain, Snow
WC	White-clothed cyclist	Cyclist dressed in white clothing standing at the center of the driving lane, straddling a bicycle, and facing the edge of the road. This represents the white-clothed cyclist condition from the ENV clear-condition study. The bicycle for this object was a fluorescent orange color.	Clear, Rain
BC	Black-clothed cyclist	Cyclist dressed in black clothing standing at the center of the driving lane, straddling a bicycle, and facing the edge of the road. This represents the black-clothed cyclist condition from the ENV clear-condition study. The bicycle used for this object was painted a mix of burgundy and black.	Clear
TT	Tire tread	A hollow tire tread placed on the roadway and straddling the white edgeline.	Clear, Rain
CB	Child's bicycle	A child's bicycle, painted green, was placed on the roadway across the white edgeline. The seat and the handlebars are tipped away from the approaching vehicle.	Clear, Rain

VES

Four different vehicles were used to provide the 11 different VESs used in the characterization activity. During the visual performance studies, participants drove a vehicle on the Virginia Smart Road and announced when they could detect and identify the objects of interest. After the participant completed a lap of the Smart Road, the VES was changed to the next configuration. This process might have required the participant to change vehicles. The VES types used are shown in table 3. Again, the IR-TIS VES from the Phase II studies was not included in this characterization effort.

Table 3. List of VES configurations.

Abbreviation	Configuration
HLB	Halogen (i.e., tungsten-halogen) low beam
Hybrid UV-A + HLB	Halogen low beam with hybrid UV-A/visible lamps
Three UV-A + HLB	Halogen low beam with three UV-A lamps
Five UV-A + HLB	Halogen low beam with five UV-A lamps
HID	High intensity discharge (metal halide) in a low-beam configuration
Hybrid UV-A + HID	High intensity discharge with hybrid UV-A/visible lamps
Three UV-A + HID	High intensity discharge with three UV-A lamps
Five UV-A + HID	High intensity discharge with five UV-A lamps
HHB	Halogen high beam
HOH	High output halogen
HLB-LP	Halogen low beam in a low profile sedan configuration. Note that this VES is the same as the visible component of the IR-TIS VES.

The headlamps used for the HLB, HID, HOH, HHB, and UV-A configurations were located on external light bars. To change from one configuration to another, the HLB and HID headlamps were moved onto, off of, and between vehicles. Each light assembly movement required a re-aiming process, which took place before starting the experimental session each night. At the beginning of the Phase II studies, a headlamp aimer was not available to the contractor, so an aiming protocol was developed with the help of experts in the field. During the photometric characterization of the headlamps, it was discovered that the maximum intensity location of the HLB, HOH, and HHB configurations was aimed higher and more toward the left than typical. This aiming method may have influenced the visual performance testing results; however, this object characterization process evaluates the objects as they were presented to the experimental participants. Details about the aiming procedure and the maximum intensity location are

discussed in ENV Volume XVII, *Characterization of Experimental Vision Enhancement Systems*.

Station

During the ENV visual performance experiments, the objects appeared randomly at one of six stations (locations) identified on the Smart Road. These stations were defined by distance from the start point of the lap (figure 1). There were three downhill stations and three uphill stations, relative to the travel direction of the experimental vehicle during a lap. As the participant drove the experimental lap on the road, objects were presented at the various stations; sometimes no objects were presented in order to reduce participant expectancy. Not all objects were used at each location. Table 4 summarizes the stations and objects presented.

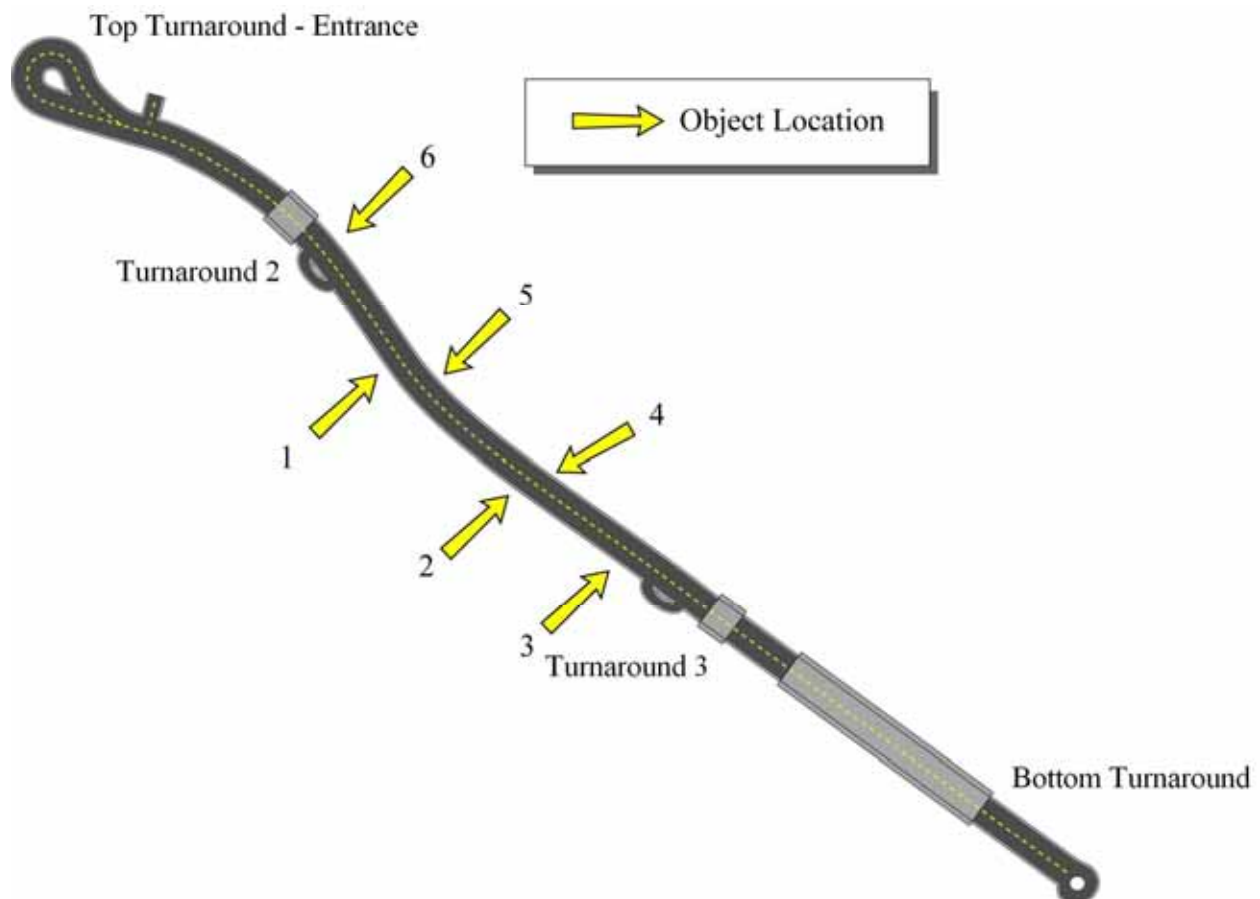


Figure 1. Diagram. Object stations (locations) on the Virginia Smart Road.

Table 4. Station and object relationship.

Station	Objects Presented
1 (downhill)	WPL, BPL, WPP, BPP, WC, BC, TT, CB
2 (downhill)	WPL, BPL, WPP, BPP, WC, BC, TT, CB
3 (downhill)	WPL, BPL, WPP, BPP, WC, BC
4 (uphill)	WPL, BPL, WPP, BPP, WC, BC, TT, CB
5 (uphill)	WPL, BPL, WPP, BPP, WC, BC, TT, CB
6 (uphill)	TT, CB

The object luminance was determined at two stations, one uphill and one downhill (station 4 and station 2). The object background luminance was established at all stations. The luminance of the objects was measured through the rain at station 2, called station R2 for this condition, to characterize the effect of rain on object visibility.

Distance

The distance from an observer to an object is also a factor in the evaluation of object visibility, affecting its visual size and the illuminance on the object. The location from which to perform the photometric characterization was determined by the closest distance of the participant vehicle to the object during the ENV visual performance experiments. The safety protocol of the Phase II experiments had directed the experimenters who stood as objects to clear the roadway when the participant vehicle was within 61.0 m (200 ft) of the station; therefore, this distance to the object became the basis for headlamp illuminance, object luminance, and background luminance measurement distances for all VES types and objects.

To more fully establish the effect of distance on visibility, object luminance, background luminance, and illuminance measurements were made at 91.5 m (300 ft), 152.5 m (500 ft), and 244 m (800 ft). Because the illuminance falls off with the square of the distance, only the white-clothed pedestrian objects were measured at these longer distances to provide the highest possible luminance of the objects, and consequently, the lowest measurement uncertainty. These measurements were made at only two of the six stations (i.e., stations 2 and 4), and the results were then applied to all stations and object types.

Because the background changed among stations, background luminance measurements were made at all of the stations from a distance of 61.0 m (200 ft). Because UV-A radiation did not

change the background luminance, only the contributing non-UV-A VESs were measured at these points. Table 5 summarizes the components of the measurement process.

Table 5. Components in the measurement process.

Station	Distance in meters (ft)	Object	VES	Purpose
2, 4	61.4 (200)	All	All	Establish background luminance, object luminance, and VES illuminance
2, 4	91.5 (300), 152.5 (500), 244 (800)	WPP, WPL	All	Establish effect of measurement distance
1, 3, 5, 6	61.4 (200)	All	HLB, HID, HHB, HOH, HLB-LP	Establish background luminance only

The final aspect of the experimental design was the weather condition. During the ENV visual performance experiments, participants were presented with the objects in rain, fog, snow, and clear conditions. The weather conditions were re-created on the Smart Road using its all-weather testing capabilities. For the object characterization, measurements to calculate atmospheric transmittance were made in all of these weather conditions. Based on this calculation, it is possible to develop factors accounting for the effect of weather on the object photometric characteristics. More information about the measurement procedures and results appear in chapter 5 of this document.

Dependent Variables

The object luminance, background luminance, and illuminance from the VES are the dependent variables in this experiment. Other calculated characteristics are discussed as part of the data analysis.

Object and Background Luminance

For each object, a series of as many as 14 luminance measurements were made including measurements of both the background and object itself.

Figure 2 and figure 3 show the measurement points for the two pedestrian object types.

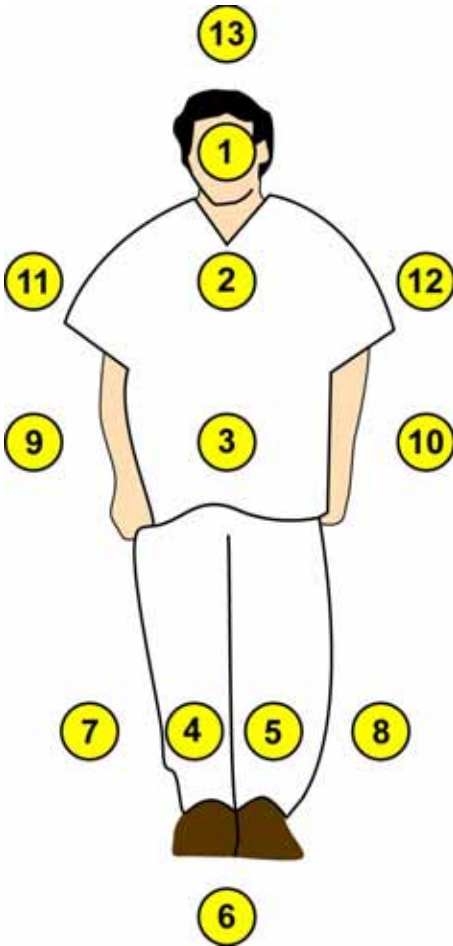


Figure 2. Illustration. Parallel pedestrian measurement points.

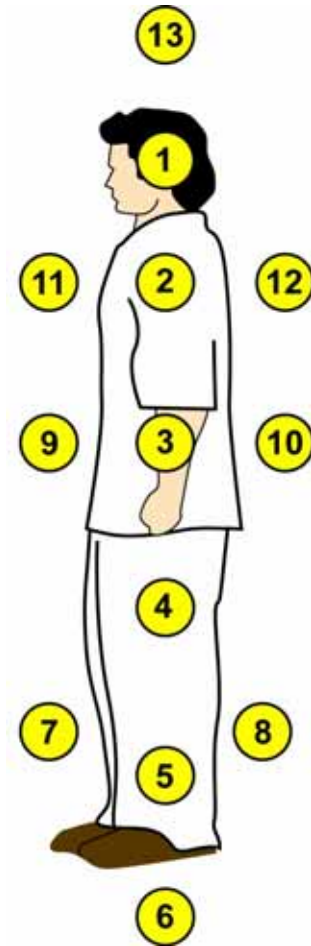


Figure 3. Illustration. Perpendicular pedestrian measurement points.

The numbers in the circles indicate the measurement point number. For the analysis, the measurement points were separated into groups, object (1 through 5) and background (6 through 13), and replaced with height and positions. This means that measurement point 3 was converted to waist height, and measurement points 9 and 10 were converted to waist-left and waist-right measurements. This was performed for the analysis so that measurements at the same height could be compared.

For the black-clothed and white-clothed cyclist conditions, the measurement points were very similar to those of the pedestrians, but the face measurement was removed from the group because it was the same regardless of the VES or object clothing. Two measurement points were

added to the bicycles themselves (i.e., points 5 and 6). These were on the wheel rims because they were the brightest parts of the bicycles. Figure 4 shows the cyclist measurement points.

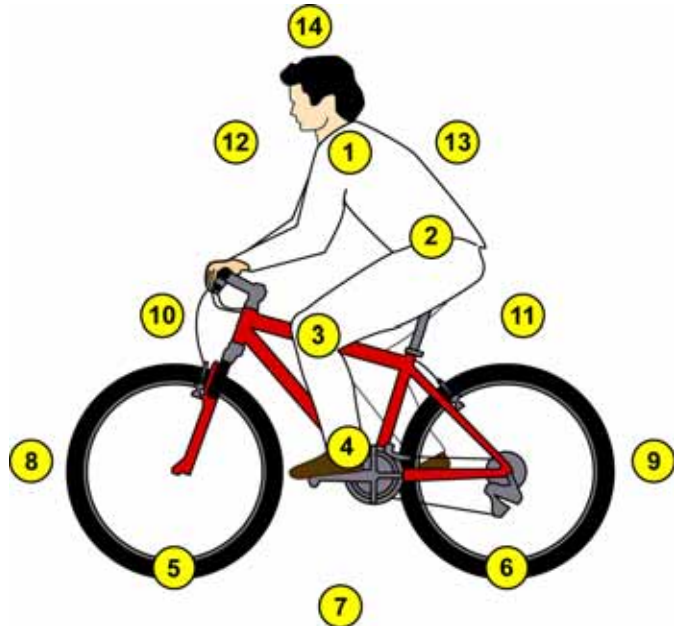


Figure 4. Illustration. Cyclist measurement points.

For the child's bicycle, two measurements were made of the frame (points 1 and 2), and four were made of the background (points 3 through 6). As with the pedestrian objects, the measurements of all objects were separated into object and background measures for analysis. Figure 5 outlines the measurements taken for the child's bicycle when it was lying horizontally.



Figure 5. Illustration. Child's bicycle measurement points.

The tire tread was similar; however, this object was measured only once (point 1), and the background was measured around it (points 2 through 5). Figure 6 shows the measurement points on the tire tread.

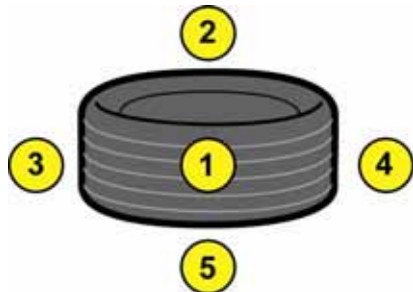


Figure 6. Illustration. Tire tread measurement points.

For measurements at stations where the background was the only measurement series of interest (stations 1, 3, 5, and 6), the object was placed at the location to ensure that the same background measurement points were used.

VES Illuminance

The illuminance falling on the objects, provided by the VESs, was measured for each object type. For the human objects, the vertical illuminance was measured at seven points. The first four points were on parts of the objects facing the vehicle and corresponding to the luminance measurement heights of chest, waist, knee, or ankle. The next three points, one at chest height on either side of the object and one behind it, were used to measure the ambient illuminance falling on each side of the object. The illuminances on the child's bicycle and the tire tread were measured at the same points as those objects' luminance measurements.

APPARATUS

The measurement apparatus used for this experiment were a photometer and an illuminance meter. The same object materials (pedestrian surgical scrubs, bicycles, tire treads) used in the ENV visual performance studies were used for the characterization.

The photometric measurements were made using a Model 1980A Pritchard[®] Telephotometer on loan from the Federal Highway Administration. The telephotometer provides five measurement

apertures ranging from $2'$ to 3° . During the experiment, the $6'$ aperture was used for all measurements made at 61.0 m (200 ft). The $2'$ aperture was used for measurements made at longer distances. The minimum sensitivities of the photometer with the $6'$ and $2'$ apertures are 3×10^{-2} candela per square meter (cd/m^2) and 3×10^{-1} cd/m^2 respectively. The uncertainty associated with the telephotometer is ± 4 percent of the measurement.

The illuminance meter used in the experiments was a Konica Minolta[®] T-10. The minimum sensitivity provided by this instrument is 0.01 lux (lx) with an uncertainty of ± 2 percent of the most significant digit; however, the meter does have an 8 percent f_1' factor. This means that the sensitivity of the detector can deviate from the response of the human eye by as much as 8 percent depending on the light source being measured. Because most of the VES types were incandescent-halogen based, the illuminance meter was calibrated with a Commission Internationale de l'Eclairage Standard Illuminant A. Consequently, measurements of HID VESs had a slightly higher uncertainty.

TESTING PROCEDURE

The testing took place on the Virginia Smart Road test facility. For each VES, the telephotometer was placed in the driver's seat of the test vehicle. A photometer operator who sat in the rear seat of the vehicle aimed the photometer at the objects. An additional experimenter sat in the front seat of the vehicle and recorded the results. This differed from the ENV visual performance studies, in which the participant and an experimenter both sat in the front seats of the experimental vehicle.

In a typical testing process, all of the measurements were performed in a series at each station, with the measurement of one object followed by the measurement of the next object until all of the objects for that station had been tested with that VES. The next step was to change the VES on the vehicle and test all of the objects with it. After all of the VESs available on one vehicle were tested, the photometer was moved to the next vehicle, until all VESs were tested. Care was taken to ensure that the warmup time and stabilization of both the photometer and the VES matched to avoid inconsistencies between conditions. After all of the objects and VES conditions were tested at a station, the setup moved to the next station, and the process continued.

As mentioned, the number and seating arrangement of vehicle occupants in the test condition differed from the configuration in the ENV detection testing. This means that the vehicle's weight distribution was not the same between the test processes of the ENV detection studies and the photometric characterization. A short comparison test was performed to investigate how the photometer operator's position affected the measurements; these measurements were for this comparison only, and they were not included in the experimental design.

For this set of data, the object and background luminance measurements were performed with the photometer operator sitting in the back seat of the vehicle, just as it was performed in the characterization activity. Then the measurements were taken again with the photometer operator sitting in the driver's seat of the vehicle; the photometer's tripod was placed in the photometer operator's lap. The measurements were made at the 244-m (800-ft) distance because it would show the greatest change resulting from the front-to-back tilt in the vehicle. The measurements were taken with the test vehicle pointed uphill toward station 4. Only the WPP, WPL, and WC objects were used for these comparisons. The VESs used were limited to the HLB, three UV-A + HLB, and five UV-A + HLB. The photometric results from the two positions were then compared using their means and standard errors.

The results for all of the measurements are seen in figure 7 for each of the UV systems. Figure 7 comprises the mean of the background and object luminance data for all objects from both of the photometer operator's positions. This figure shows that the two photometer operator positions yielded similar measurements.

Back Seat and Driver's Seat Photometer Operator Position Comparison by UV Type

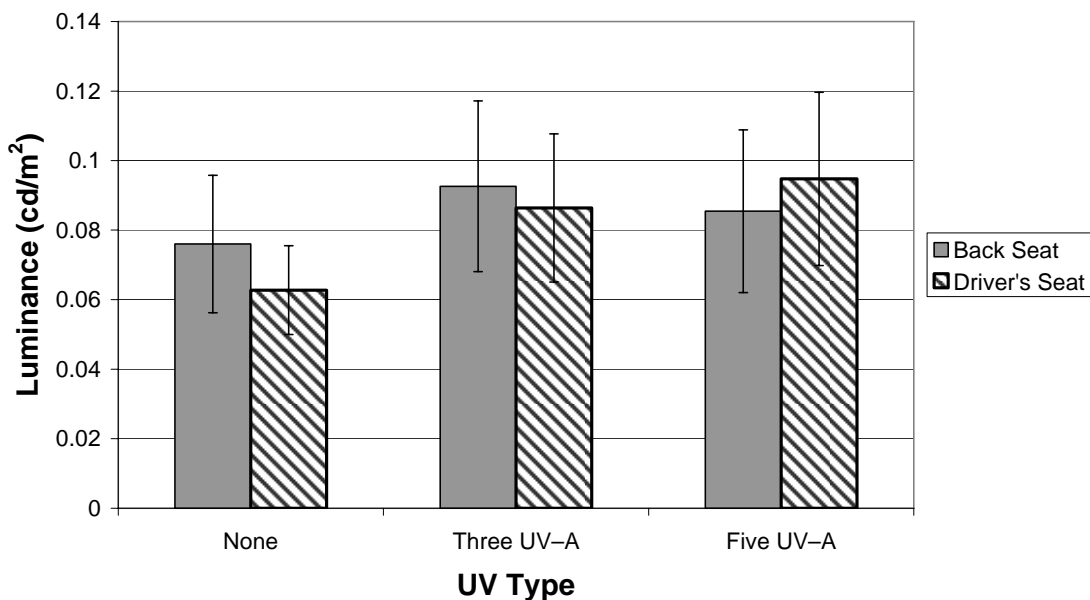


Figure 7. Bar graph. Comparison of the mean of background object luminance for HLB combined with different UV-A levels when the photometer operator is in the back seat or the driver's seat.

To further review these results, the data for the object luminance were considered separately because these data were more likely to have been affected by the change in the tilt of the vehicle than the background luminance data. The bar graph in figure 8 shows a slight difference between the object measurements for the two positions of the photometer operator for the HLB VES; however, there was no such significant difference for the HLB VESs with UV-A. From this data, it can be seen that the standard error associated with the measurements was greater than any difference produced by the position of the photometer operator. Based on this analysis, it was decided that the measurement procedure with the photometer operator in the back seat of the vehicle was valid, and the position did not influence the measurement results.

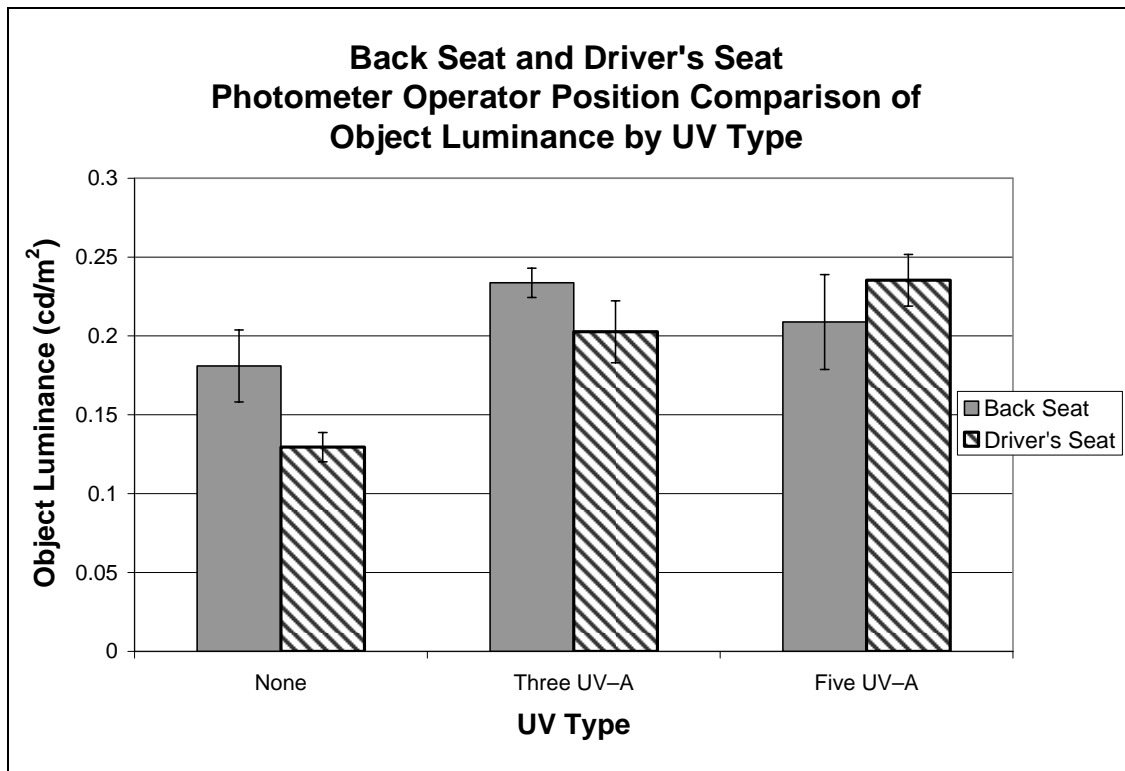


Figure 8. Bar graph. Comparison of object luminance for HLB combined with different UV-A levels when the photometer operator is in the back seat or the driver's seat.

DATA ANALYSIS

The dependent variables measured on the Smart Road were used to derive several other metrics, namely the object reflectivity, object fluorescence, contrast, and visibility level.

Reflectivity

The reflectivity of the object can be calculated using the assumption that the object of interest is a Lambertian (diffuse in all directions) reflector. If this assumption is made, the reflectivity is calculated from the incident illuminance and the object luminance. This is determined through the equation shown in figure 9.

$$\rho = \frac{L\pi}{E}$$

Figure 9. Equation. Lambertian reflection.

In this equation, ρ is the reflectivity, E is the incident illuminance, and L is the object luminance. The reflectivity of most of the objects was determined using this relationship.

Some objects in this study did not reflect diffusely, but rather, they acted specularly. These were the shiny objects such as certain parts of the bicycles. This means that reflectivity has a directional component, and thus the Lambertian assumption is not valid. For such objects, the specular reflectivity in a given direction is calculated using the equation in figure 10.

$$\rho = \frac{L}{E}$$

Figure 10. Equation. Specular reflection.

In both cases, the reflectivity is a ratio usually expressed in percent, and it does not have specific units.

It is important to note that the reflectivity of the objects can be established only for the non-UV–A containing VESs. If the UV–A containing VESs are used, the measured luminance contains both the reflected light and the light generated through the fluorescence of the clothing material and possibly the paint on the bicycle used in the cyclist conditions and the child's bicycle.

Fluorescence

The contribution of the UV–A to the appearance of the material can be assessed by examining the increase in the object’s luminance with the various UV–A VES configurations. To establish the fluorescence of the material, the reflectance of all of the object and VES combinations was calculated. These combinations included VESs with a UV–A component. The reflectance with these UV–A combinations could be much greater than 100 percent because the luminance was generated not only from the reflected visible light but also from the emitted fluorescence due to the UV. The fluorescence was calculated as the ratio of the object reflectance in a UV–A condition to that of the same object in a non-UV–A condition with the same visible-light headlamps. Figure 11 shows this relationship.

$$\% Fluorescence = \left(\frac{\rho_{Fluorescent}}{\rho_{Non-Fluorescent}} \right) \bullet 100$$

Figure 11. Equation. Object fluorescence.

The equation in figure 11 assumes that the UV–A reflectance will always be greater than the non-UV–A reflectivity. This relationship established the fluorescent activation capability of each of the object types and each of the VESs. Note, a *%Fluorescence* value of 100 percent indicates no increase in the object’s luminance with the various UV–A VES configurations.

Contrast

The contrast of the object to the background can be expressed as the simple difference between the luminance of the object and the luminance of the background or as a ratio of the object and background luminance difference to the background luminance as shown in figure 12.

$$C = \frac{L_{Object} - L_{Background}}{L_{Background}}$$

Figure 12. Equation. Contrast ratio.

When the object is darker than the background, the relationship is negative; it is referred to as a “negative contrast condition.”

In addition to the other analyses, the contrast of the human objects in the experiment was evaluated in two ways. The first was to use the average of the background measurements and the average of all of the object measurements in the contrast equation. The second was to evaluate the contrast at the various measurement heights (ankle, knee, waist, and chest) using the object measurement and the two corresponding (left, right) background measurements. This provided an idea of a contrast gradient on the object. The contrasts for the tire tread and the child's bicycle were evaluated only as the average of the background versus the average of the object luminance measurement.

Visibility Level

The visibility level (VL) was calculated based on Adrian's object visibility model, in which the threshold luminance difference (ΔL_{th}) is defined as the value of the difference between the luminance of a target and the luminance of the background that allows an observer to barely detect the presence of the object.⁽¹⁾ His model is defined for mesopic viewing conditions and assumes no impact due to color differences and spectral sensitivity. The ΔL_{th} is calculated according to the model, and it is based on the size of the object, background luminance, observation time, age of the observer, and polarity of the contrast.

The Adrian model is calculated using a basic formula with situational factors to modify the result for various conditions. The basic calculation is shown in the equation in figure 13.

$$\Delta L_{th} = k \left(\frac{\phi^2}{\alpha} + L^2 \right)^2$$

Figure 13. Equation. Basic ΔL_{th} model.

The models for ϕ and L are both functions of the background luminance, and they are defined in the model. α is the angular size of a target in minutes of arc. To calculate the target size, the solid angle of the actual onroad object was calculated, and then a circular object of equivalent size was chosen. The circular object's diameter was used as the target size in minutes of arc. The factor k is a constant that scales the ΔL_{th} result to a probability factor. For the 99.9-percent probability of detection, k would equal 2.6; for the 50-percent probability of detection, k would equal 1.

The basic ΔL_{th} function was developed using a 2-s observation time. A time factor was developed to account for shorter observation times. The general form of the time factor is shown in the equation in figure 14.

$$TF = \frac{a(\alpha, L_B) + t}{t}$$

Figure 14. Equation. Time factor for the ΔL_{th} model.

The function $a(\alpha, L_B)$, representing the observation time, is defined in the model.

According to the Adrian model, targets that appear in negative contrast (i.e., object is darker than background) are more easily seen than those that appear in positive contrast (i.e., object is lighter than background).⁽¹⁾ A factor for negative contrast was also developed. This factor (F_{CP}) is based on the target size and background luminance.

The final variable that must be accounted for is the age of the observer. The basic model was developed for a 23-year-old observer. To account for different age groups, a final factor was used. The format for the factor is shown in the equation in figure 15.

$$AF = \frac{(Age - a)^2}{b} + c$$

Figure 15. Equation. Age factor for the ΔL_{th} model.

The value of the constants of a , b , and c are dependent on the age, and the values are presented in Adrian's document.

The final model of the ΔL_{th} calculation is shown in figure 16.

$$\Delta L_{th} = k \left(\frac{\phi^2}{\alpha} + L^2 \right)^2 \cdot TF \cdot F_{CP} \cdot AF$$

Figure 16. Equation. Complete ΔL_{th} model.

As a metric for visibility, the VL is the ratio of the actual luminance difference and ΔL_{th} . The formula for this calculation is seen in figure 17, where C stands for contrast.

$$VL = \frac{\Delta L_{Actual}}{\Delta L_{Threshold}} = \frac{L_{Object} - L_{Background}}{\Delta L_{Threshold}} = \frac{C_{Actual}}{C_{Threshold}}$$

Figure 17. Equation. Visibility level.

In this calculation, a VL of 1 would imply the detection threshold; however, in a driving task the threshold increases to allow for driver distraction and workload. Because there are no correction factors for driver distraction and workload, the Illuminating Engineering Society of North America RP-8-00 recommends that a VL of 2.6 to 3.8 be used in practice to account for those issues.⁽²⁾

The Adrian model was used to calculate the VL of all of the objects used in this ENV object characterization. For this calculation, the observation time was set to 0.2 s. The target size was calculated based on the height of the object and the observation distance. The objects' dimensions are summarized in table 6. A 99-percent detection confidence interval was used with a k factor of 2.9.

Table 6. Object dimension summarization.

Object	Height (ft)	Width (ft)
Pedestrians/cyclist (WPL, BPL, WPP, BPP, WC, BC)	6.00	1.00
Child's bicycle (CB)	0.75	2.25
Tire tread (TT)	0.75	2.25

1 ft = 0.305 m

CHAPTER 3—RESULTS

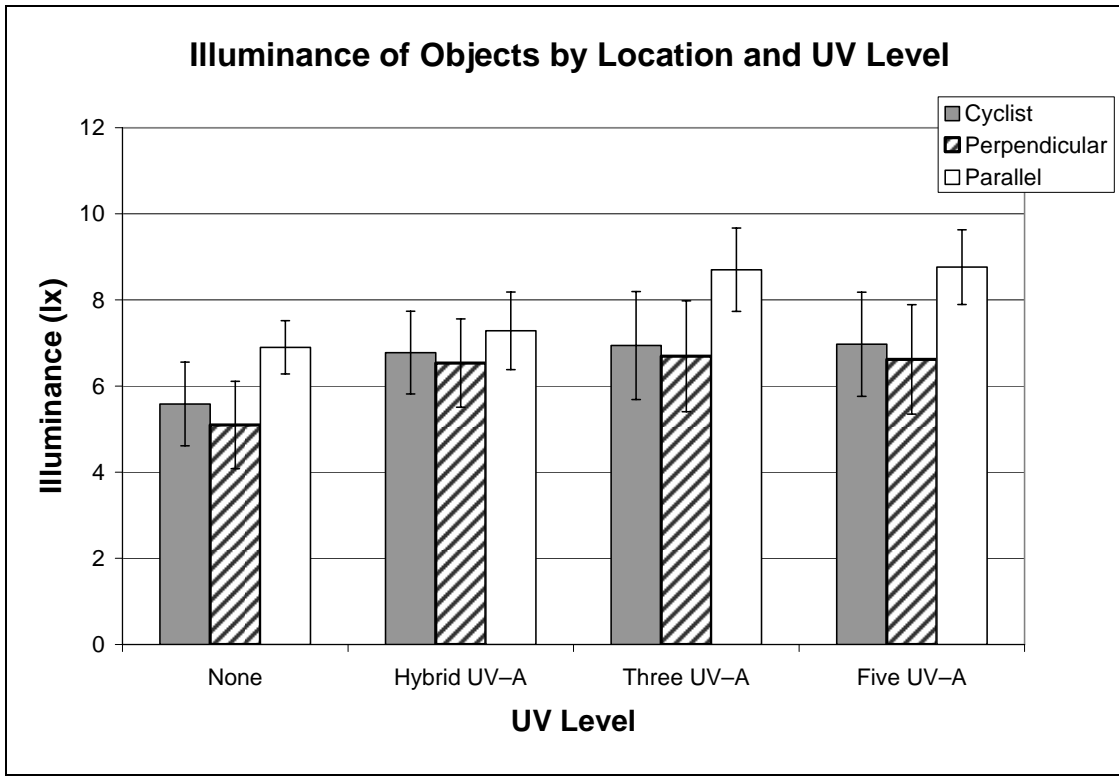
The results from this measurement activity are presented below. The measured values of headlamp illuminance, object luminance, and background luminance are presented followed by the calculated metrics of reflectance, fluorescence, contrast, and VL.

ILLUMINANCE FROM THE HEADLAMPS

The illuminance from the headlamps was measured at points corresponding to the luminance measurement points. For the analysis, an analysis of variance (ANOVA) that considered the effect of the UV–A systems on the illuminance was conducted. Then the data were analyzed in terms of the pedestrian objects (which included the cyclist), the child’s bicycle, and the tire tread.

UV–A Illuminance

Because UV–A is outside of the human visual range, the UV–A sources should not contribute to the illuminance on the object; however, the UV–A systems used, particularly the hybrid source, did have some output in the visible range. Thus a comparison of the measurement results with and without the UV–A systems was used to investigate their effect on the illuminance. The object position was considered as a factor because the illuminance contribution from the UV–A sources may have varied across the roadway. That is to say, the parallel and static objects on the shoulder of the road might have received a different level of illuminance from the UV–A sources than did the objects in the center of the road such as the cyclist and the perpendicular objects. The results of this comparison are shown in figure 18.



All measurements taken from a distance of 61.0 m (200 ft).

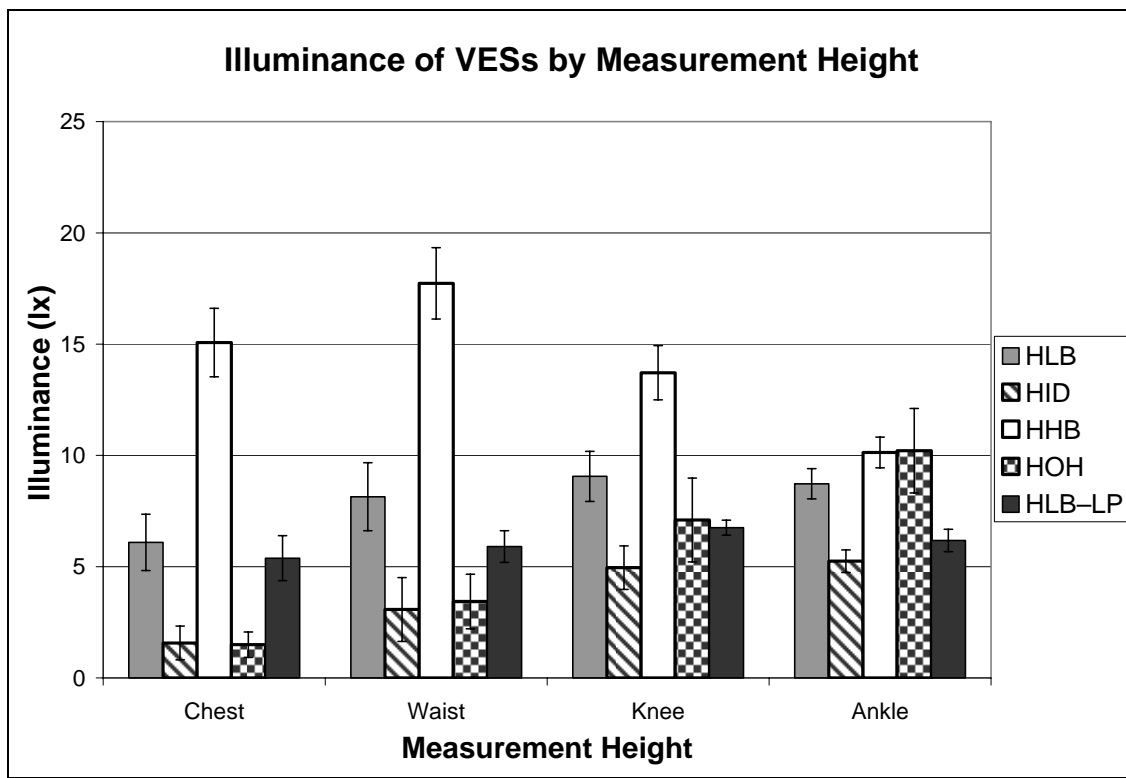
Figure 18. Bar graph. Object illuminance by UV-A level.

This interaction of position and UV-A shows that there is a slight increase in illuminance on all the objects, with the greatest increase on the parallel object at the side of the road; however, the increase remains within the standard error of the measurements made without UV-A sources. Because neither effect was significant, the UV-A sources were not considered in the analysis of the headlamp illuminance.

Pedestrian and Cyclist Objects

The parallel pedestrian, perpendicular pedestrian, and cyclist were considered together in this group. The results for the black-clothed objects and the white-clothed objects were averaged because the illuminance on an object is independent of the object itself. The results were then summarized by measurement height, position of the object on the roadway, and the distance from the VES to the object.

Figure 19 shows illuminance results for the different VESs and the measurement height. It is interesting that with the exception of the HHB light source, the illuminance decreased as the measurement height increased, meaning that the headlamps primarily lit the lower portions of objects, which were closer to the roadway. This is to be expected because headlamps are designed to limit the projected light above the horizon that could cause glare for oncoming drivers. The HHB light source illuminated the higher portions of the object better than they did the lower portions. This is also to be expected because the HHB typically is aimed to provide illumination farther down the roadway.



All measurements taken from a distance of 61.0 m (200 ft).

Figure 19. Bar graph. Illuminance from each VES by measurement height for the pedestrian object types.

The next aspect of the illuminance results is the performance for the three object positions on the roadway, shown in figure 20. Through review of the standard error, this relationship shows that the HLB and the HLB–LP similarly illuminated all three objects. The noteworthy result is that the HID and the HOH headlamps lit the pedestrian at the side of the road (parallel pedestrians) more than they lit those in the center of the road (cyclists and perpendicular pedestrians). Conversely, the HHB headlamps lit objects in the center of the road more than it did the objects on the side of the road.

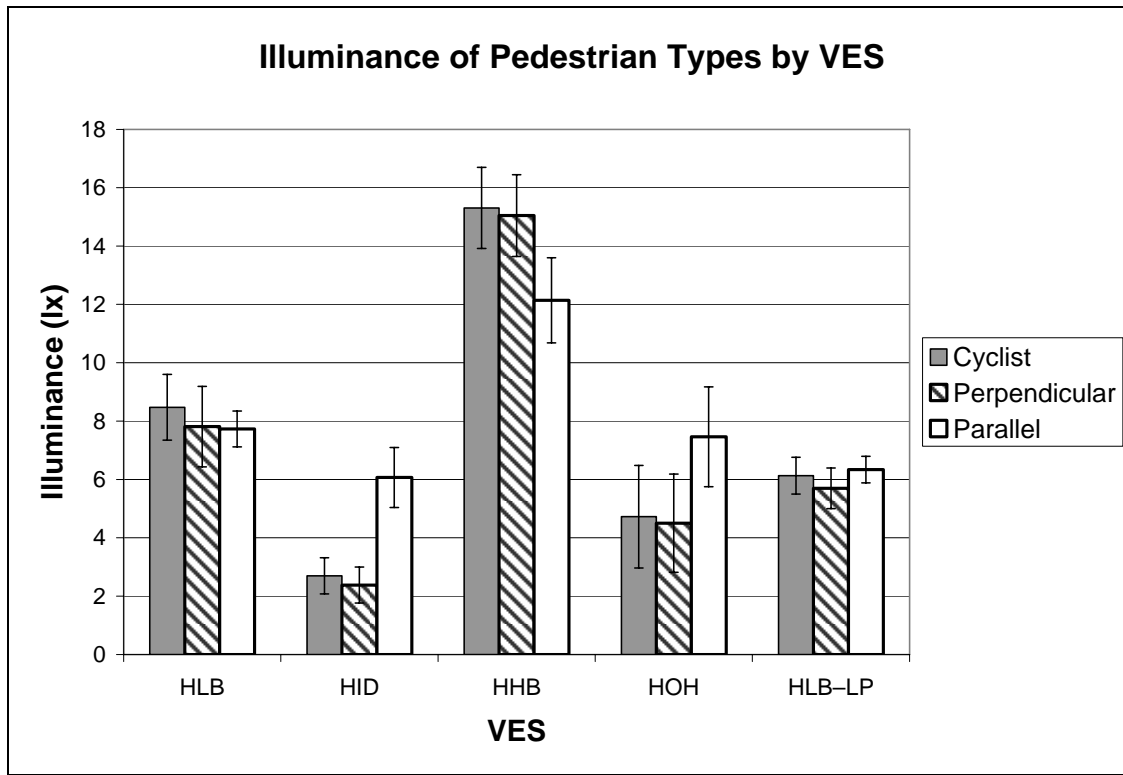


Figure 20. Bar graph. Illuminance from each VES by object position for the pedestrian object types.

The other aspect of interest for the illuminance is the relationship of the illuminance to the distance between the object and the vehicle as shown in figure 21. This relationship should follow the inverse square law, which is shown as the line on the figure. The difference between the HID and HLB headlamp types as well as the relationship between the chest and the waist measurement appears to be consistent, and the difference followed the inverse square trend.

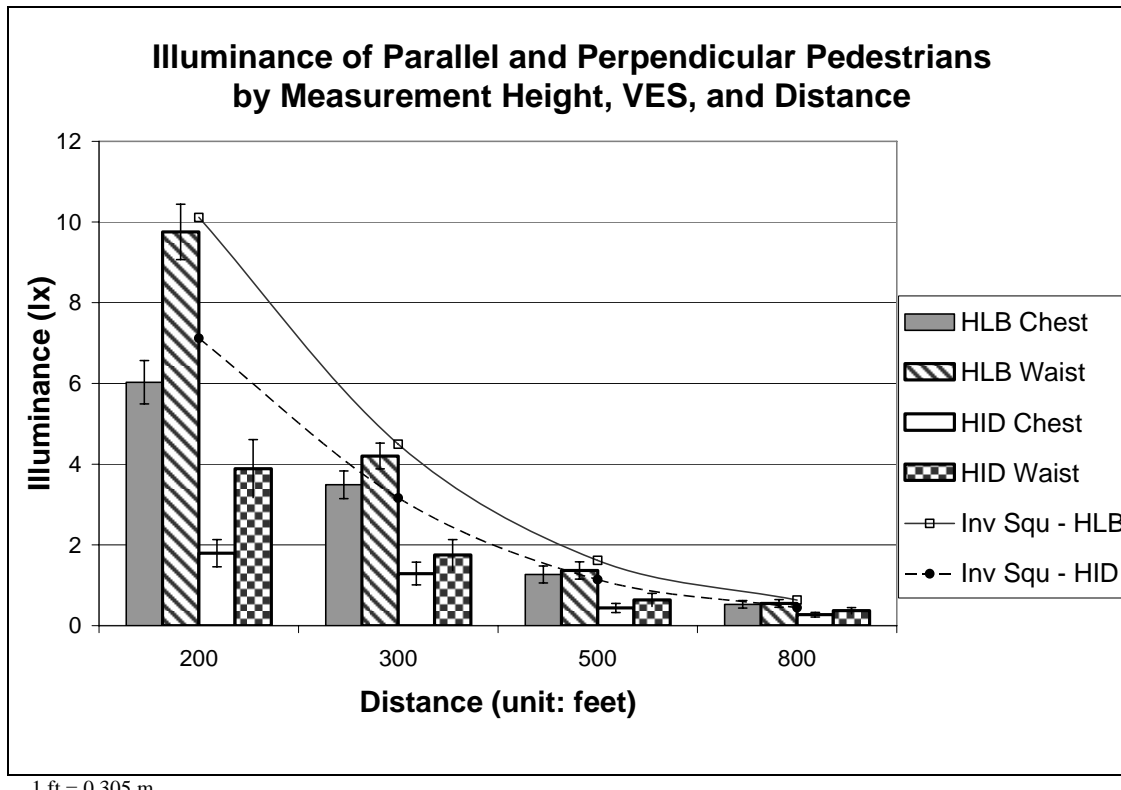


Figure 21. Bar graph. Illuminance and distance relationship by lamp and measurement location with the inverse square law trends for the pedestrian object types.

Child's Bicycle and Tire Tread Objects

The results for the tire tread and the child's bicycle are shown in figure 22. Both of these objects were at the side of the road and close to the road surface, and as a result, the illuminance on these objects followed the relationship of the ankle measurement for the pedestrian objects as seen in figure 19. Generally, the illuminance on the two object types was the same for all of the headlamps except HLB and HID. It is not clear what caused the difference between the tire tread and the child's bicycle for the HLB and the HID light sources.

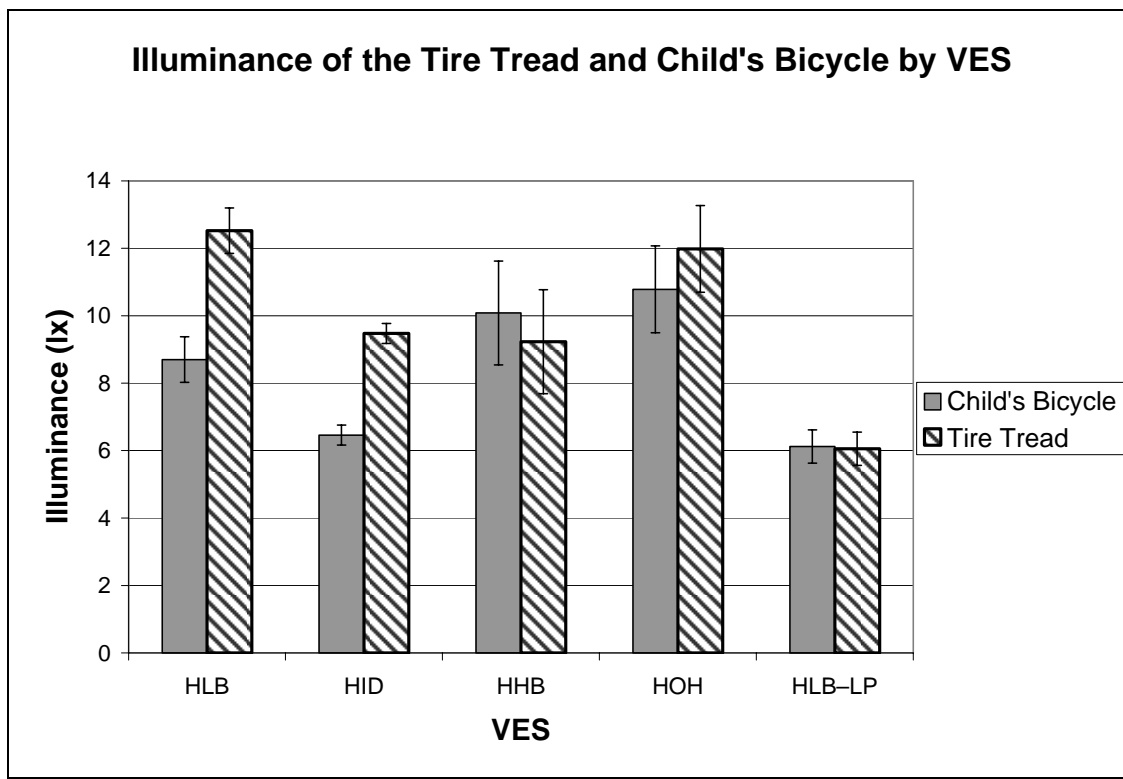


Figure 22. Bar graph. Illuminance on the child's bicycle and the tire tread for each VES type.

OBJECT LUMINANCE

For analysis, the object luminance was broken into three categories. As with the illuminance data, the pedestrians and cyclists, the child's bicycle, and the tire tread were all analyzed separately. The pedestrians and cyclists were further broken into white- and black-clothed groupings for analysis.

The measurement method for both the object luminance and the background luminance was designed such that a first measurement series was performed with 61.0 m (200 ft) between the experimental object and the vehicle to establish the object luminance. The next series of measurements was performed at 91.5 m (300 ft), 152.5 m (500 ft), and 244 m (800 ft) to establish the effect of distance on the luminance.

Pedestrian and Cyclist Objects

The overall effect of VES types on the object luminance is shown in figure 23 for the black- and the white-clothed pedestrians and cyclist. In this case the HID, HOH, and HLB-LP provided a lower level of luminance than the HHB, which had the highest value, and HLB, which had an intermediate level. Figure 23 also shows the effect of the UV-A source on the luminance of the white-clothed objects; as the UV-A level increased from none to five UV-A, the luminance of the objects also increased. This is evident for both the UV-A + HID and UV-A + HLB combinations; however, the most obvious significant difference is the effect on object luminance of the white and black clothing, which was analyzed separately to review this difference in more detail. Results follow the figure.

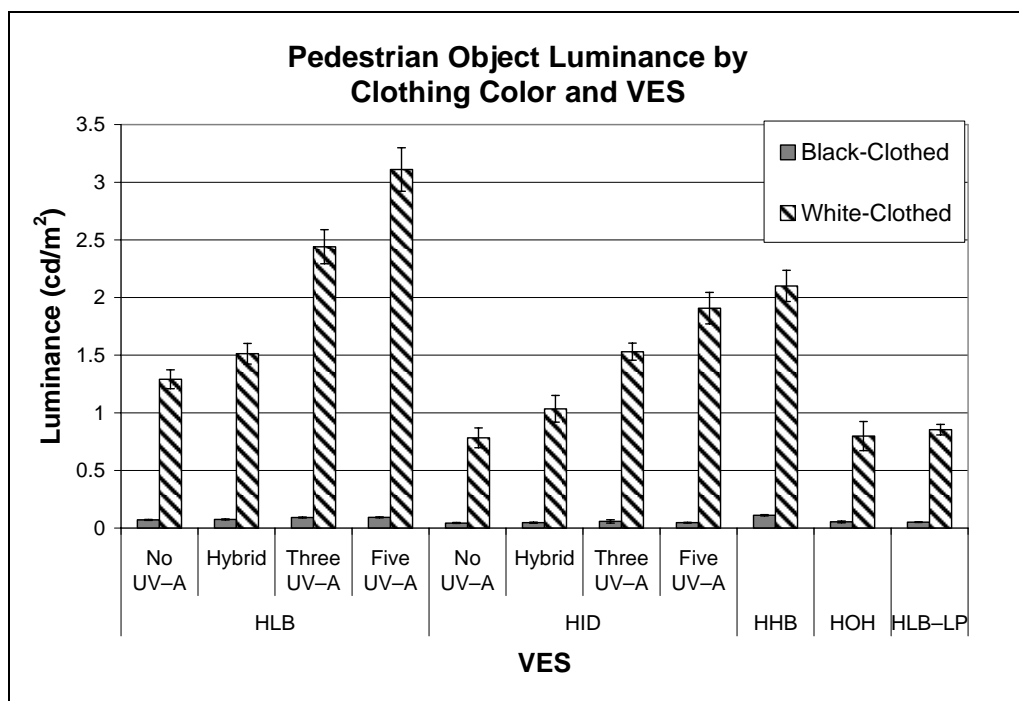
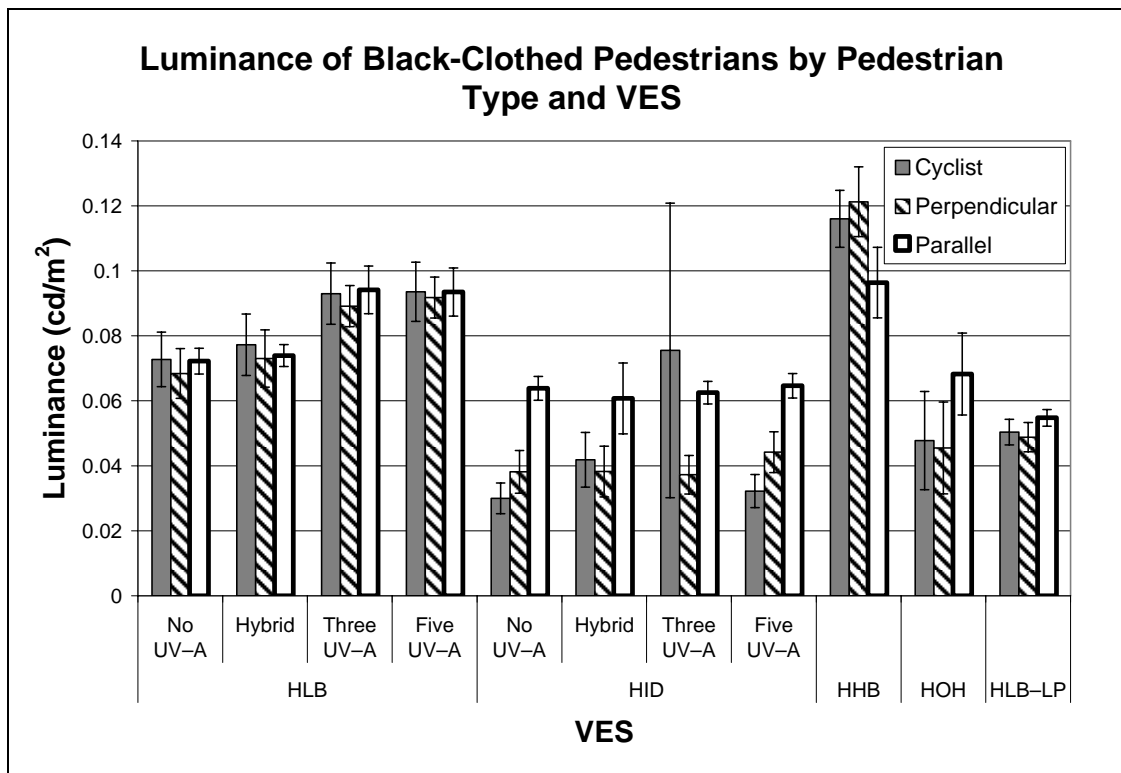


Figure 23. Bar graph. Object luminance by VES for white- and black-clothed pedestrians.

Black-Clothed Objects

The black-clothed objects included the cyclist and the perpendicular and parallel pedestrians. Figure 24 shows the object luminance for VES for each of these object classes.



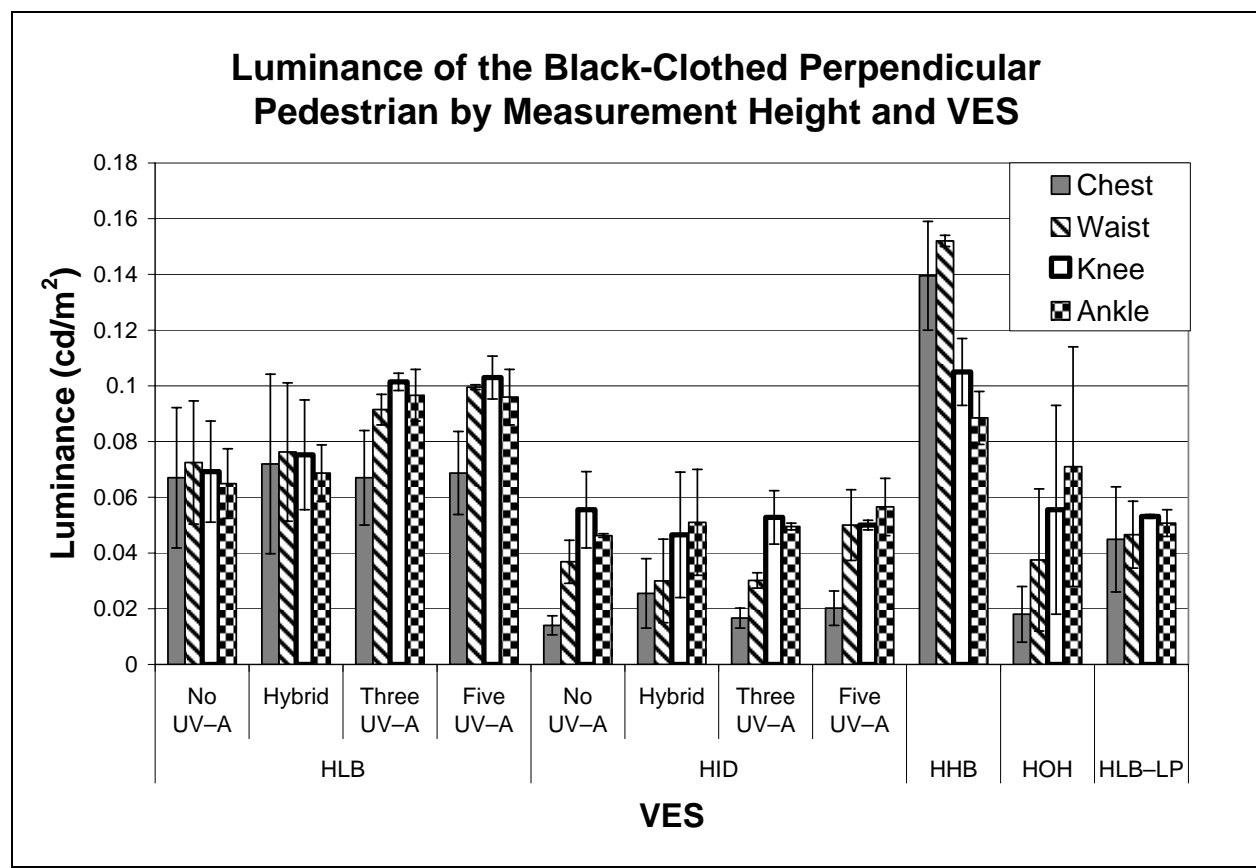
All measurements taken from a distance of 61.0 m (200 ft).

Figure 24. Bar graph. Object luminance by VES for black-clothed pedestrians and cyclist by object position.

All of these measurements were taken from a distance of 61.0 m (200 ft). With the exception of the HID class of headlamps, the object luminances were not statistically different between the black-clothed objects. For the HID class of headlamps, the parallel position had a consistently higher luminance than the perpendicular position and the cyclist. This probably indicates that the beam distribution of the HID headlamps is wider than the other headlamp types. A wider beam will illuminate the object at the side of the road to a greater extent than narrower beams. The contribution of the UV-A to the luminance of the black-clothed objects appears to have been minimal. There was slight contribution of the three and five UV-A designs with the HLB headlamp, but there was no contribution from the hybrid UV-A with HLB or any of the UV-A headlamps with the HID headlamp. Finally, the HHB provided the highest values for object

luminance; the values for the perpendicular pedestrian and cyclist were slightly greater than the luminance for the parallel pedestrian, which also is indicative of beam pattern. The HHB headlamps are designed to cast more light straight down the roadway rather than to the side. This design would illuminate the objects at the center of the road more clearly than it would those on the shoulder. The HOH shows the opposite characteristics; it provided more light to the side than the center. In terms of the non-UV-A systems, the HOH and the HLB-LP provided equivalent lighting levels, with the HID series being the lowest, the HHB being the highest, and the HLB being between these values.

The influence of the measurement height on the objects is shown in figure 25.



All measurements taken from a distance of 61.0 m (200 ft).

Figure 25. Bar graph. Object luminance by VES for black-clothed perpendicular pedestrians by measurement height.

For most VESs, the luminance at the chest measurement height was lower than the luminance at the other measurement heights. The exceptions to this trend were the HLB and the hybrid UV-A + HLB, which showed no significant differences between the measurement

heights, and HHB, which showed greater luminance at the chest and waist than at the knee and ankle. These results are to be expected because the HLB and HHB headlamps do not have a significant intensity cutoff; however, the similarity in object luminance with height for HLB and the HHB VES types might have been exacerbated by aiming issues associated with these headlamps. For more information about this issue, please refer to ENV Volume XVII, *Characterization of Experimental Vision Enhancement Systems*. The UV–A headlamps showed no significant effect on the black clothing and the measurement height. There were also no significant differences among the other VES types.

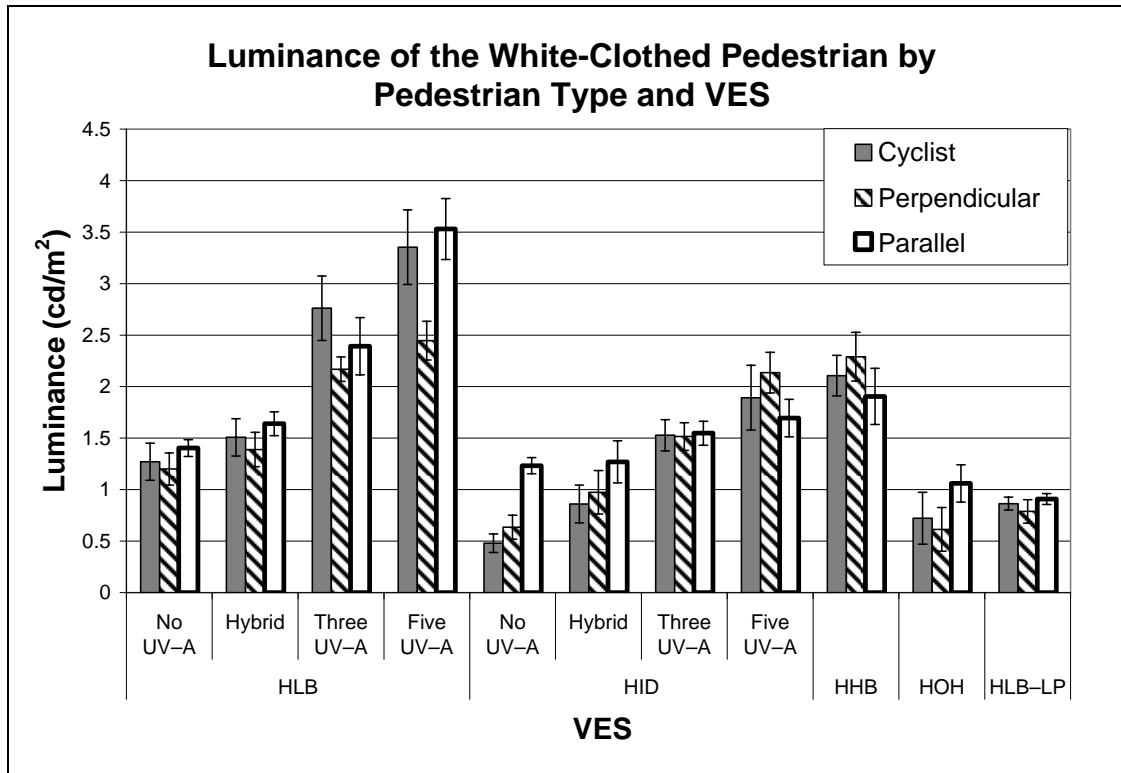
White-Clothed Objects

The luminance of all the white-clothed objects was first measured at 61.0 m (200 ft), and then the luminance of the parallel and perpendicular pedestrians was measured at 91.5 m (300 ft), 152.5 m (500 ft), and 244 m (800 ft) to establish the influence of distance on the luminance. The analysis of these white-clothed objects was first performed at 61.0 m (200 ft), and then the effect of distance was considered.

As with the black-clothed object, the white-clothed object appeared in perpendicular, parallel, and cyclist configurations. As mentioned, in addition to these, the white-clothed pedestrian was also presented in a static configuration in which the pedestrian stood on the shoulder of the road, approximately 0.3 m (1 ft) from the white roadway edgeline, and faced the approaching participant vehicle. For characterization purposes, this object was considered to be the same as the parallel object, so the static condition was not explicitly considered in any of the analyses.

The influence of the object position on the measurements is shown in figure 26. In this relationship, the influence of the UV–A sources on the luminance of the white-clothed objects is evident. The luminance for the five UV–A + HLB VES was the highest, followed by the three UV–A + HLB VES. The hybrid UV–A also indicated a slight increase in luminance over the HLB with no UV–A condition. The HHB and the three UV–A + HLB VESs were not statistically different. The lowest-performing VESs were the HOH and the HLB–LP, which had similar luminance levels. One of the more interesting results is the luminance of the parallel pedestrian under the HID-based VESs. In the HID configuration with no UV–A contribution, the parallel pedestrian had the highest luminance, which is indicative of the beam pattern of the HID

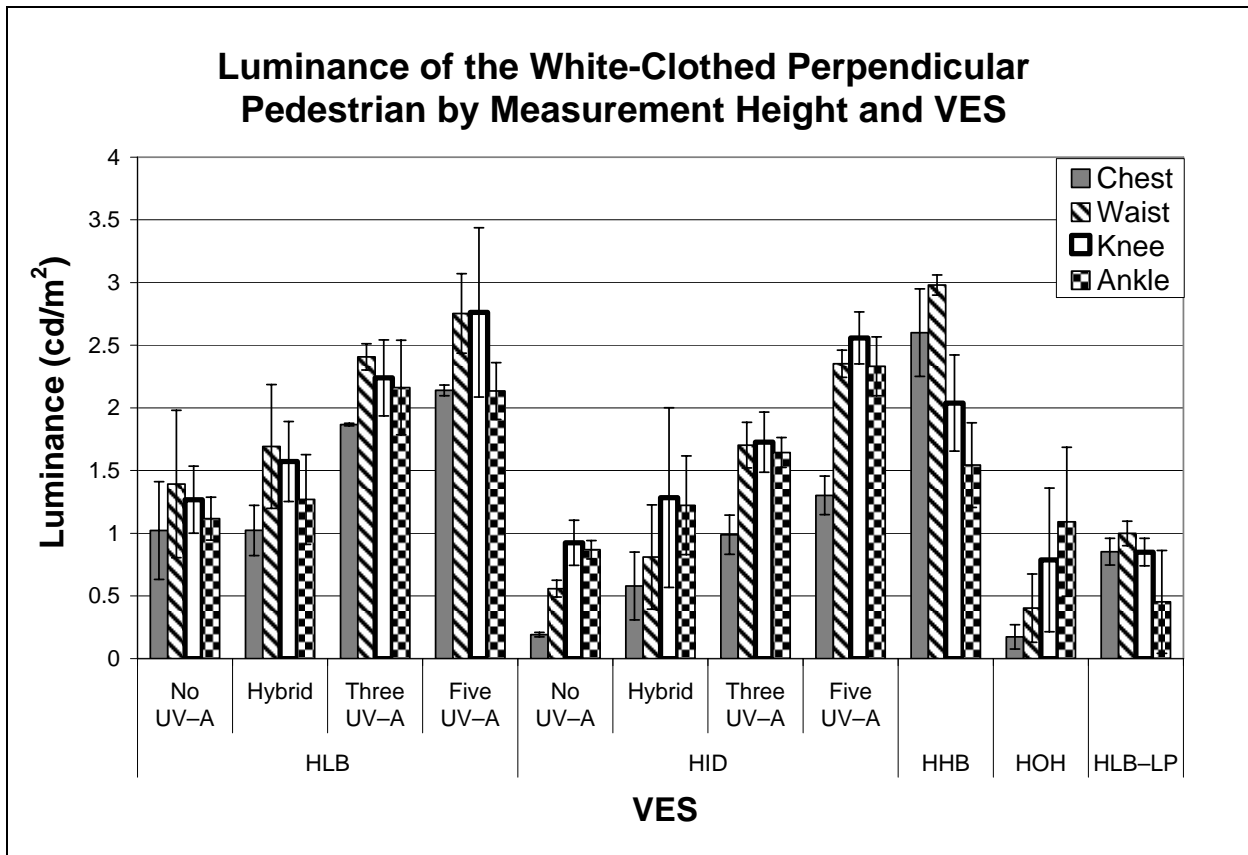
luminaires. However, as the UV-A contribution is added, the influence of the UV-A on the cyclist and the perpendicular pedestrian was greater than on the parallel pedestrian, which had the lowest luminance of the three configurations at the five UV-A level.



All measurements taken from a distance of 61.0 m (200 ft).

Figure 26. Bar graph. Object luminance by VES for white-clothed pedestrians by object position.

The influence of the measurement height on the object luminance is shown in figure 27. This influence was very similar to that on the black-clothed objects. The headlamps that have a sharp cutoff, such as the HID headlamps, had a much lower luminance on the chest of the object than the other locations. The HHB headlamp showed a higher luminance on the chest than the ankle because of its higher aiming point.



All measurements taken from a distance of 61.0 m (200 ft).

Figure 27. Bar graph. Object luminance by VES for white-clothed perpendicular pedestrian by measurement height.

The effect of the measurement distance on the object luminance is shown in figure 28. As expected, the luminance decreased as the distance increased. Because the headlamps were the only source of illumination, this would follow the same relationship as the object illuminance and the inverse square law. The change in the luminance for the VESs with the UV-A contribution also showed a decrement with distance. For the HLB configurations, the luminance levels appeared to become statistically similar at 152.5 m (500 ft). For the HID configurations, the luminance appeared to become statistically similar at 91.5 m (300 ft).

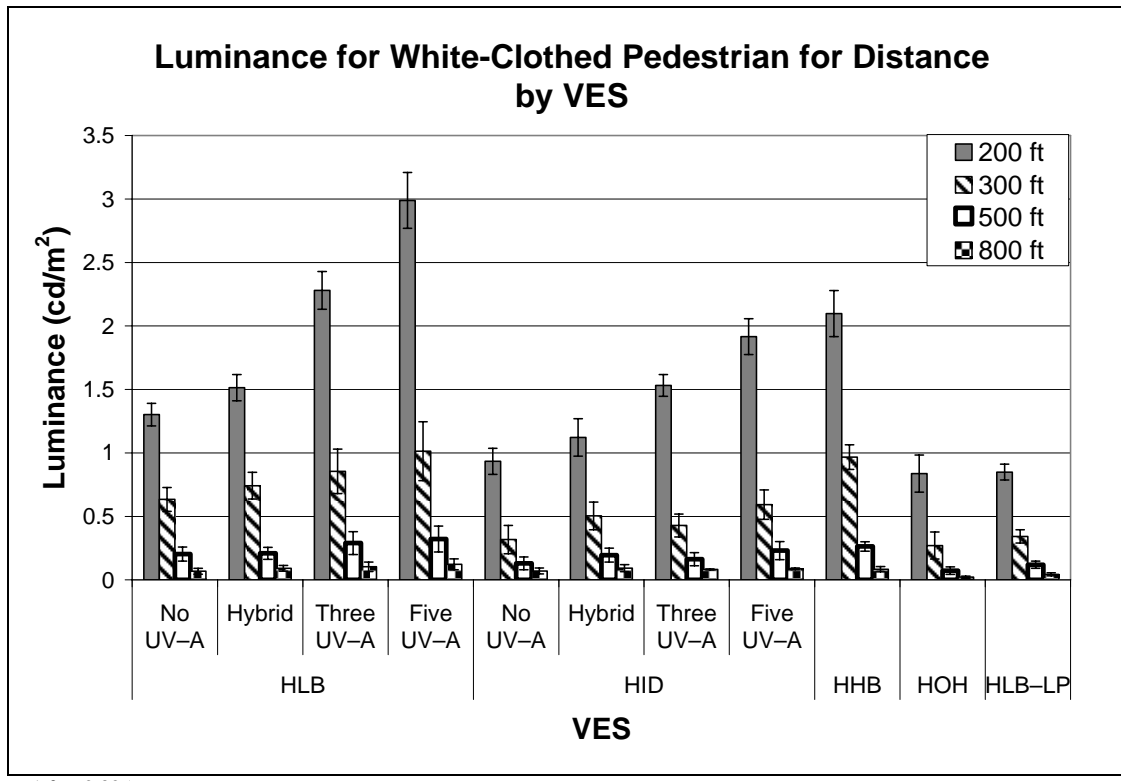


Figure 28. Bar graph. Object luminance by VES for white-clothed pedestrians by measurement distance.

Child's Bicycle

The luminance of the child's bicycle was measured at 61.0 m (200 ft). The results are presented in figure 29. This relationship shows that the UV-A configurations provided a higher object luminance than their baseline counterparts; however, unlike the pedestrian and cyclist objects, the HID configurations outperformed the HLB-LP. The HLB and the HID performed equivalently, and the HOH performed slightly higher. Because the child's bicycle was placed at the edge of the road and close to the road surface and because the HID has a wider beam than the HHB, this would result in a higher object luminance, as was found.

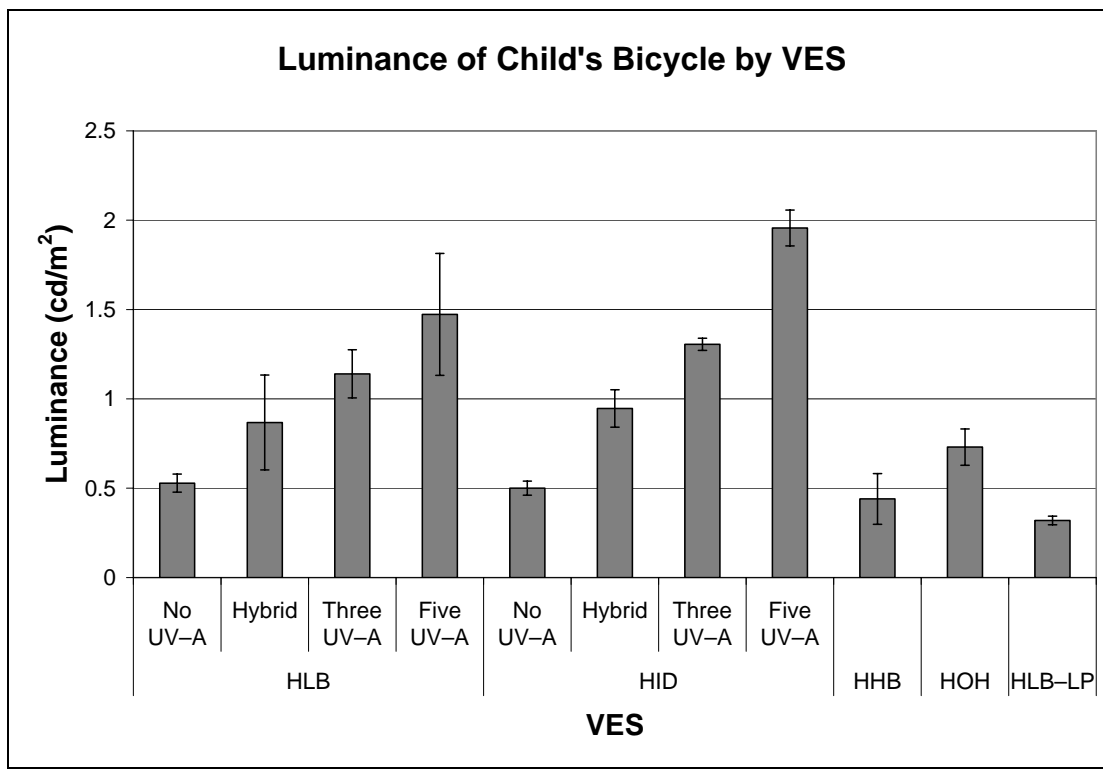


Figure 29. Bar graph. Object luminance by VES for the child's bicycle.

Tire Tread

The tire tread object was measured at 61.0 m (200 ft), and the results are shown in figure 30. Similar to the child's bicycle, the HLB, HHB, and HID conditions were all similar, with the HLB–LP having a lower luminance and the HOH having a higher luminance. Again, this appears to result from the nature of the beam pattern for these headlamp types. The HID beam is wider and would illuminate the tire tread at the side of the road better than the beam profile of the HLB–LP. There was no significant contribution to the luminance of the tire tread by the UV–A sources except for the three and five UV–A configurations with HLB, which showed a significantly higher luminance level. This contribution of the UV–A to the tire tread luminance was not expected.

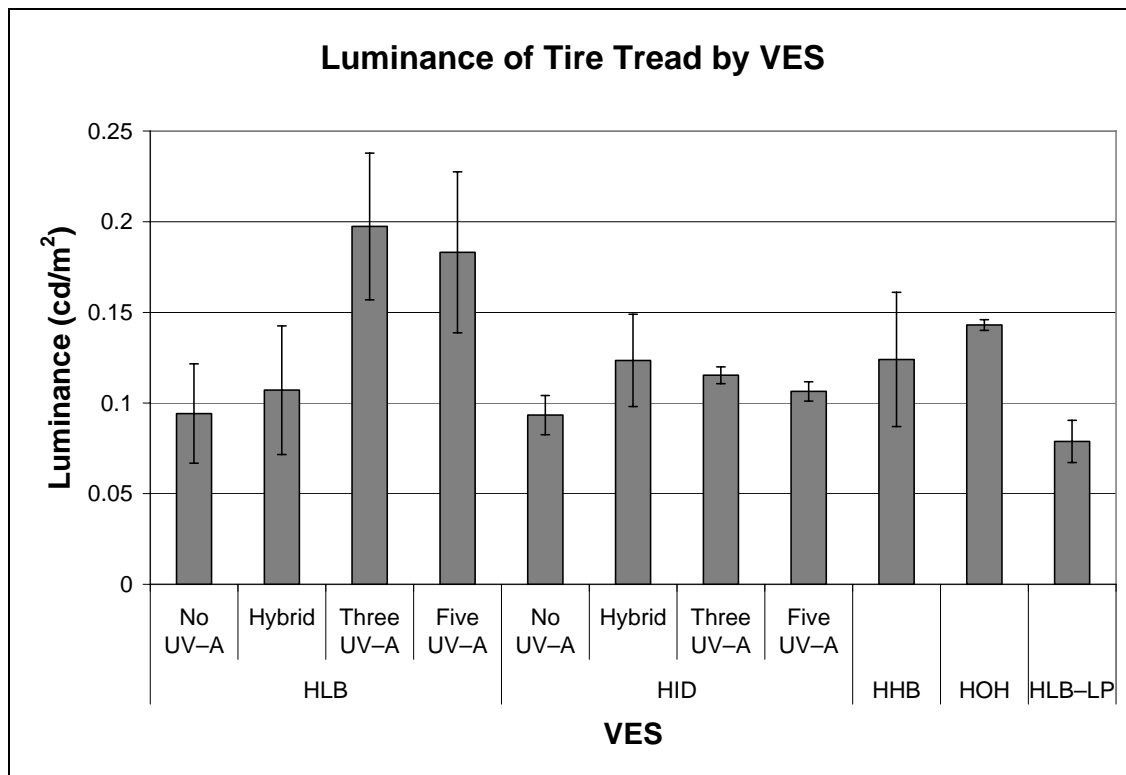
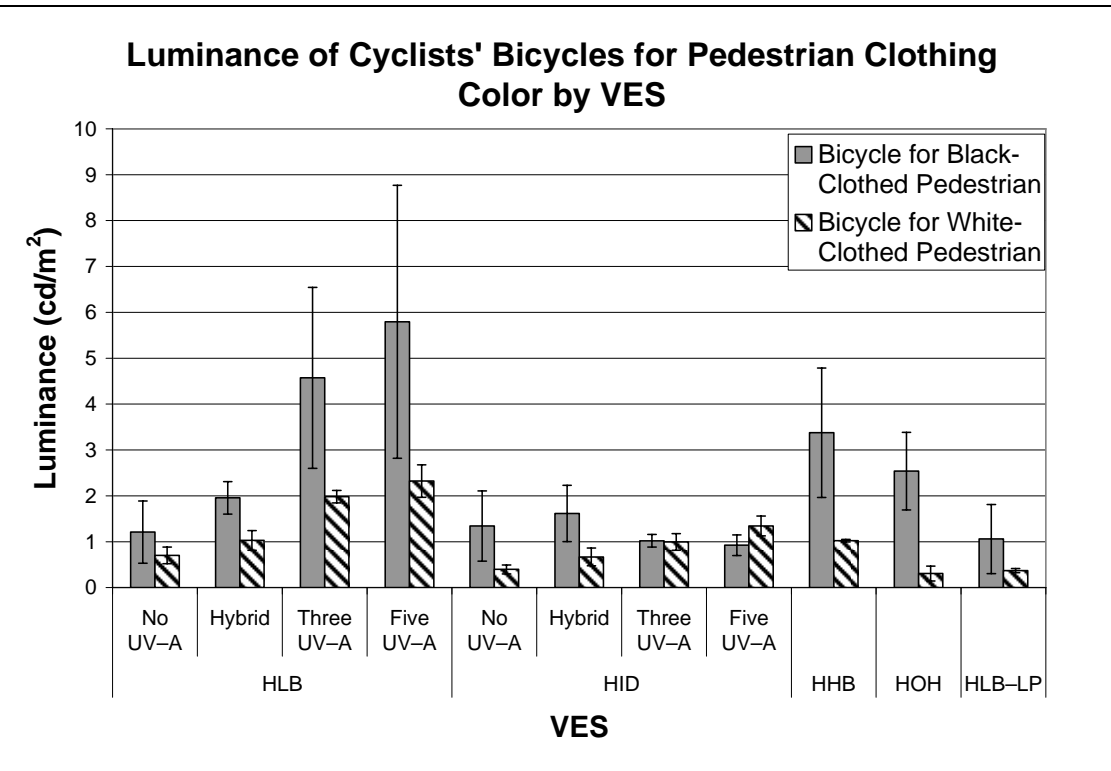


Figure 30. Bar graph. Object luminance by VES for the tire tread.

Cyclist Bicycles

The bicycle used by the black-clothed cyclist was a dark color, while the bicycle used by the white-clothed cyclist was painted with light-colored fluorescent paint. The wheel rims of the two bicycles also differed. The dark bicycle had shiny chrome rims, and the fluorescent bicycle had black rims. The measurement points were the brightest locations, so on the dark bicycle, the chrome rims were used for the measurement. The luminance relationship for these objects is shown in figure 31. The luminance performance was similar to the other objects, with the HHB providing a high level of luminance as compared to the other non-UV-A configurations. The important issue is the overall luminance level as compared to the cyclist alone. For the black-clothed cyclist, the luminance level ranged from 0.2 to 1.2 cd/m², and the bicycle for the same object ranged from approximately 1 to close to 6 cd/m². For the white-clothed cyclist, the luminance ranged from 0.5 to 3.5 cd/m², and the bicycle ranged from 0.25 to 2.25 cd/m². This indicates that the bicycle for the black-clothed cyclist was much brighter than the cyclist associated with it, which was not the case for the white-clothed cyclist's bicycle. During the ENV visual performance experiments, the brightness of the bicycle, rather than the luminance of the cyclist, may have provided the visibility to the participant. Unfortunately, this cannot be ascertained from the experimental results of the visibility investigation for the ENV clear condition.



All measurements taken from a distance of 61.0 m (200 ft).

Figure 31. Bar graph. Object luminance by VES for the cyclists' bicycles.

OBJECT BACKGROUND LUMINANCE

The object background luminance was measured for all VESs and objects at stations 2 and 4 at a distance of 61.0 m (200 ft). The effects of the measurement distance and the different station locations were also assessed during the measurement process. As with the object illuminance, the effects of the UV-A sources on the background measurements were assessed first. The analysis then continued with the assessment of the objects themselves.

Two factors should not have had an influence on the measurements made of the background luminance: the UV-A sources and the color of the object's clothing. For UV-A to affect photometric measurements, the radiation must come into contact with an object that fluoresces. In a typical background scene, fluorescent behavior is not evident. The object type, in particular the color of the pedestrian's or cyclist's clothing, also should not have an influence on the background measurement because the background is not influenced by the reflectance of the object. To verify this, the means of the data measured at the 61.4-m (200-ft) distance were compared in figure 32. This analysis included all of the VES configurations that included UV-A

and their baseline headlamps as well as the background measurement for the black- and white-clothed pedestrian and cyclist objects.

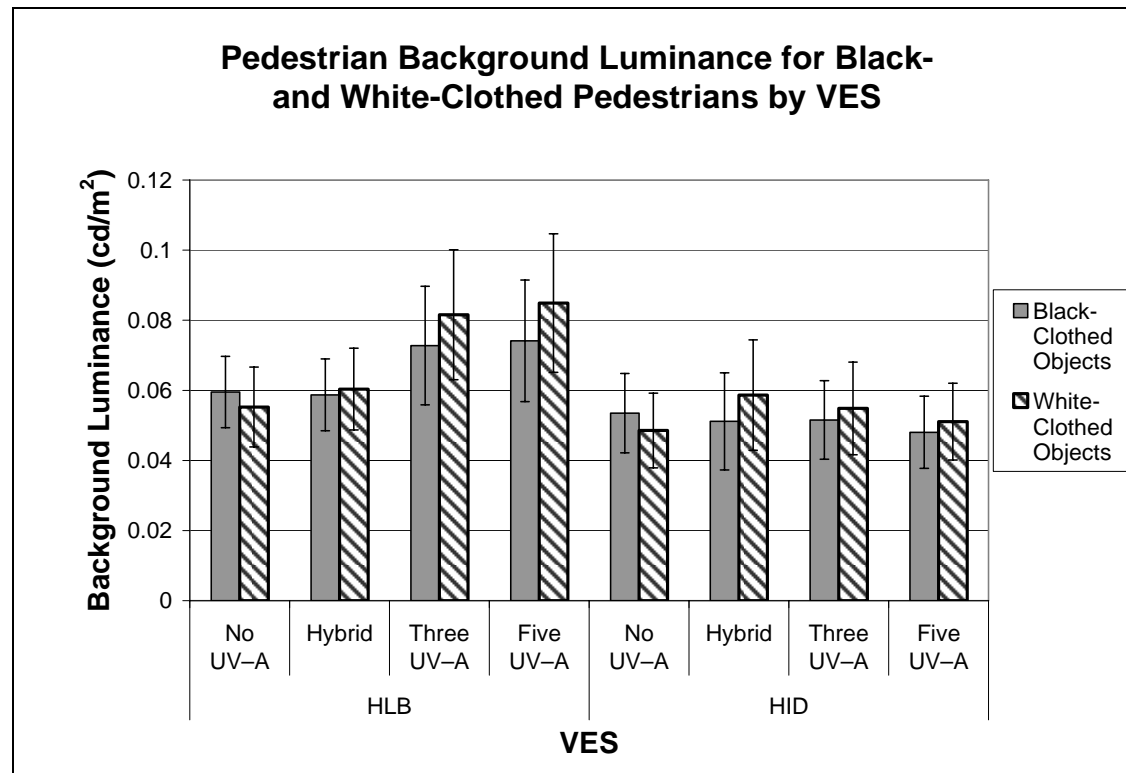


Figure 32. Bar graph. Background luminance for white- and black-clothed pedestrians by UV-A-based VES.

Figure 32 shows that the UV contribution does not influence the background luminance measurement. This is particularly true for the HID-based VESs. The HLB with three UV-A and five UV-A show an increase over the other measurements, but the differences are not statistically significant. This trend is similar to the trend for object luminance of the black-clothed perpendicular pedestrian. The results also show very little difference between the backgrounds of the two clothing colors. These results show that the UV-A sources and the object clothing color were not significant in the background luminance results and so were not included in any other analysis of the background luminance.

Pedestrian and Cyclist Objects

For the pedestrian and cyclist objects, eight luminance measurements of the background were made at varying heights. The heights matched those used for the object luminance measurements. These measurements were made for all of the VESs at each of the object presentation stations. The analysis of the data consisted of first summarizing the effect of the VES on the background measurements. Figure 33 shows this relationship by object position; the mean background luminance was not influenced by the position of the object on the roadway. The HLB, HHB, and HOH sources appear to have provided similar background luminance levels, with the HLB–LP and the HID providing slightly less.

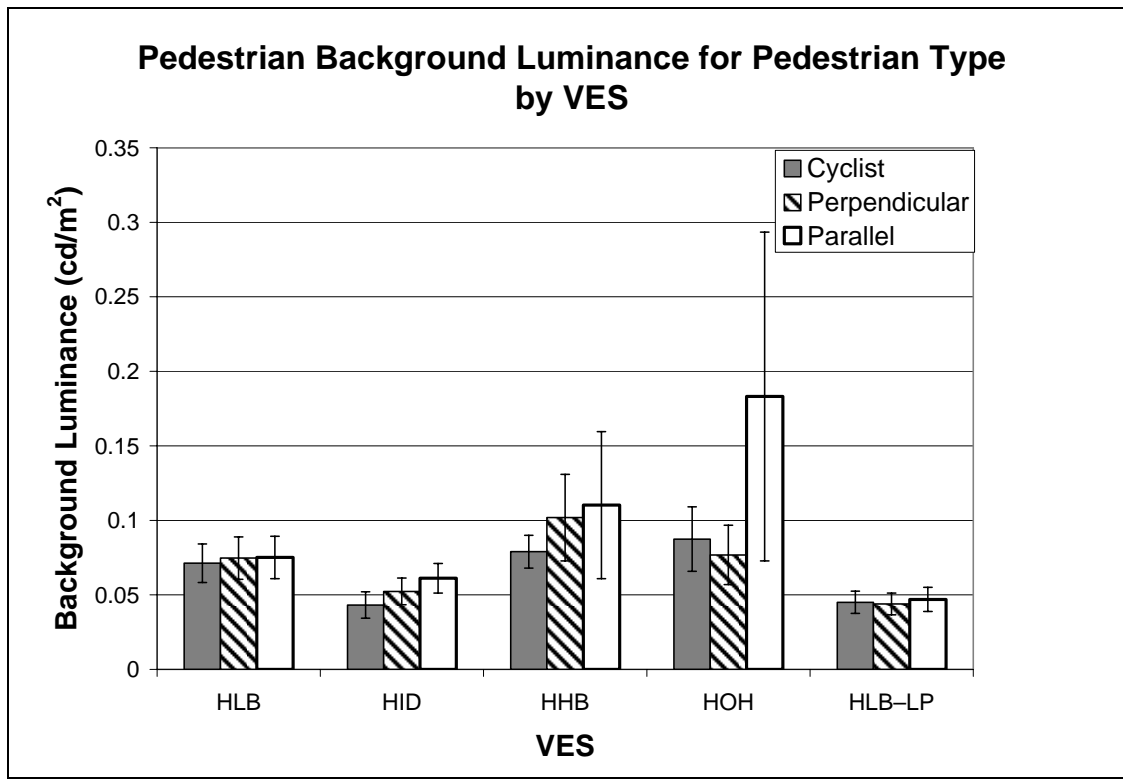


Figure 33. Bar graph. Influence of VES on background luminance by pedestrian position.

The relationship of the measurement height to the object background is interesting. Figure 34 shows this relationship for each VES. In this figure, the background luminance is shown to increase as the measurement height decreases. This is to be expected because the road surface came into the view of the photometer at low measurement heights. The other interesting increase is that of the HOH. In this case, the pavement marking may have been included as part of the background, which explains why the HOH VES showed the highest background luminance for the parallel pedestrian.

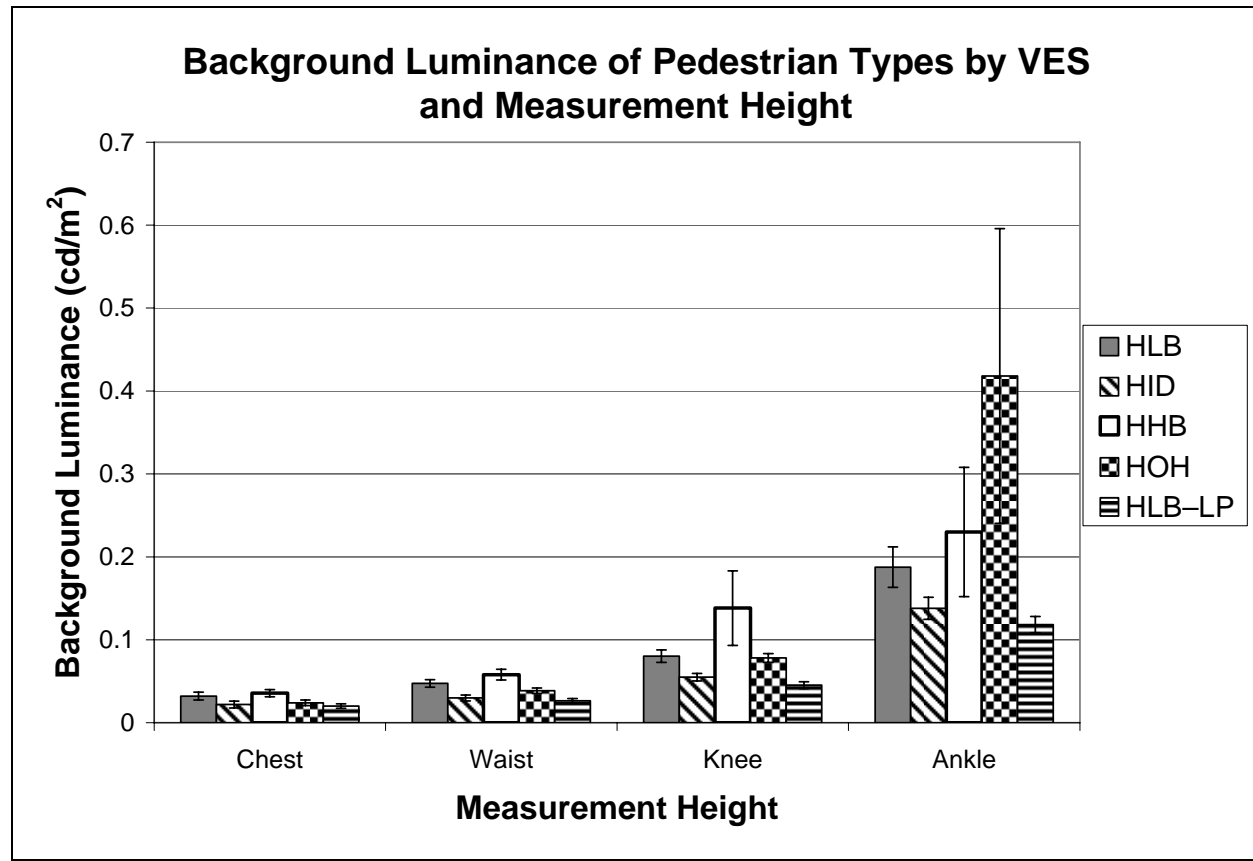


Figure 34. Bar graph. Influence of VES on background luminance by measurement height.

To investigate this further, the interaction of the measurement height and the object position is shown in figure 35. The parallel pedestrian shows a higher background luminance for the ankle measurement than all of the other measurement heights. This is particularly pronounced for the HOH and the HHB measurements. Here again, the background for the parallel pedestrian may have included the pavement marking, whereas the perpendicular pedestrian and the cyclist locations included only the pavement surface itself.

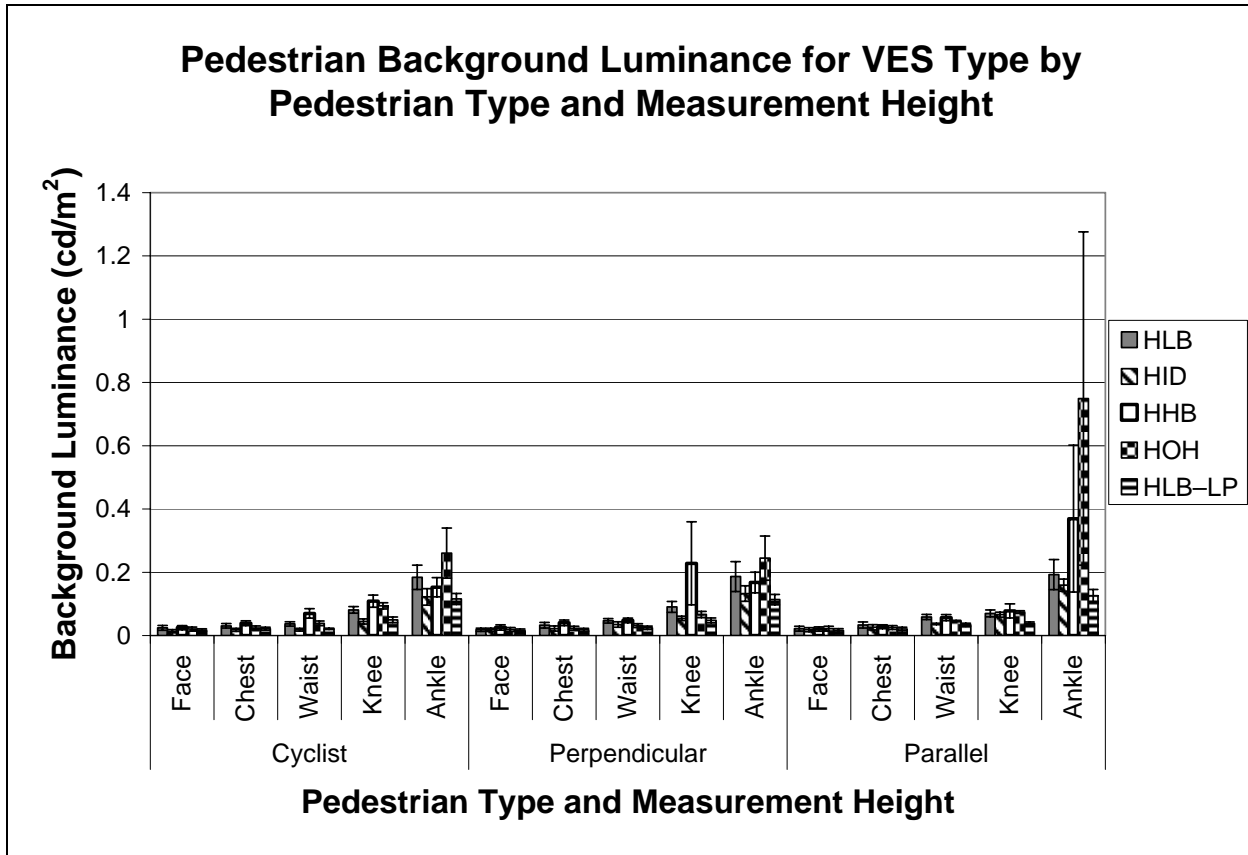


Figure 35. Bar graph. Influence of VES on background luminance by pedestrian type and measurement height.

The influence of the measurement distance on the background luminance for the pedestrian objects is shown in figure 36. Here the high measurements of the HOH and HHB VESs are significantly higher than the other VESs for the 61.4-m (200-ft) measurement. For the 91.5-m (300-ft), 152.5-m (500-ft), and 244-m (800-ft) measurements, the influence of the VES was not significant. An example inverse square relationship has been added to this figure also. Because the illuminance from the headlamps followed the inverse square relationship, it would be expected that the background luminance would have followed the same relationship; however, from the figure, this does not seem to be the case because there was no significant difference between the measurements at 61.0 m (200 ft) and 91.5 m (300 ft) for the HLB, HID, and HLB-LP VES types, and for all of the VESs, there was no significant difference between the 152.5-m (500-ft) and 244-m (800-ft) measurement distances. The background luminance seems to have reached a minimum ambient luminance at these distances, and the inverse square law did not apply.

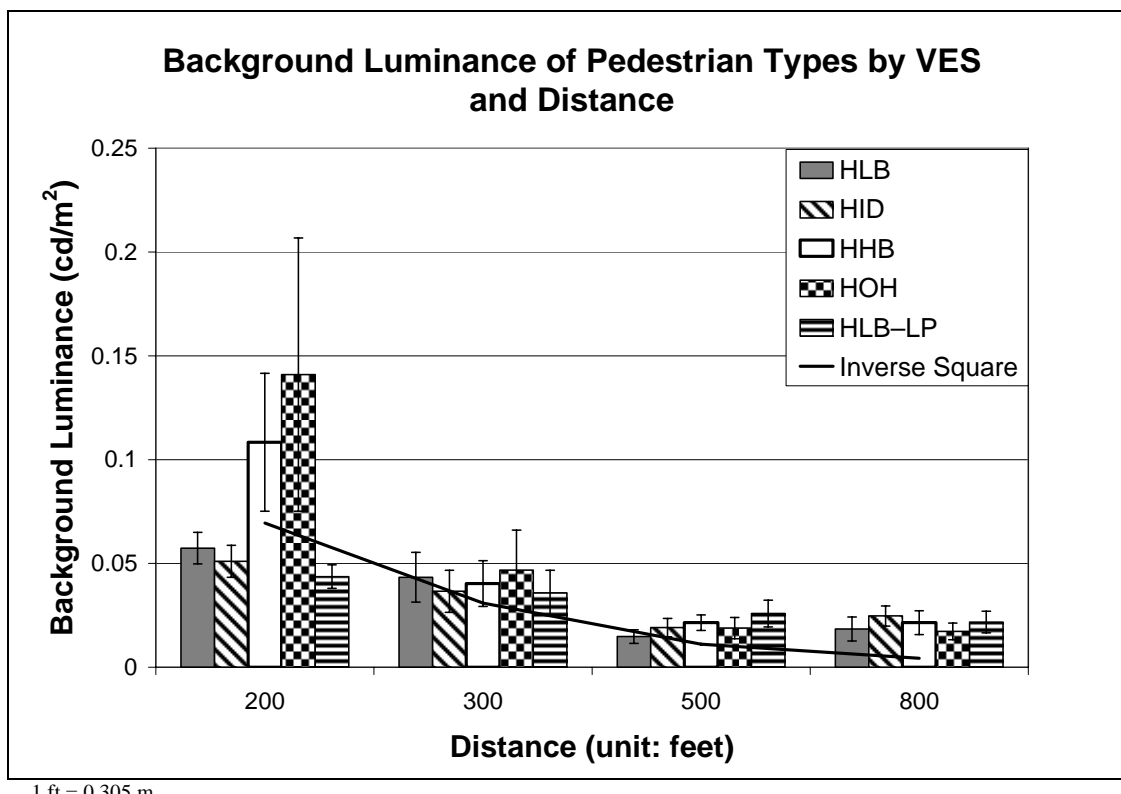


Figure 36. Bar graph. Influence of VES on background luminance by measurement distance.

The influence of the object station on the background luminance is shown in figure 37. For most VESs, there were no significant differences among the stations; however, the HOH measurement did show a higher result at station 4, which again probably was a result of the pavement marking influencing the measurement. The HOH measurement was made from the pickup truck vehicle that was used for this VES and represents the highest observation location with one of the shorter observation distances, which may have allowed the pavement marking to play a more significant role in the measurement with this VES than the other VESs.

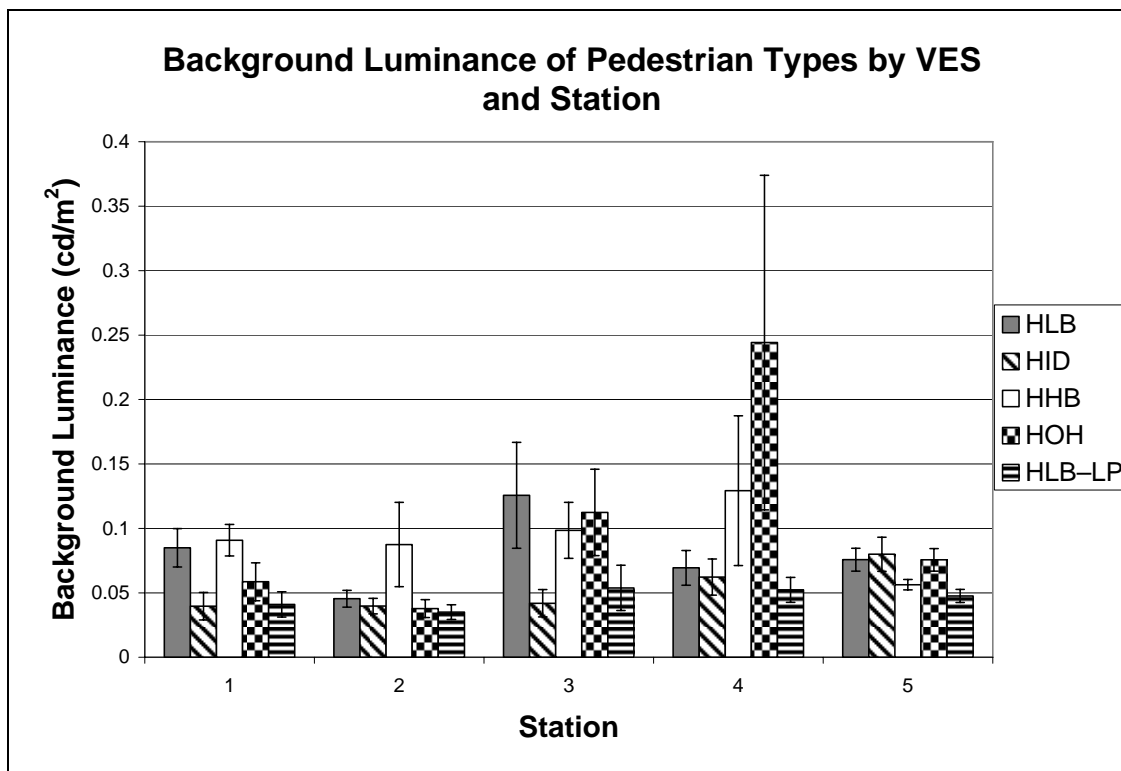
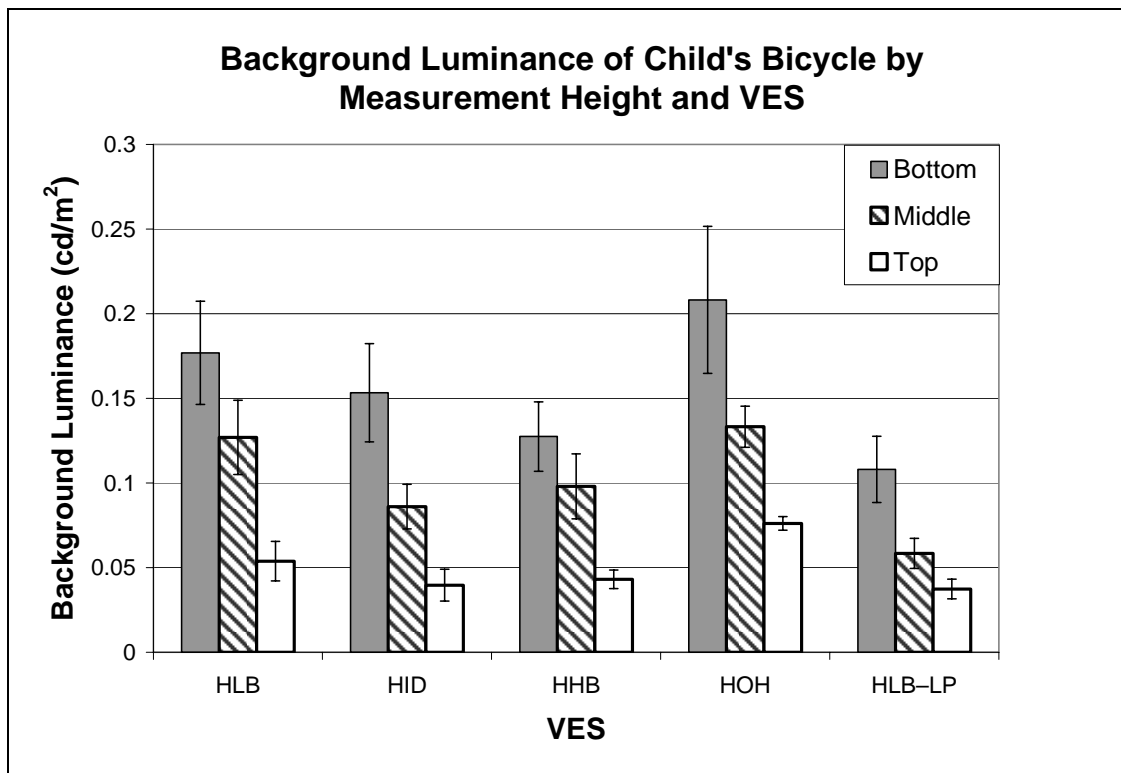


Figure 37. Bar graph. Influence of station on background luminance for pedestrians by VES.

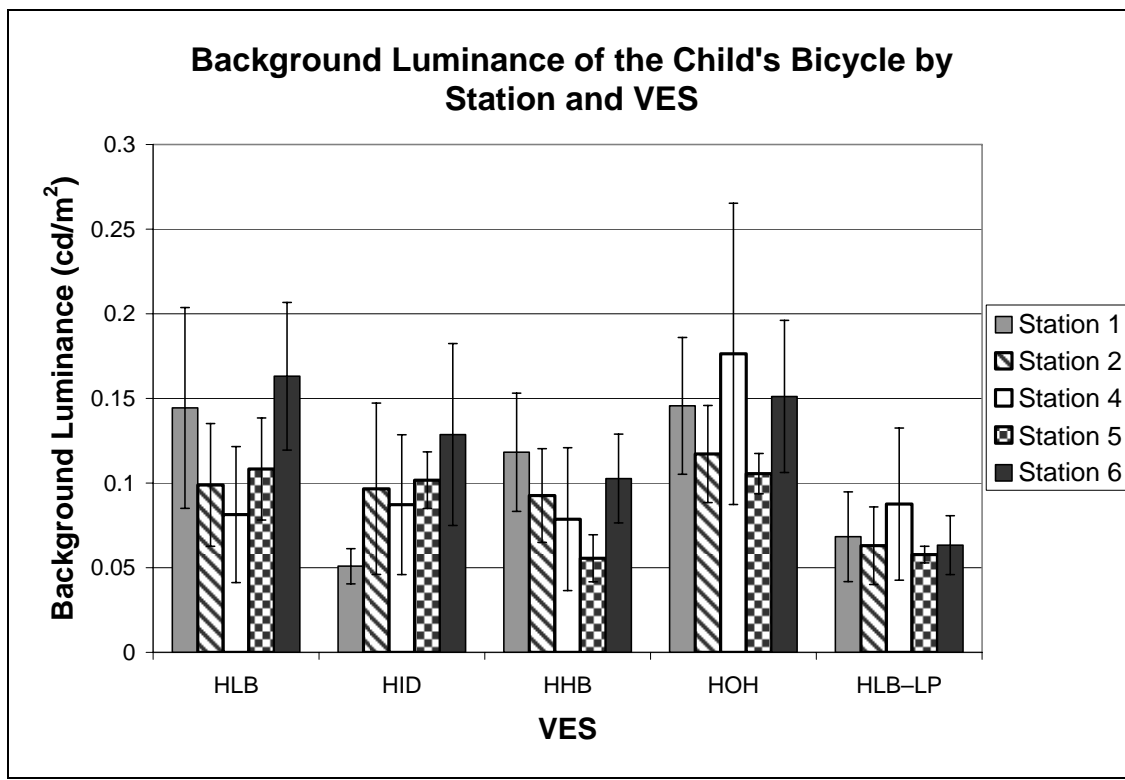
Child's Bicycle

For the child's bicycle, the background luminance was considered two ways. The first was the influence of the measurement height, and the second was the influence of the object station. Figure 38 shows the influence of the measurement height on the background luminance for this object. For this relationship, the primarily pavement background behind the bicycle's bottom-measurement height had the greatest luminance, with the middle- and the top-measurement heights showing a lower luminance. This trend was the same for all VESs, with the HOH being the highest, followed in order by the HLB, HID, HHB, and HLB-LP. In terms of significant differences among the VESs, some of these may be grouped as having differences; however, there were no meaningful differences among all of the VESs. The background luminance of the child's bicycle is shown in figure 39 for each of the object stations. It should be noted that the child's bicycle never appeared at station 3. Neither the VES nor the station had an influence on the background luminance for this object.



All measurements taken from a distance of 61.0 m (200 ft).

Figure 38. Bar graph. Influence of measurement height on background luminance of child's bicycle by VES.

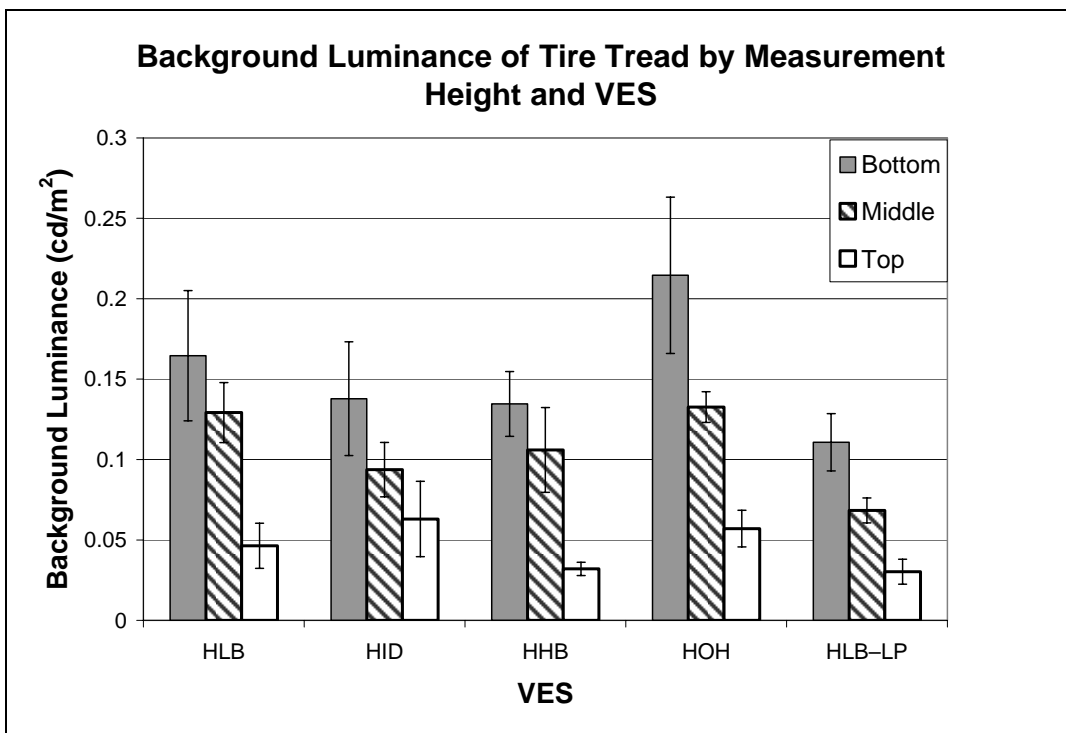


All measurements taken from a distance of 61.0 m (200 ft).

Figure 39. Bar graph. Influence of station on background luminance for the child's bicycle by VES.

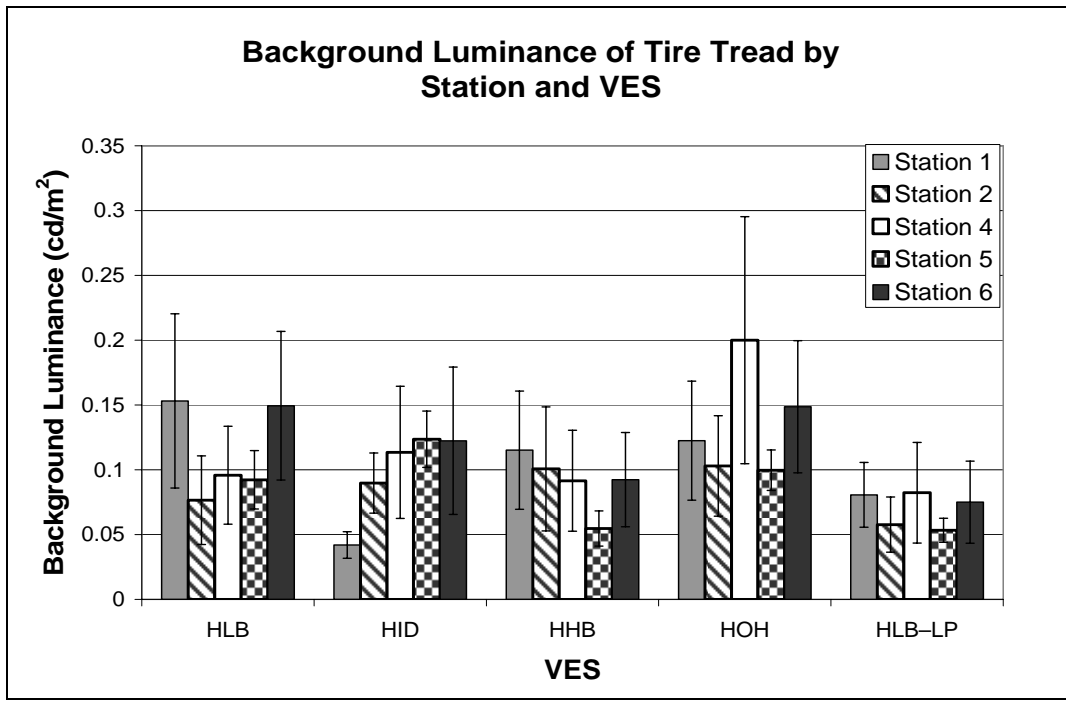
Tire Tread

As with the child's bicycle, the tire tread's background luminance was analyzed first by measurement height and then by object station; the tire tread did not appear at station 3. The tire tread showed the same trends in all of the relationships shown. The influence of the measurement height is shown in figure 40. Just below the object, or the bottom-measurement height, had the highest measured luminance, followed by the middle- and the top-measurement heights. Similarly, the HOH had the highest result, followed in order by the HLB, HID, HHB, and the HLB-LP. The relationship for the background luminance and the object station is shown in figure 41. Here again, neither the VES nor the station influenced the background luminance results.



All measurements taken from a distance of 61.0 m (200 ft).

Figure 40. Bar graph. Influence of measurement height on background luminance for the tire tread by VES.



All measurements taken from a distance of 61.0 m (200 ft).

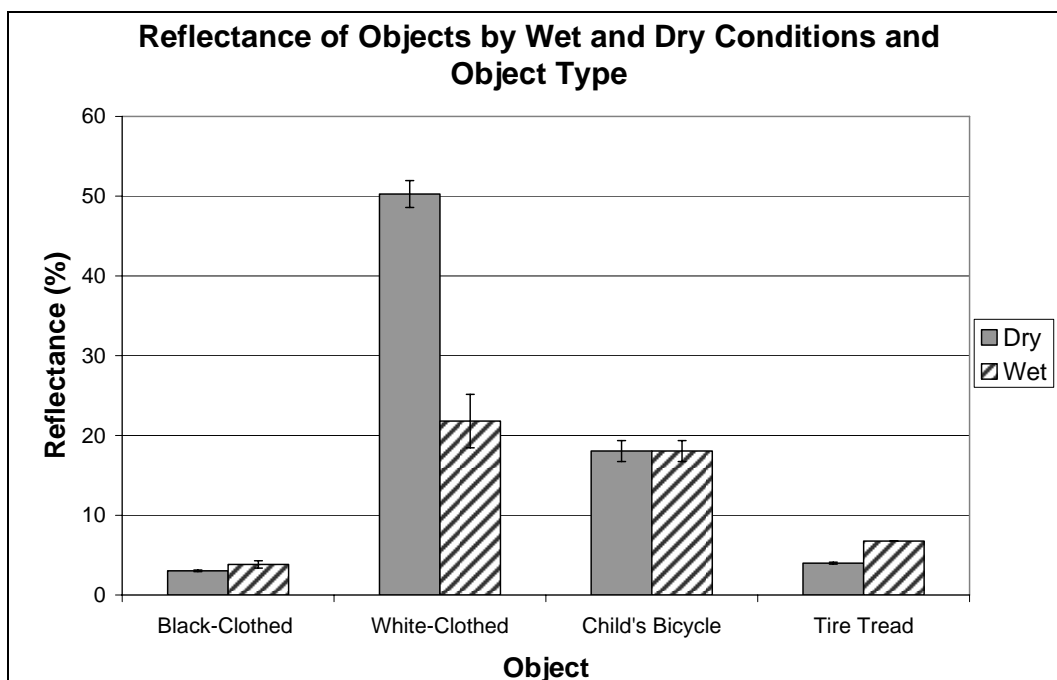
Figure 41. Bar graph. Influence of station on background luminance for the tire tread by VES.

OBJECT REFLECTANCE

The reflectance was calculated for all of the objects used in the experimental conditions. The calculation was performed only for VES conditions with no UV–A contribution. In the case of the human objects, all black-clothed and white-clothed objects were grouped, and the reflectance values calculated for these conditions were averaged. These calculations were performed for the objects when they were dry, as they were in the clear and fog conditions, as well as wet, as they were in the rain and snow conditions. White clothing became significantly less reflective under the wet condition, while the black clothing became slightly more reflective. The tire tread object developed specular reflective attributes, as evidenced by an increase in its reflectivity for the wet condition. The reflectance of all the objects is summarized in table 7. Figure 42 also shows these values.

Table 7. Object reflectance summary.

Object	Dry	Wet
Black Clothing	3.02	3.83
Tire Tread	4.00	6.76
Child's Bicycle	18.00	18.00
White Clothing	50.30	21.80



All measurements taken from a distance of 61.0 m (200 ft).

Figure 42. Bar graph. Reflectance of all objects both dry and wet.

The other reflective characteristic for the cyclists were the bicycles themselves. The black-clothed cyclist rode a bicycle of a dark color, which was a mix of burgundy and black, but the wheel rims were chrome. The white-clothed cyclist rode a bicycle painted with a fluorescent orange paint, and the wheel rims were painted black. For these objects, the specular (non-Lambertian) reflection was measured. These results are presented in figure 43 for the dry conditions. As this figure indicates, the bicycle associated with the black-clothed cyclist had a much higher reflectance than that associated with the white-clothed cyclist. As discussed under object luminance, this might indicate that the bicycle used by the dark-clothed cyclist was more visible than the cyclist for this object presentation.

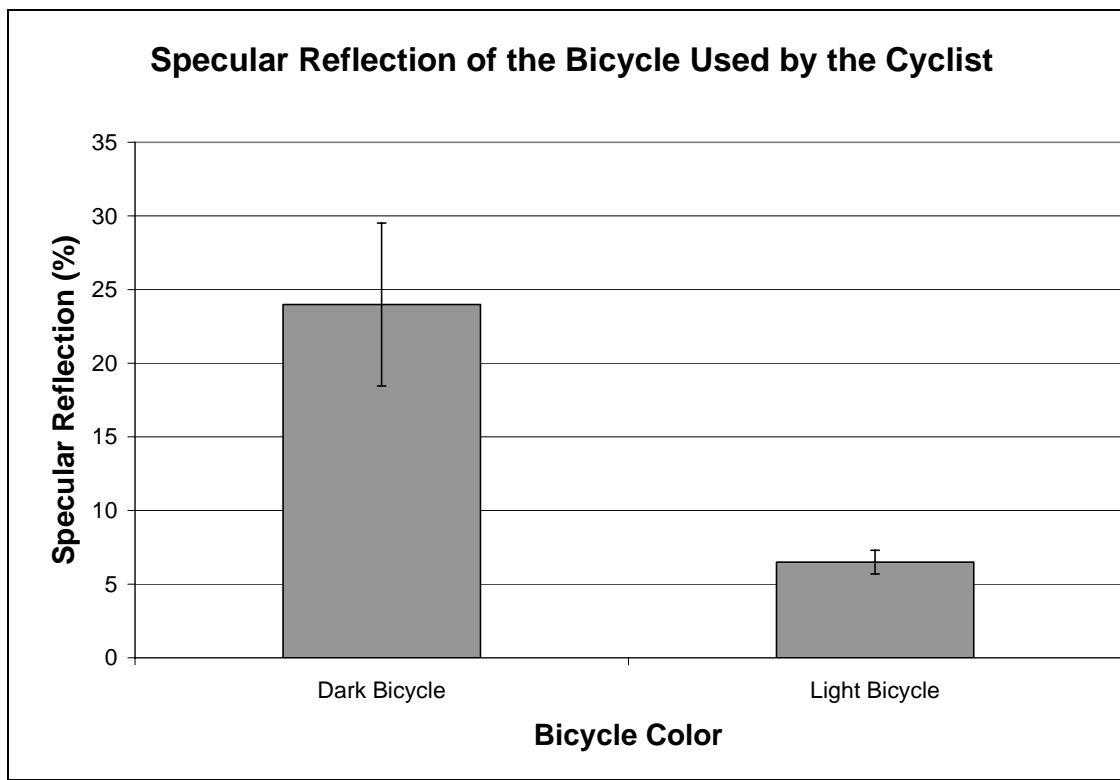


Figure 43. Bar graph. Specular reflection of all bicycle objects for both black-clothed and white-clothed cyclist.

OBJECT FLUORESCENCE

The object fluorescence was calculated for all VES configurations that included UV-A radiation, using the equation in figure 11. These included hybrid UV-A + HLB, three UV-A + HLB, five UV-A + HLB, hybrid UV-A + HID, three UV-A + HID, and five UV-A + HID. As a comparison, the base conditions of HID and HLB were used as the nonfluorescent comparison conditions. The means of the results are plotted for black-clothed and the white-clothed objects in figure 44 by their position on the roadway and in figure 45 by the VES type. Both figures indicate that the black-clothed objects showed no significant fluorescent behavior; however, the white-clothed objects showed fluorescence that increased with the higher levels of UV-A, as seen in figure 45.

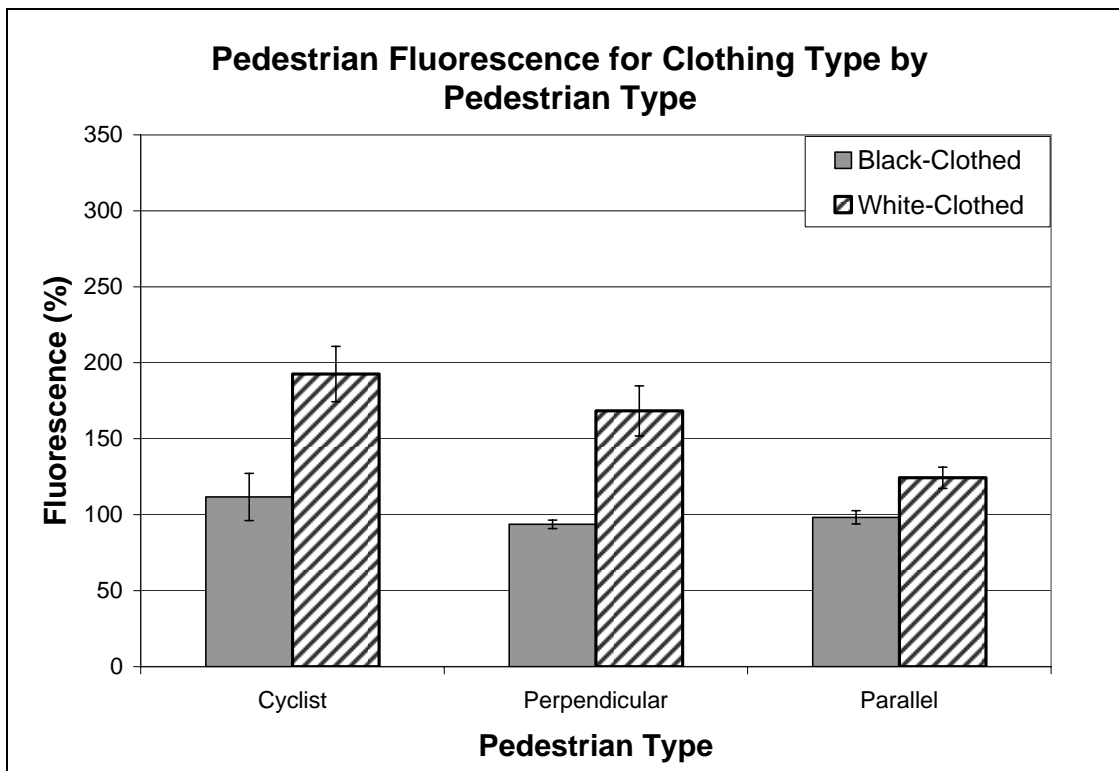


Figure 44. Bar graph. Fluorescence for the black-clothed and white-clothed pedestrians by roadway position.

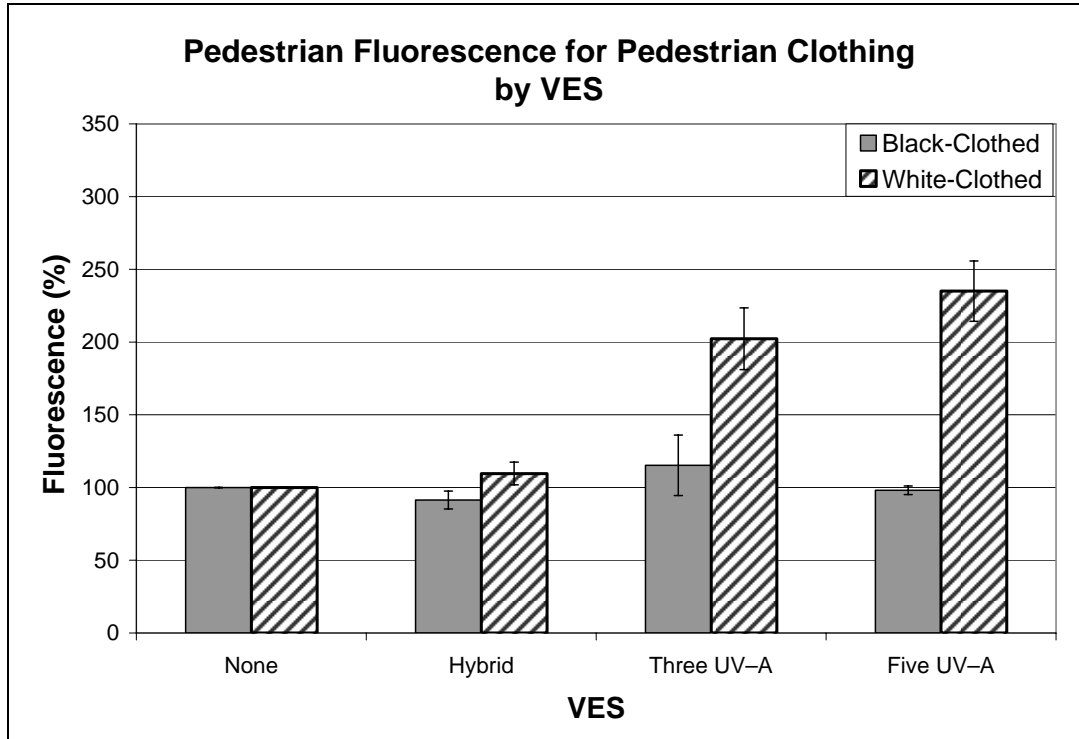


Figure 45. Bar graph. Fluorescence for the black-clothed and white-clothed objects by VES type.

The fluorescence level also varied by the position on the roadway. The parallel pedestrian object showed a significant difference from the perpendicular pedestrian object and the cyclist object. This is to be expected because the UV-A systems are aimed toward the direction of travel of the vehicle, and therefore, they do not provide as high an irradiance level on objects located on the side of the road as they do on objects in the middle of the roadway. Figure 46 shows the interaction of the VES type and the object position for the white-clothed objects only. In this figure, the effect of increasing the UV-A content, such as adding two more UV-A sources to the three UV-A configuration, was smaller than expected. Similarly, the performance of the hybrid source was not significantly different than having no UV-A contribution at all.

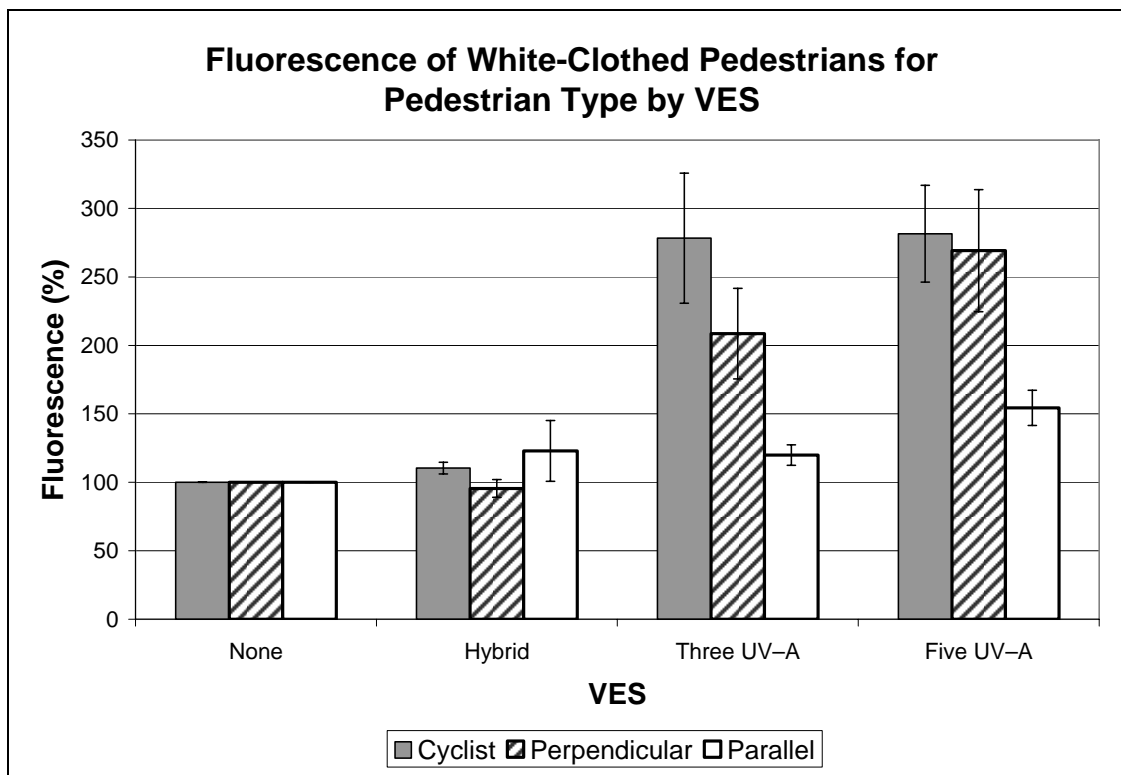


Figure 46. Bar graph. Fluorescence for the white-clothed objects by VES type and position on the roadway.

Because the child's bicycle was painted with fluorescent paint, that object's fluorescence could also be calculated; the results of this calculation are shown in figure 47 by VES type. This figure shows the response of the paint to the increasing levels of UV-A, with each level being significantly different than all of the other levels. The child's bicycle was placed at the side of the roadway in a similar location to that of the parallel pedestrian, but it showed a more consistent increase than the pedestrian. This response is likely due to the paint used on the child's bicycle, which was a fluorescent paint that would have had a linear response to the UV-A contribution of the VES as compared to the clothing.

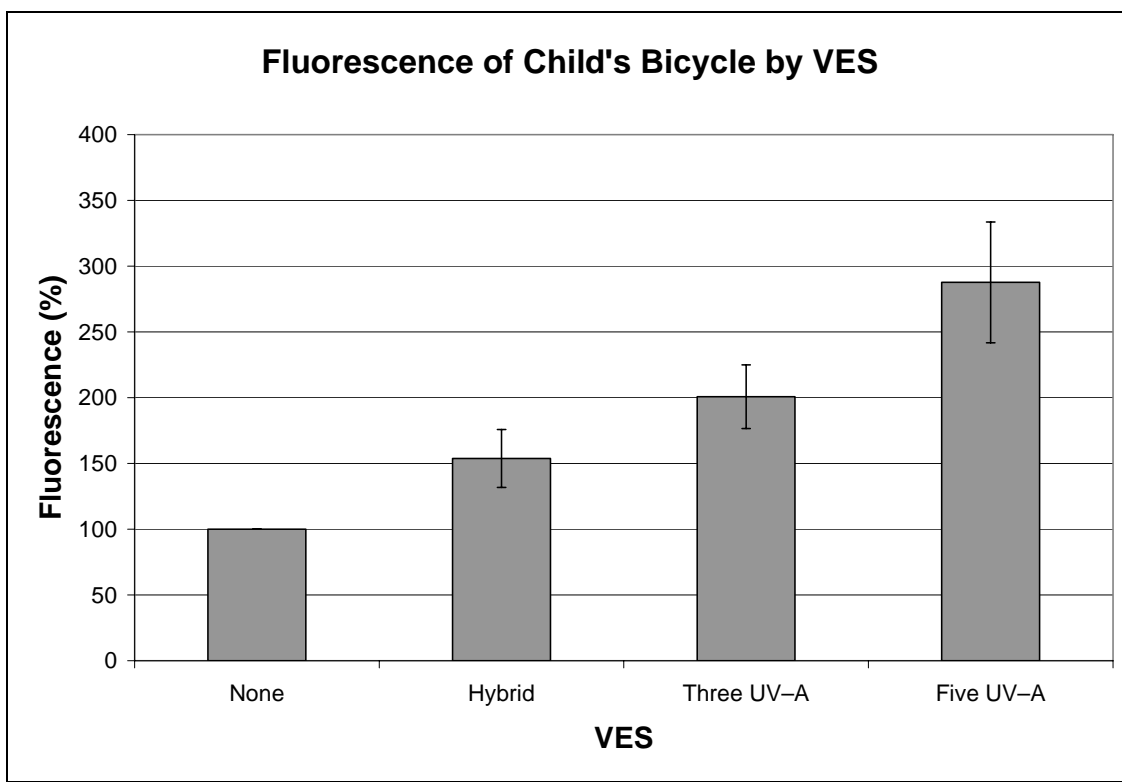


Figure 47. Bar graph. Fluorescence of the child's bicycle by VES type.

The tire tread was not considered in this analysis because it was black rubber and, much like the black-clothed pedestrian, it would not fluoresce.

LUMINANCE DIFFERENCE

The difference in the luminance between each object and its background (ΔL) was calculated for all of the objects at all of the measured distances. The luminance difference was calculated by

subtracting the background luminance from the object luminance (this is the same value as ΔL_{Actual} , used in the calculation of VL). Thus, ΔL can be positive or negative, depending on if the background luminance is the lesser or greater of the two values. Contrast, which is defined as the ratio of the luminance difference to the background luminance, will be considered later. Note that a positive ΔL indicates positive contrast, while a negative ΔL indicates a negative contrast between the object and its background.

The change in the object luminance as a result of the change in the measurement distance for the white-clothed objects was applied to the black-clothed objects to calculate the change in their luminance because the influence of distance was not measured for the black-clothed objects. Similarly, the effect of the measurement distance on the background measurements for the white-clothed objects was used for the black-clothed pedestrians to establish their background luminance. For these background calculations, there was no effect of the UV-A system applied to the calculation.

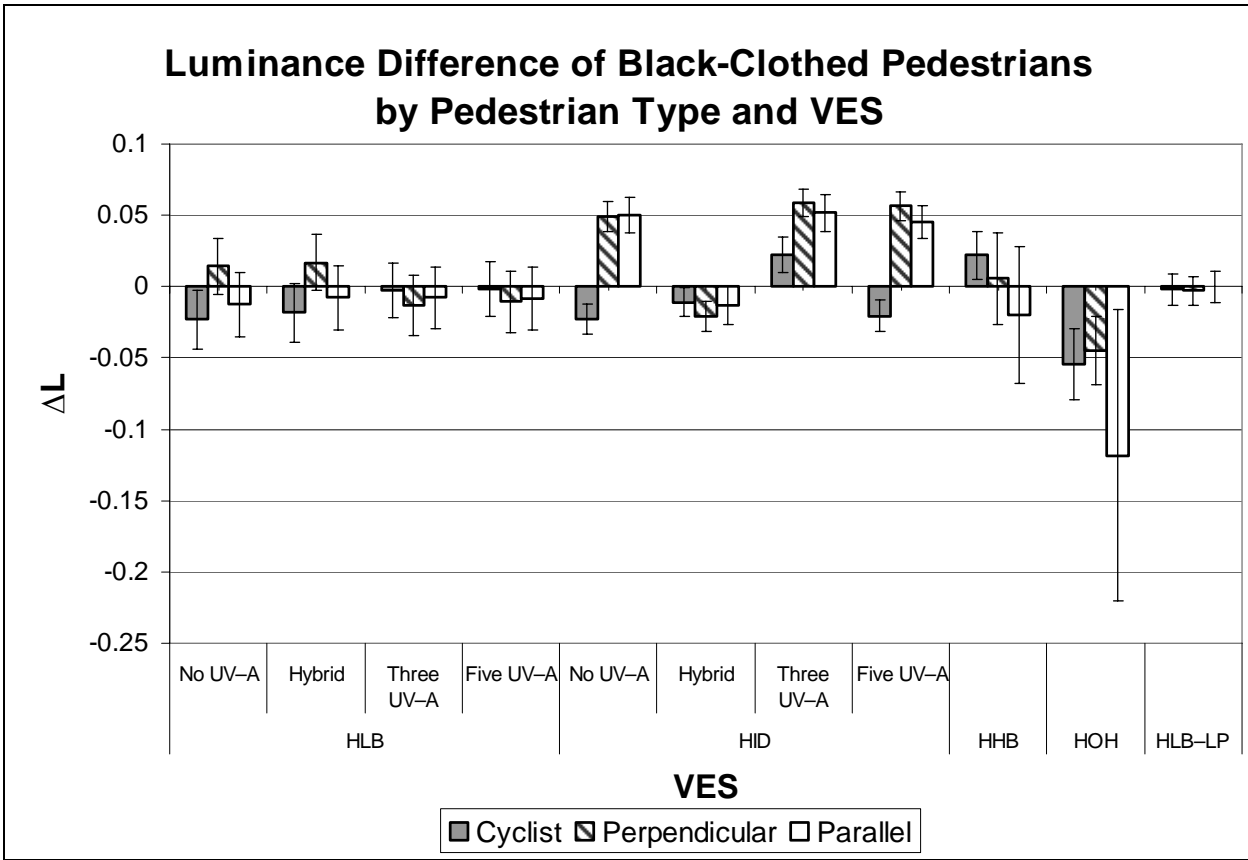
As in the object luminance analysis, the ΔL analysis first considered the pedestrian and cyclist objects and then the child's bicycle and the tire tread.

Pedestrian and Cyclist Objects

Based on the differences between object luminance of the white-clothed and the black-clothed objects, ΔL also should have been significantly different. For this reason, the two clothing colors were investigated individually.

Black-Clothed Objects

The first relationship considered in this analysis was the influence of object position on ΔL , which is shown in figure 48. In general, the position had very little effect on ΔL . There were some transitions from positive to negative values for the headlamps that incorporated HID. In these transitions, the cyclist had a negative ΔL , whereas the parallel and perpendicular pedestrians had positive values of ΔL . The other major transition was that of the HOH VES. With that VES, all of the objects had negative values of ΔL because the VES provided a high background luminance and a low object luminance.



All measurements taken from a distance of 61.0 m (200 ft).

Figure 48. Bar graph. Luminance difference by VES for black-clothed pedestrians by object position.

The next relationship is the change in ΔL with the measurement height. Shown in figure 49, the consistent relationship shown is the negative values for ΔL measured at the ankle height of the object; however, this resulted from the appearance of the object against the immediate background, which in this case was the road surface. It is to be expected that the luminance difference at this level would have been negative, with the black object against the gray pavement. For the measurement height and VES combinations, few significant changes were shown by the calculations.

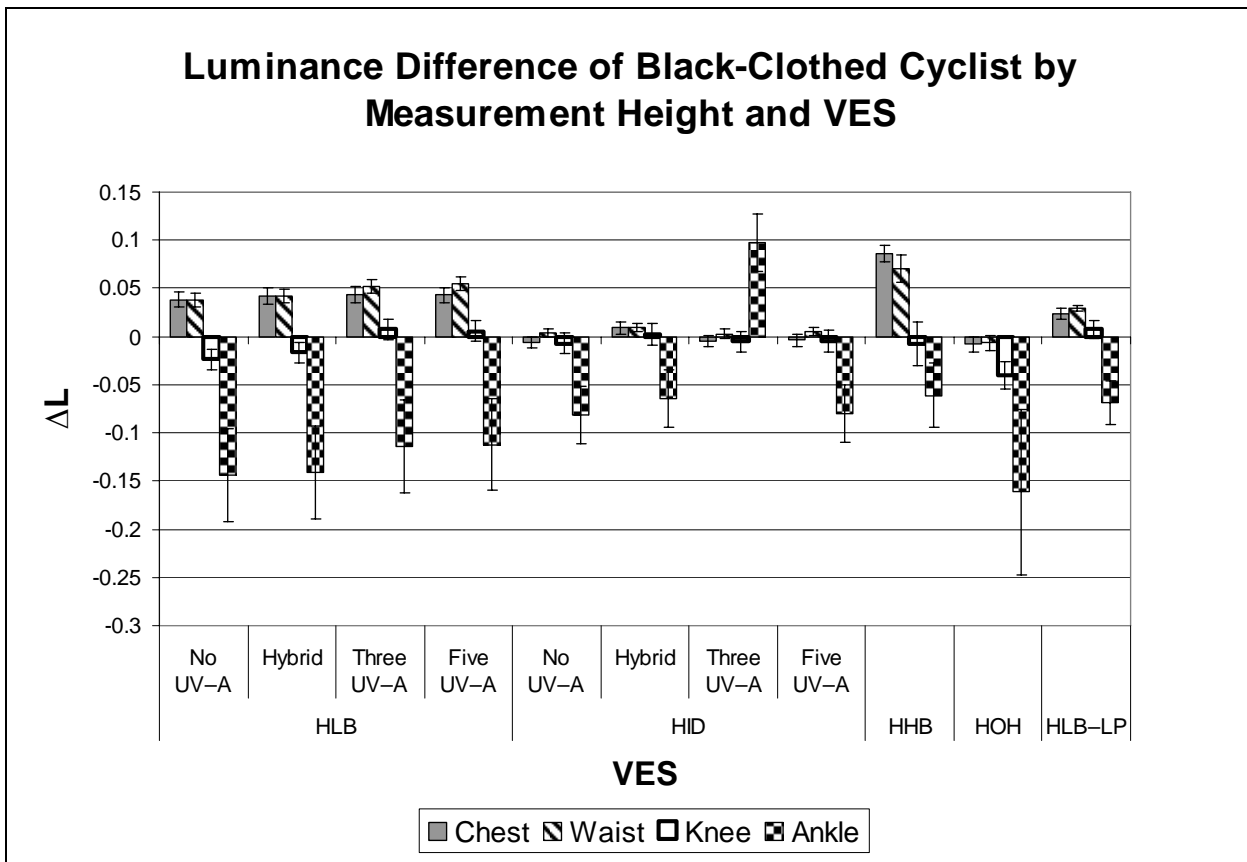


Figure 49. Bar graph. Luminance difference by VES for black-cladpedestrians by measurement height

The final aspect of the black-clothed pedestrian object is the effect of distance on ΔL . This relationship is shown in figure 50. Because the UV-A did not affect the black-clothed object, this relationship is shown for the visible-light-based VESs only. The important issue in this relationship is the apparent lessening of ΔL as the vehicle approached the object. From farther away, the object would have appeared dark against the light pavement, thus providing a negative contrast situation. As the vehicle approached, more light was cast on the front vertical side of the object, and the object luminance increased, thereby reducing the luminance difference. However, as the vehicle approached the object, the visual size got bigger, reducing the threshold difference and possibly offsetting the effect on visibility due to the reduction of the difference in luminance. For the HID-based VESs and HHB, ΔL actually changed from negative to positive as the vehicle approached, which means that the object would have gone through a transitional point where it had zero luminance difference and would have been invisible at that distance.

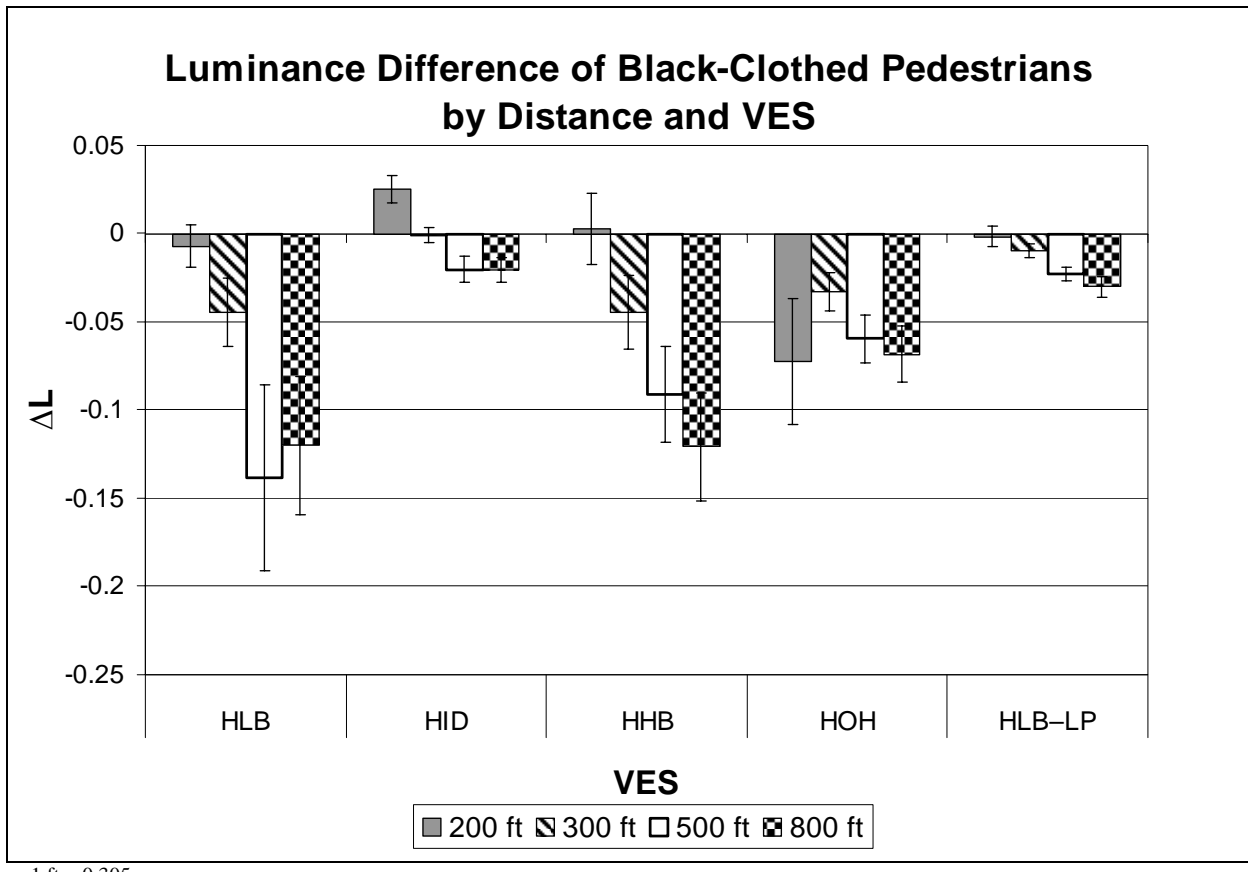


Figure 50. Bar graph. Luminance difference by VES for black-clothed pedestrians by measurement distance.

White-Clothed Objects

The luminance difference for the white-clothed objects was evaluated in the same manner as for the black-clothed objects. The first relationship considered is shown in figure 51. In this relationship, the luminance of the white-clothed object was so dominant as compared to the background at 61.0 m (200 ft) that ΔL was driven by object luminance value. This would also have applied to the values of ΔL by measurement height relationship, so it is not shown here.

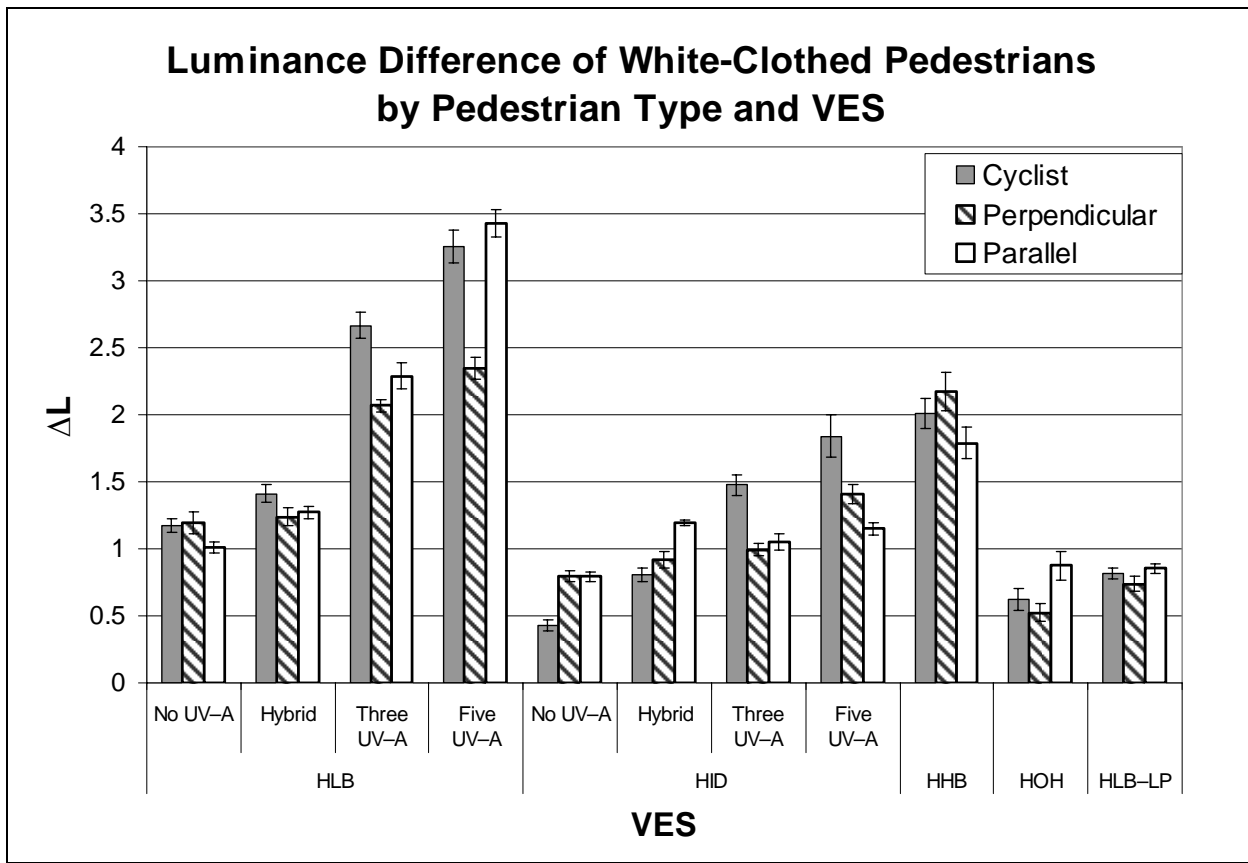


Figure 51. Bar graph. Luminance difference by VES for white-clothed pedestrians by object position.

The other relationship of interest is the change in ΔL with distance, which is shown in figure 52. Like the other relationships, ΔL was dominated by the object luminance; however, at greater distance, the object luminance fell closer to the background luminance, reducing the magnitude of ΔL . For the HLB, hybrid UV-A + HLB, HHB, and the HOH lamps, ΔL transitioned to negative values, which caused the same through-zero transition mentioned for the black-clothed object. It is noteworthy that ΔL for the HID-based systems did not fall as much as for the other VESs. It is not clear if this resulted from the headlamp cutoff or the strength of the HID light source.

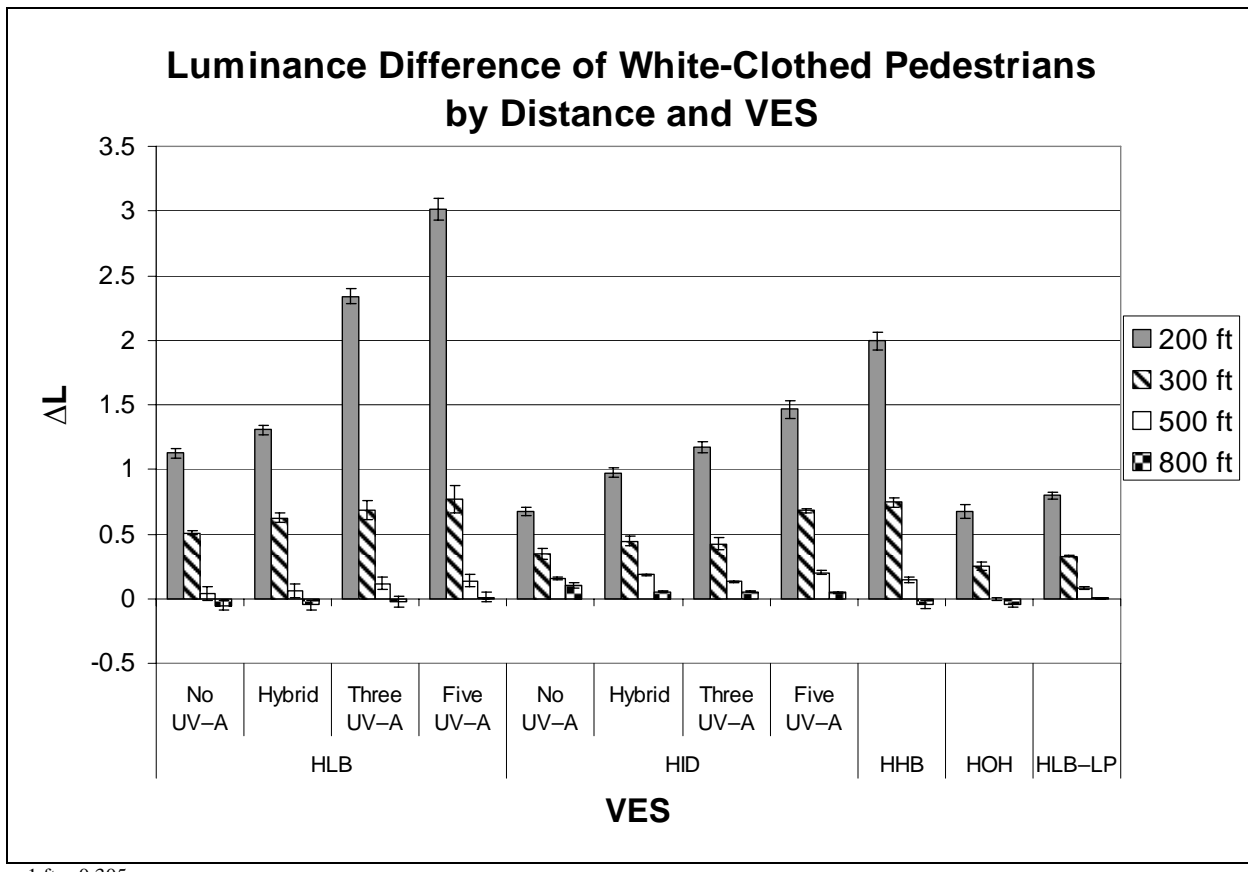


Figure 52. Bar graph. Luminance difference by VES for white-clothed pedestrians by measurement distance.

Child's Bicycle

As with the white-clothed object, ΔL for the child's bicycle was primarily dependent on the object luminance, as seen in figure 53. In this case, the background luminance from each of the VESs did not show a dramatic difference. This lack of change resulted in ΔL of the bicycle following that of the object luminance. All of the ΔL values for the VESs were positive, with the HLB- and HID-based VESs providing the highest values of ΔL and the HLB-LP providing the lowest values.

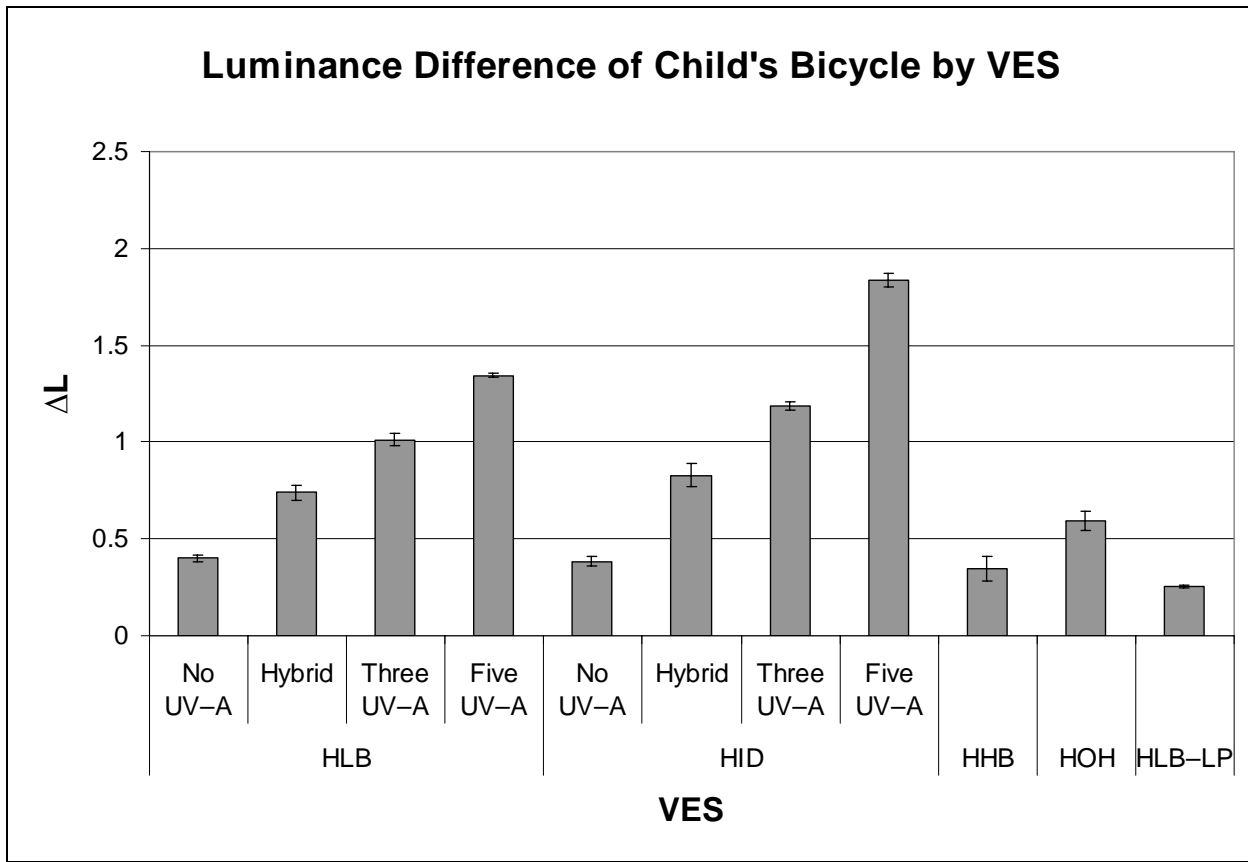


Figure 53. Bar graph. Luminance difference by VES for the child's bicycle.

Tire Tread

The ΔL of the tire tread is shown in figure 54. In this relationship, the tire tread appeared with both positive and negative values for ΔL based on the performance of the VES. The HLB had the highest negative ΔL , with the HHB providing the highest positive ΔL .

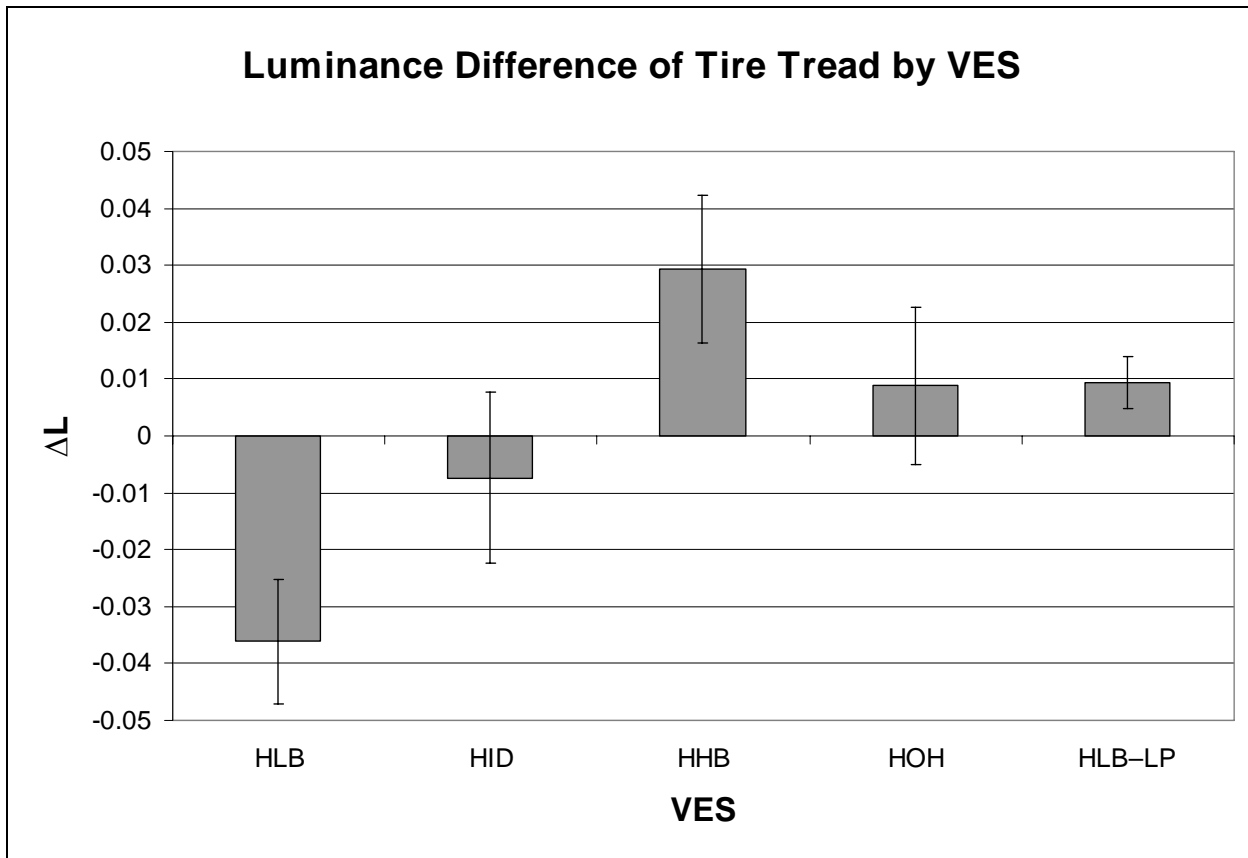


Figure 54. Bar graph. Luminance difference by VES for the tire tread.

VISIBILITY LEVEL

As mentioned, the visibility level (VL) metric considers all of the measurements already mentioned; however, the VL is also dependent on the age of the participant. For this analysis, the age of the observer was considered for a young (23-year-old) observer, a middle-aged (45-year-old) observer, and an older (70-year-old) observer. The VL was analyzed in the same manner as the other measurements; the pedestrians were considered first, followed by the child's bicycle and then the tire tread.

Pedestrian and Cyclist Objects

The mean VL for the pedestrian and cyclist objects are shown in figure 55. All of these measurements were taken at the 61.4-m (200-ft) measurement distance. The VL trend followed that of the object luminance. The addition of the UV-A increased the VL, with the effect on the halogen-based VESs being higher than that on the HID-based VESs. The resulting VL for the HHB was lower than that of the five UV-A + HLB, and it was not significantly different than the five UV-A + HID. The HOH provided the lowest VL, with the HLB-LP performing on par with the HLB. The age of the observer reduced the VL by approximately one-third for each age group. That is to say, the middle-aged group had about two-thirds the VL of the younger group, and the older group had about one-third the VL of the younger group.

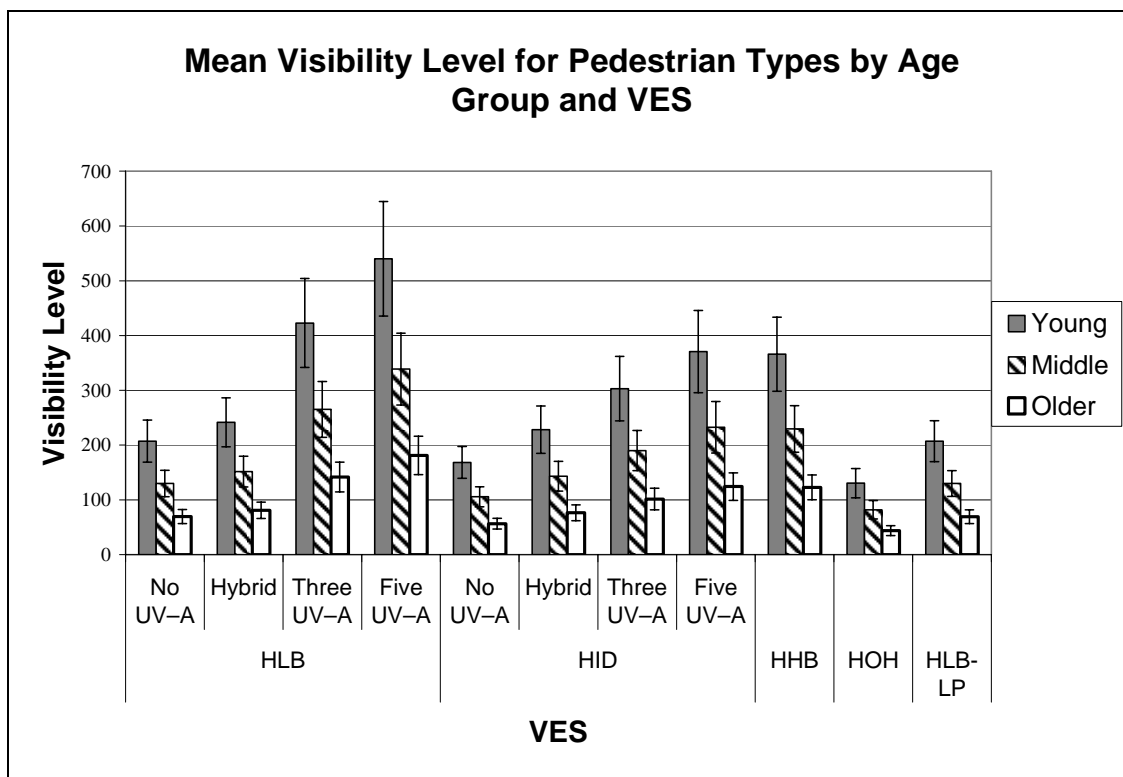


Figure 55. Bar graph. Visibility level by age and VES for the pedestrian objects.

The VL analysis then considered each of the pedestrian types individually. According to the Adrian model, the ratio with respect to age will be the same for all of the VESs considered, and so it was not included in the remaining VL analyses.⁽¹⁾

Black-Clothed Objects

For the black-clothed objects, the addition of the UV–A sources did not make a significant difference to the object luminance, so only the non-UV–A VESs were considered as part of this analysis. Figure 56 shows the VL by pedestrian type for all of the black-clothed objects. In this relationship, the parallel object showed the highest VL for HID, HHB, and the HLB–LP VESs, with the perpendicular object having lower values and the cyclist having the lowest values. For the HOH VES, there was no difference among the object locations, and for the HLB, there was no difference between the parallel and perpendicular objects, with the cyclist being slightly lower.

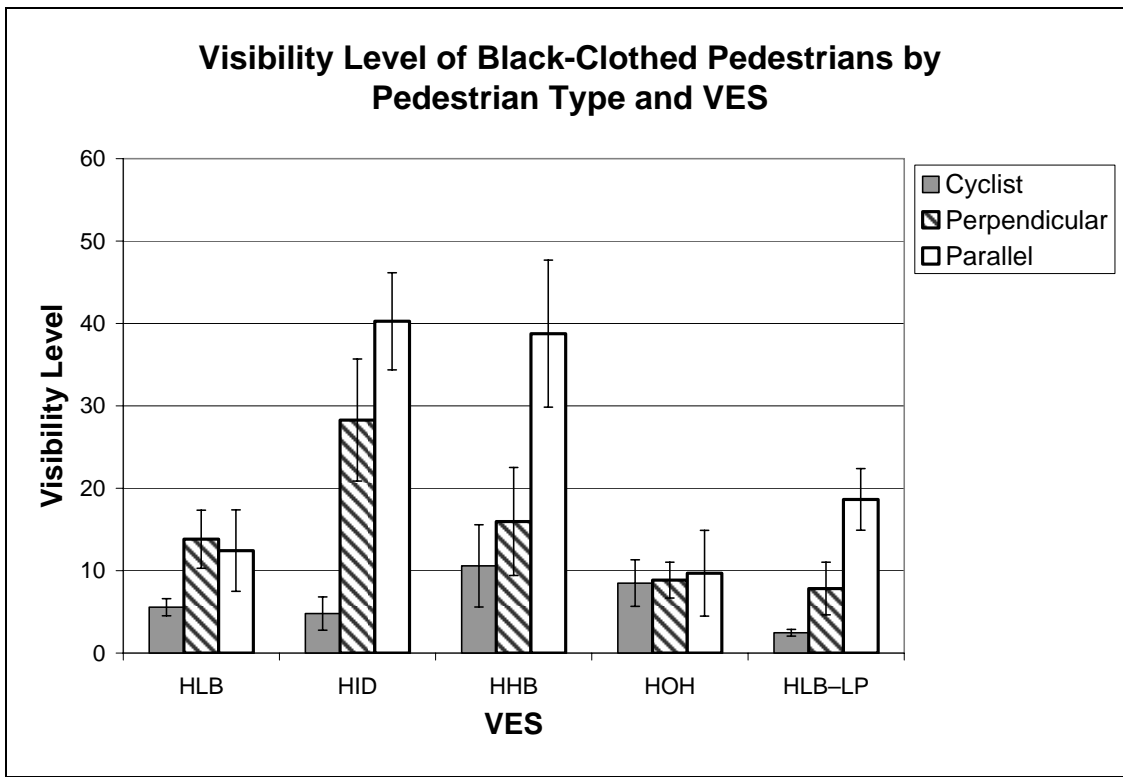


Figure 56. Bar graph. Visibility level by VES for the black-clothed pedestrian objects by position.

The effect of the distance on the VL is shown in figure 57. As the vehicle approached the object, the visual size of the pedestrian increased, so the object became easier to see. In terms of the VL, the increase in the size would have caused the VL to increase. This was seen in the HLB and the HLB-LP VESs, but the other VESs did not show the same trend. For the HID VES, the VL actually decreased for the 91.5-m (300-ft) and 152.5-m (500-ft) distances and then increased again at the 61.4-m (200-ft) distance. Compare these values to the contrast values shown in figure 50; there was a negative to positive transition of contrast with distance that impacted the calculated value of VL. This means that the object could be seen at 244 m (800 ft), then was more difficult to see at 152.5 m (500 ft) and 91.5 m (300 ft), and then was more easily seen at 61.0 m (200 ft). The HOH VES showed the opposite behavior, where the VL was higher at 91.5 m (300 ft) and 152.5 m (500 ft). The HHB VES performed in a much less predictable manner with a low point at 91.5 m (300 ft) and reached the highest point at 152.5 m (500 ft). This was not expected because the contrast for the same VES is a linear change with distance.

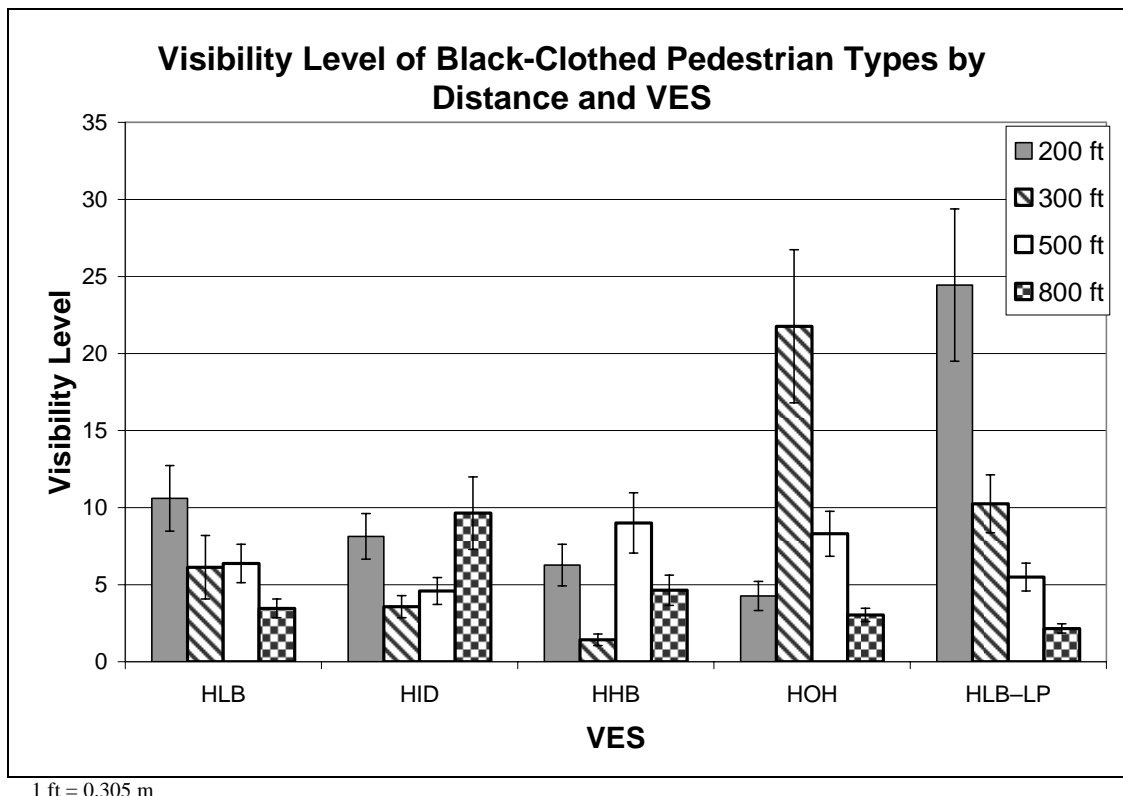
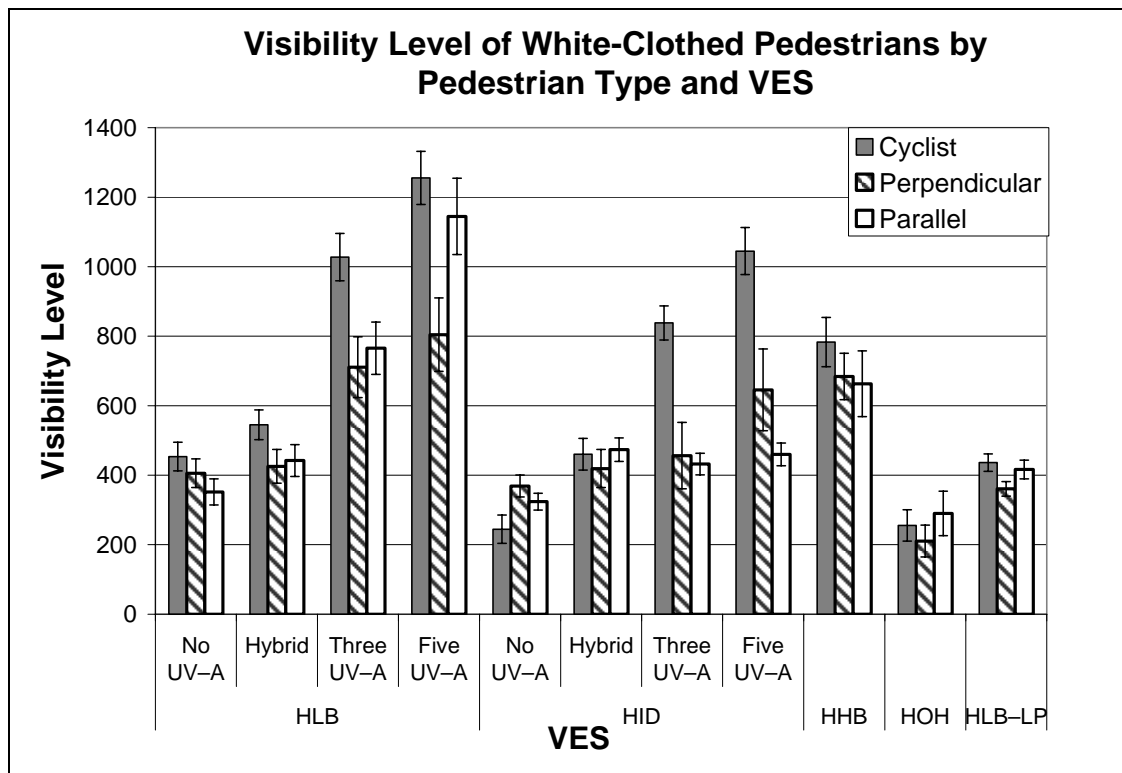


Figure 57. Bar graph. Visibility level by VES for the black-clothed pedestrian objects by distance.

White-Clothed Objects

The VL for the white-clothed objects followed the same path as the object luminance, with the influence of the UV–A contribution increasing the VL over the base condition as shown in figure 58. The change for the white-clothed objects as compared to the black-clothed objects was that the cyclist had a higher VL than the parallel and perpendicular pedestrians for almost all of the tested VESs. The other interesting result is that the VESs with a UV–A component were as high as or higher in VL than the HHB. The HOH continued to perform the worst, and the HLB and HLB–LP conditions performed the same. The other point is that in both conditions that included the hybrid UV–A headlamp, the gain in VL was just barely significant as compared to the contributions from the other UV–A sources.



All measurements taken from a distance of 61.0 m (200 ft).

Figure 58. Bar graph. Visibility level by VES for the white-clothed pedestrian objects by position.

For the influence of the distance, as shown in figure 59, all of the VESs performed in a similar manner, with the VL increasing as the distance decreased. This is to be expected when comparing the contrast results in figure 52. There is a constant rise in the contrast as the distance decreases with only a few negative to positive transitions at the 152.5-m (500-ft) to 244-m (800-ft) distance. This trend for contrast and the increase in the object size as the distance closes will result in an increase in the VL.

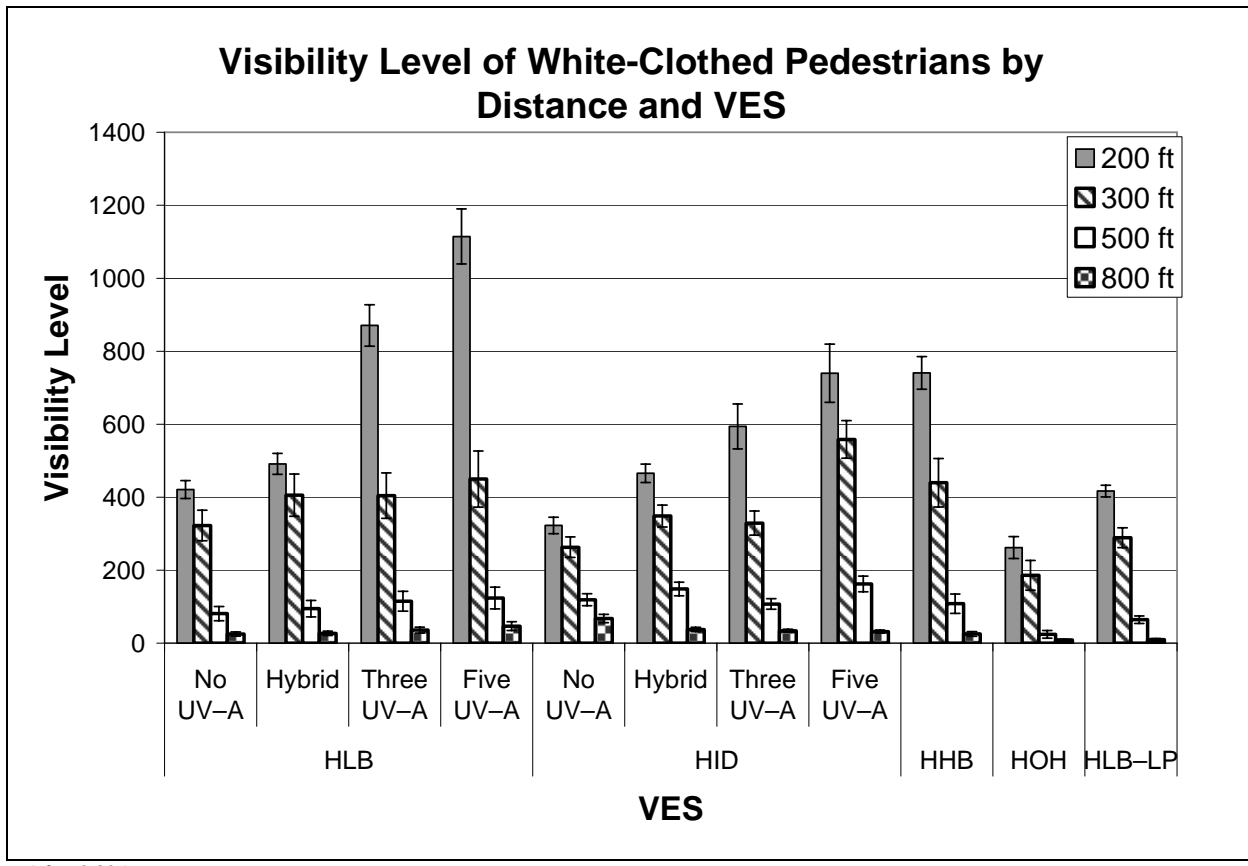
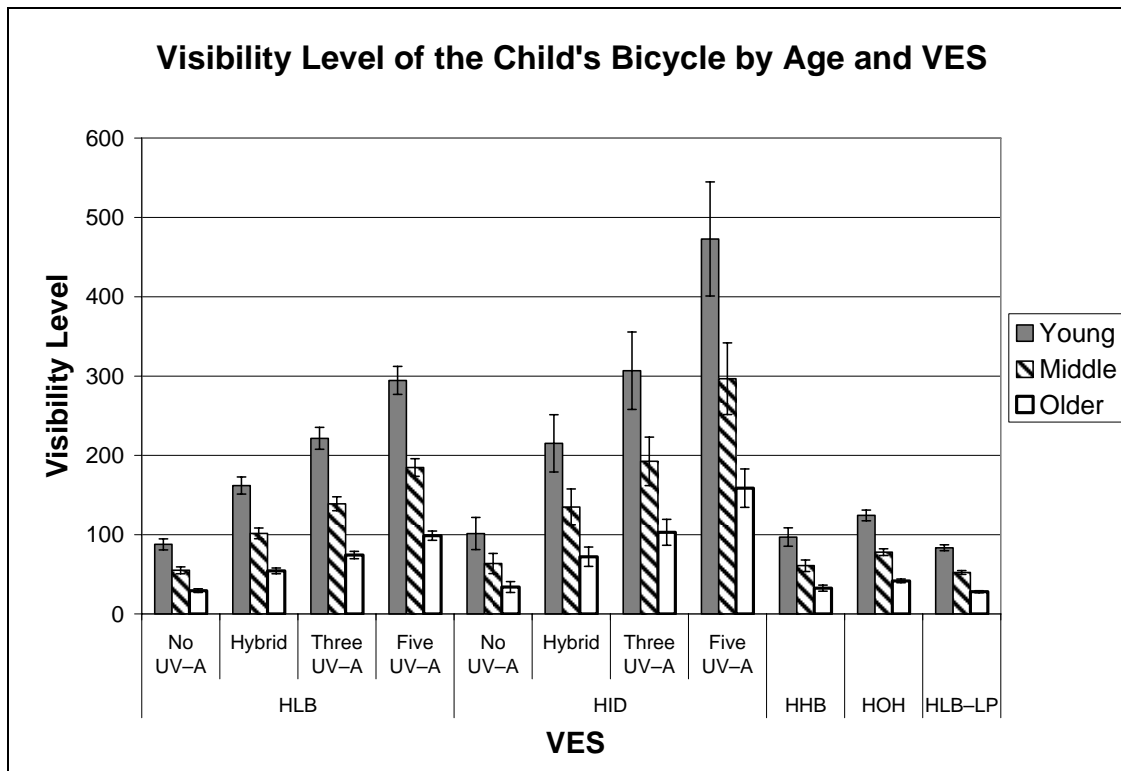


Figure 59. Bar graph. Visibility level for the white-clothed pedestrians by distance and VES.

Child's Bicycle

As with the white-clothed objects, the VL for the child's bicycle followed the object luminance (figure 60). The HID system with the sharp cutoff had the best performance, followed by the HLB-based systems. The HHB, HOH, HLB, and HLB-LP showed no significant differences between the VESs. The effect of age, about one-third for each age step, was the same as for the pedestrian objects.



All measurements taken from a distance of 61.0 m (200 ft).

Figure 60. Bar graph. Visibility level for the child's bicycle by age and VES.

Tire Tread

The VL for the tire tread at 61.0 m (200 ft) is shown in figure 61. The UV–A effect is not shown because the tire tread was not influenced by the UV–A. In this relationship, the HHB showed the highest VL, followed by the HOH and HID VESs, and then the HLB and HLB–LP configurations. Comparing these values to the contrast results shown in figure 54, the VL generally followed the contrast, with the highest contrast belonging to the HHB system. As with the other objects, the effect of age followed the same trend of one-third increase or decrease per age group.

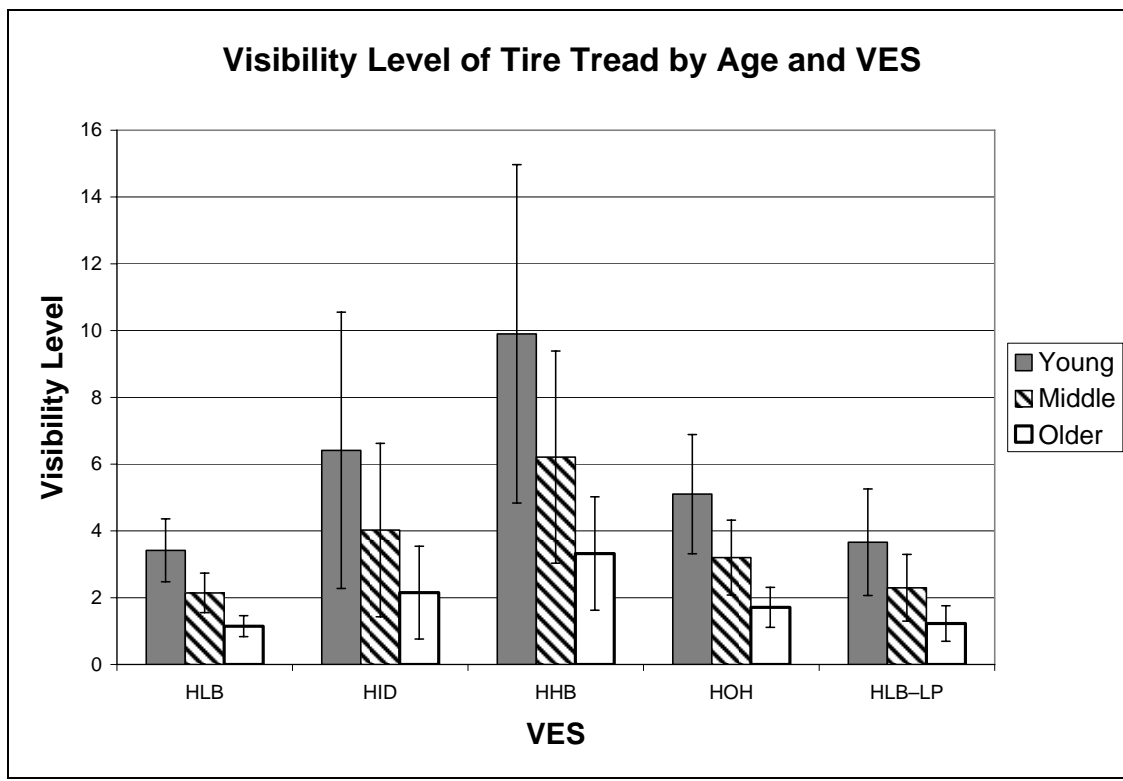


Figure 61. Bar graph. Visibility level for the tire tread by age and VES.

CHAPTER 4—DISCUSSION

The measurement results show several different analyses of photometric data obtained for all of the objects with all of the VESs. To relate these results to those of the ENV visual performance testing, the metrics calculated here must be related to the measured visibility distances from the ENV clear-condition study. To answer the research questions, the data for both the visual performance and the object characterization studies have been combined to provide an analysis of the most suitable photometric performance indicator or object detection and recognition and the threshold values obtained for the measurements. For details on the visual performance measurements, please refer to ENV Volume III, *Visual Performance During Nighttime Driving in Clear Weather*. Following is a list of the research questions posed for this investigation and a discussion of the findings.

What is the correlation between the photometric performance of the VESs and the visual detection and recognition performance from the ENV visual performance studies?

The correlation of the visual performance results with those of the photometric characterization was performed using a Pearson correlation method. In this process, the correlation coefficients for the detection and recognition distance results were calculated for the object luminance, background luminance, luminance difference, contrast, and VL. The parallel pedestrian data was used to represent the correlations relating to the static pedestrian because the photometric characterizations of those two pedestrian objects were the same. The data for the IR-TIS VES were not included in the correlation calculation because this VES is based on a camera system that was not photometrically analyzed.

In addition to contrast as defined earlier, another formulation of contrast was used in this correlation analysis. This is the Weber ratio, shown in figure 62, which typically is used for complex images. In this case, the positive and negative aspect of the relationship is removed, and the maximum and minimum luminance values are used.

$$C = \frac{L_{Maximum} - L_{Minimum}}{L_{Minimum}}$$

Figure 62. Equation. Weber ratio contrast equation.

For all conditions of age, VES, and object type, the Pearson correlation coefficient was calculated between the detection and recognition distance and all of the photometric measures at 61.0 m (200 ft). This distance was used because it generally represents the performance of the metrics at all distances as shown in the results. The correlation results are shown in table 8.

Table 8. Pearson correlation coefficients between detection and recognition distances and measured and calculated values for all age, VES, and object types.

	Detection Distance	Recognition Distance
Object Luminance	0.596	0.577
Background Luminance	0.040	0.063
ΔL	0.603	0.583
Contrast	0.657	0.626
VL	0.621	0.601
Weber Ratio	0.674	0.659

N = 1,207

In this table, the results show detection distance correlation coefficient values of between 0.596 and 0.673 for all the metrics but background luminance. Similarly, the range of correlation coefficients for the recognition distance is 0.576 to 0.658, with the Weber ratio as the highest value. Because the background luminance shows no relationship to the data, it will not be considered further. Also, because the results for the detection and recognition distance are similar and the detection of objects is more important for driver safety, only the detection distance will be considered further.

In the next correlation analysis, participant age was considered separately. The results for the correlation analysis by age are shown in table 9. These results show that all of the Pearson r-correlation coefficients are within approximately the same range, and the Weber ratio shows the highest correlation to the detection distance results for each age group. In general, the correlations are similar between the different age groups for all of the metrics.

Table 9. Pearson correlation coefficients between detection distance and measured and calculated values for all VES and object types by age.

	Young N = 391	Middle N = 419	Older N = 297
Object Luminance	0.587	0.611	0.606
ΔL	0.595	0.618	0.612
Contrast	0.660	0.669	0.657
VL	0.657	0.673	0.661
Weber Ratio	0.676	0.690	0.671

The next analysis was the correlation of the detection distances and the photometric variables by the object type. The correlation results for the cyclist, parallel pedestrian, perpendicular pedestrian, static pedestrian, child's bicycle, and tire tread are shown in table 10. The results for the cyclist, perpendicular pedestrian, and parallel pedestrian are all relatively high. In each of these object types, the Weber ratio performs the best and the VL performs the worst. The correlation values for the static pedestrian, child's bicycle, and tire tread are very low, showing that the visual performance results are not strongly related to the photometric results for these objects. Their poor performance may be a result of these objects being located at the side of the road, but this effect was not evident for the parallel pedestrian; however, the background pavement marking came into play for these objects, and it may have influenced their visibility from the moving vehicle. The visual performance study's parallel pedestrian was dynamic, and the other objects in this location were stationary, which may have made it more easily seen and more highly correlated to the photometric measurements.

Table 10. Pearson correlation coefficients between detection distance and measured and calculated values for all ages and VESs by object types.

	Cyclist N = 293	Parallel N = 259	Perpendicular N = 279	Static N = 147	Child's Bicycle N = 130	Tire Tread N = 99
Object Luminance	0.578	0.686	0.704	0.066	0.070	0.099
ΔL	0.570	0.673	0.702	0.038	0.059	-0.166
Contrast	0.455	0.658	0.612	-0.095	-0.024	-0.263
VL	0.510	0.576	0.657	-0.053	0.116	-0.179
Weber Ratio	0.631	0.738	0.702	0.002	0.063	-0.182

The final aspect of the correlation analysis is the correlation by the VES type, shown in table 11. The results of the analysis show that either the object luminance or the Weber ratio had the highest correlation to the visibility distance results; the VL or the contrast had the lowest. Generally, the relationships are in the same range for all of the VES types, with the HLB values being the highest overall and the five UV-A + HID values being the lowest. For the HLB-based VESs, the addition of UV-A to the system seemed to maintain the same levels of correlation as those of the HLB baseline, whereas the addition of UV-A to the HID-based VESs seemed to degrade their correlations. This effect might be a result of two issues. The first is the cutoff of the light distribution pattern because the HLB did not have a cutoff and the HID did. The second

might be the aiming issues mentioned previously. Because the UV–A sources were aimed directly in front of the vehicle, it would be expected that the cutoff area of the light source would be filled in by the UV–A emission, which may affect the correlation performance.

Table 11. Pearson correlation coefficients between detection distance and measured and calculated values for all age and object types by VES.

	HLB N = 269	Hybrid UV-A + HLB N = 270	Three UV-A + HLB N = 270	Five UV-A + HLB N = 270	HID N = 270	Hybrid UV-A + HID N = 270	Three UV-A + HID N = 270	Five UV-A + HID N = 270	HHB N = 270	HOH N = 270	HLB-LP N = 261
Object Luminance	0.714	0.690	0.723	0.699	0.652	0.671	0.569	0.527	0.806	0.622	0.747
ΔL	0.712	0.690	0.724	0.699	0.657	0.686	0.584	0.537	0.795	0.549	0.748
Contrast	0.592	0.547	0.581	0.575	0.627	0.708	0.615	0.609	0.718	0.518	0.679
VL	0.580	0.587	0.611	0.596	0.623	0.644	0.624	0.620	0.649	0.457	0.684
Weber Ratio	0.710	0.704	0.688	0.660	0.565	0.674	0.578	0.612	0.745	0.639	0.715

From the correlation analysis, it appears that the Weber ratio may be the measure most highly correlated to the detection distance. This appears to be true for all of the objects, ages, and VESs investigated. The other metrics also performed well and showed a reasonable correlation to the results. The VL, which in general performed the worst, still had a mean correlation coefficient of 0.556 as compared to 0.651 for the Weber ratio. Based on these results, it is likely that any of the metrics would provide an equally adequate representation of the visibility distance.

Of the visibility metrics analyzed, what threshold values are required for the detection and recognition of the objects tested?

The threshold is the point at which the participant detected the object, and the threshold value is the value of the metric when this occurred. For this aspect of the analysis, the threshold values were calculated from the distance relationships shown earlier in the photometric data results.

Linear interpolation was used to estimate the parameter values at the midpoints between successive measurement distances. That is to say, if a participant had a detection or recognition distance of 183 m (600 ft), the threshold value was determined by linear interpolation between the 152.5-m (500-ft) and 244-m (800-ft) photometric measurements. This calculation was performed for all of the calculated and measured metrics. Because the photometric performance data is in the range of 61.0 m (200 ft) to 244 m (800 ft), any detection or recognition performed by a participant outside of these limits was not used in this analysis.

In terms of visual object detection, there are two laws that define the threshold of vision and the photometric conditions at that threshold contrast. The first is Ricco's law, which states that the product of the luminance of an object and the visual or angular size of the object is a constant. This means that the smaller the angular size of an object, the more luminous the surface must be to be seen. This relationship holds until a certain angular size is met, at which point the addition of more luminance will not make the object any more visible. After the object reaches this critical size, Weber's law is evident; the size no longer contributes to the detectability of the object, and the threshold contrast is determined only by the magnitude of the background luminance. The critical size at which an object changes between the Ricco relationship and the Weber relationship defines the limit of human spatial-visual summation, and it is called the Ricco area. According to Hood and Finkelstein, the Ricco area is on the order of 6 minutes of

arc.⁽³⁾ Using this value, a critical distance can be calculated that defines the point where the visual angle of the object is large enough to make Ricco's law unusable and make Weber's law the dominant visual relationship. These distances have been calculated for the objects in this investigation, shown in table 12.

Table 12. Critical distance calculation for the objects based on a 6 minute of arc Ricco area.

Object	Height (inches)	Width (inches)	Area (ft ²)	Critical Distance (ft)
Pedestrian/cyclist	70	12	5.83	781
Tire tread	9	27	1.69	420
Child's bicycle	8	27	1.50	396

1 ft² = 0.09 m²

1 inch = 2.54 cm

For any object with a detection distance shorter than the critical distance, where Weber's law dominates, it would be expected that during the object detection task the object would be visible to the participant when a certain combination of object luminance and background luminance was reached. The object size is not critical within this distance, and the threshold values should be the same for all the conditions of object and VES. For objects outside of this critical distance, the threshold values should increase with the visual size of the object.

The threshold values for the Weber ratio, which was the highest-performing metric in the correlation analysis, are presented in figure 63 for the black-clothed objects and figure 64 for the white-clothed objects. It should be noted that for brevity, only the data for the older participants are presented here because this age group had the highest number of detection data points within the required distance range. Because the critical distance for these pedestrian and cyclist objects is 238 m (781 ft), which is close to the limit of the measurements, all of the objects in this figure would be expected to be based on Weber's law, so the resulting threshold values should be close to equivalent. It appears from the figure that this is generally true. This is particularly true of the white-clothed objects; there are no significant differences among their Weber ratios for the VESs, with the exception of the UV-A + HID combinations.

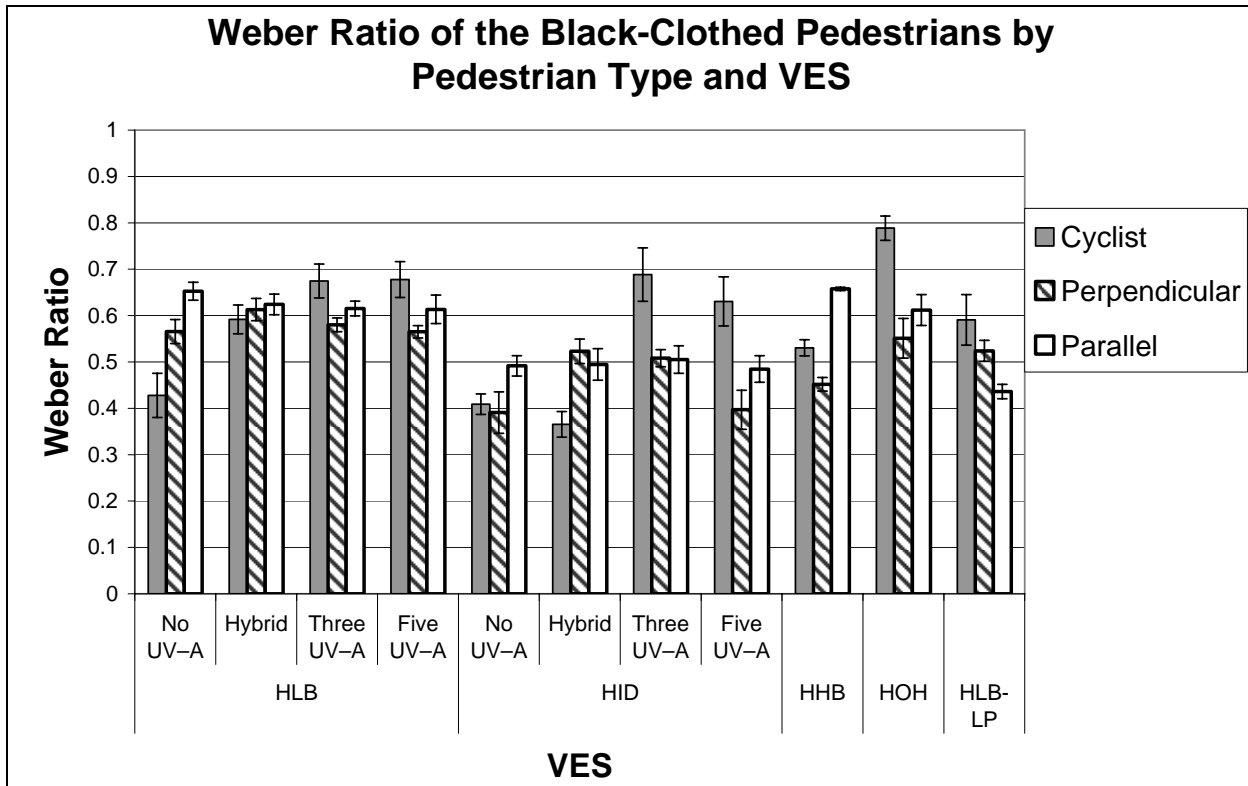


Figure 63. Bar graph. Threshold Weber ratio for black-clothed pedestrian objects.

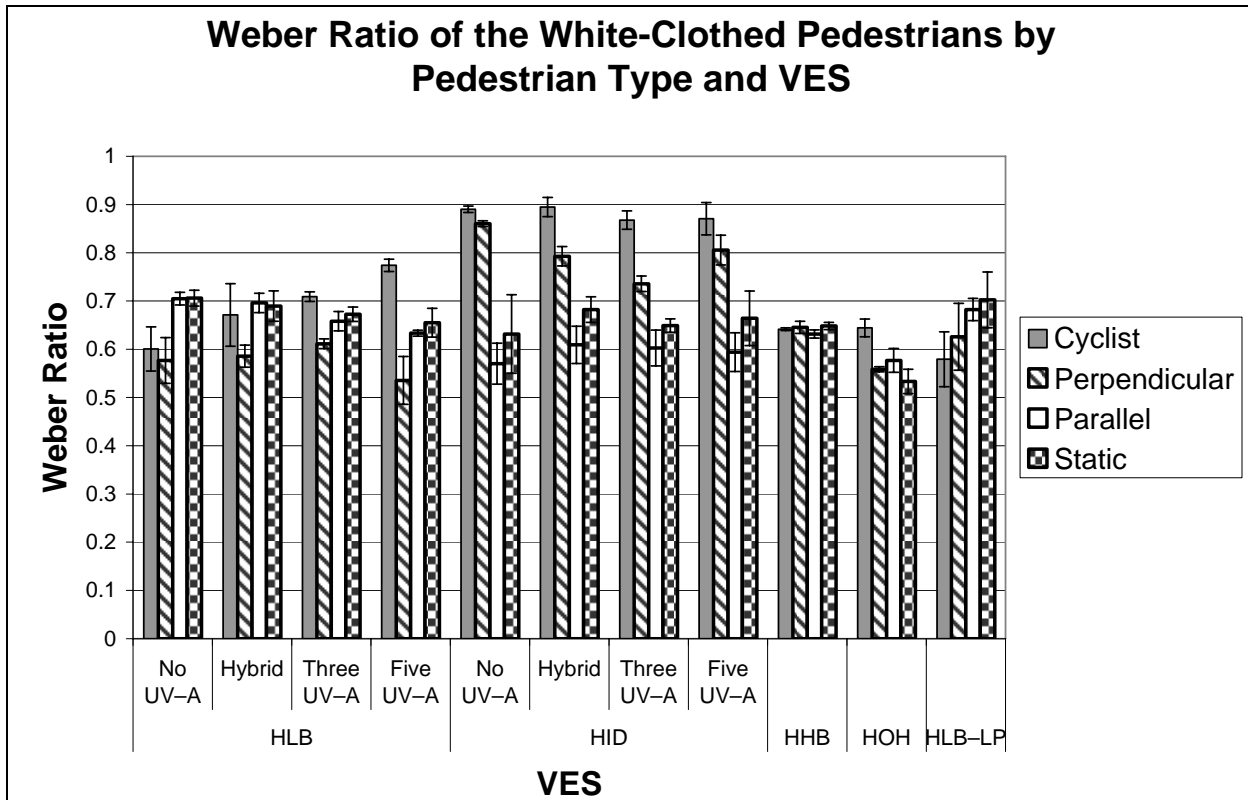


Figure 64. Bar graph. Threshold Weber ratio for white-clothed pedestrian objects.

One of the limitations of the Weber contrast ratio is that visual object size is not a component of its calculation. This results in the use of the critical distance to define the expected behavior of the relationship; however, the VL is designed to account for both Ricco's and Weber's laws. Although the VL metric was generally the least correlated to the detection and recognition results, consideration of the threshold values provides some interesting insight into the VL results. It would be expected that the threshold values would result in the same VL.

The threshold VL values for the black-clothed objects are shown in figure 65. It is interesting that the values are not consistent across all of the VESs; however, for the HHB, HOH, HLB-LP, and HLB-based VESs, they appear to be very similar to each other. The addition of the UV-A to the HID-based VESs appears to cause some variation, which is interesting because the earlier analysis showed that the UV-A should have no effect on the black-clothed objects. Another interesting result is that of the black-clothed cyclist. Most of the threshold values for the black-clothed cyclist are close to or below 1, where the object should be invisible, indicating that the shiny rims of the bicycles were the key to the visibility of those objects, not the cyclists themselves. The final aspect of note in this figure is that the threshold value ranges between 2 and 4 for pedestrians with the exception of the cyclist and the HID-based VESs. This is consistent with the recommendations of the IESNA RP-8-00.⁽²⁾

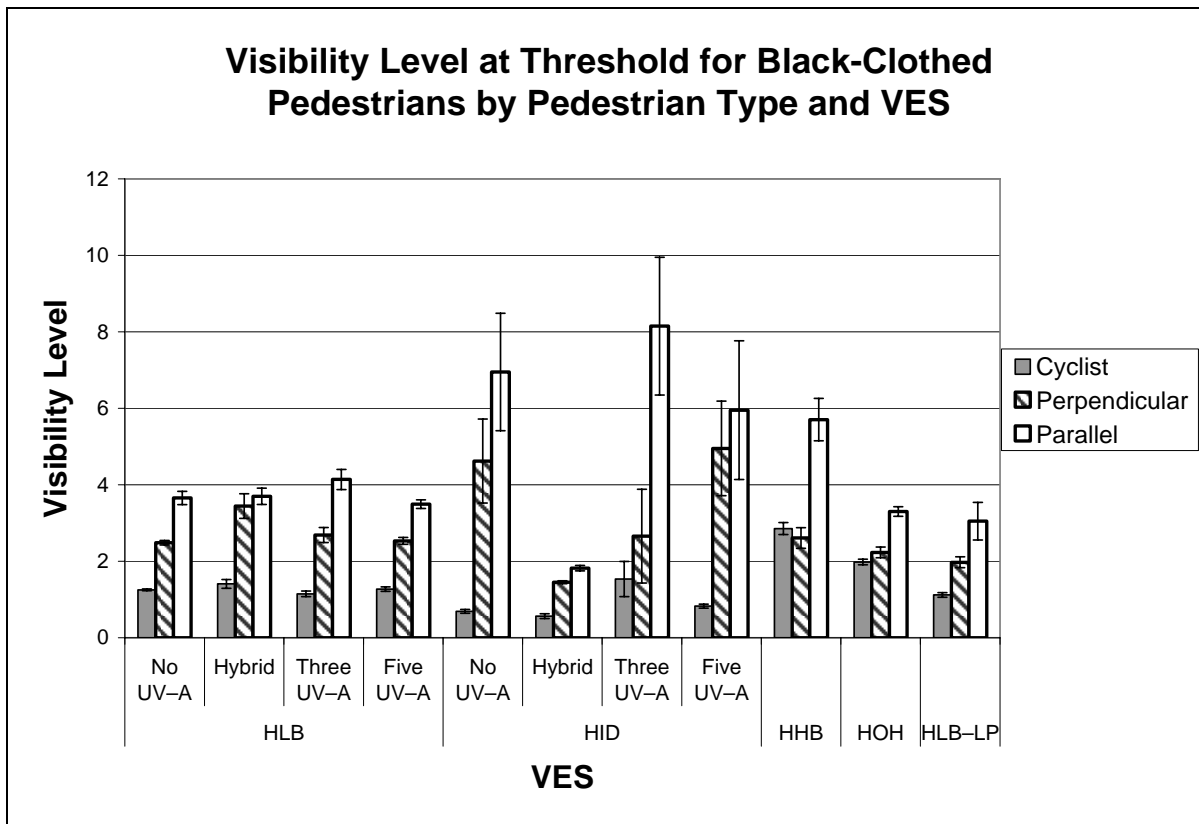


Figure 65. Bar graph. Threshold visibility level for black-clothed pedestrian objects.

The threshold VLs for the white-clothed objects show more variation for these objects than for the black-clothed objects (figure 66); however, the same general relationships are evident. The HID-based VESs have higher values than the others, and the HOH, HHB, and HLB–LP and HLB-based VESs all show similar results to each other, although the HOH performed slightly lower. It is interesting that, unlike the results for the black-clothed cyclist, the results for the white-clothed cyclist were not different than those of the other objects. This indicates that the participant was looking at the cyclist and not at the bicycle itself. The most important aspect of note, however, is the comparison of the white-clothed objects' results to the black-clothed objects' results. The range for the white-clothed objects is between 5 and 45, whereas the range for the black-clothed objects is between 1.5 and 8 (excluding the cyclist). This indicates that the threshold VL does not completely describe the photometric requirements for vision.

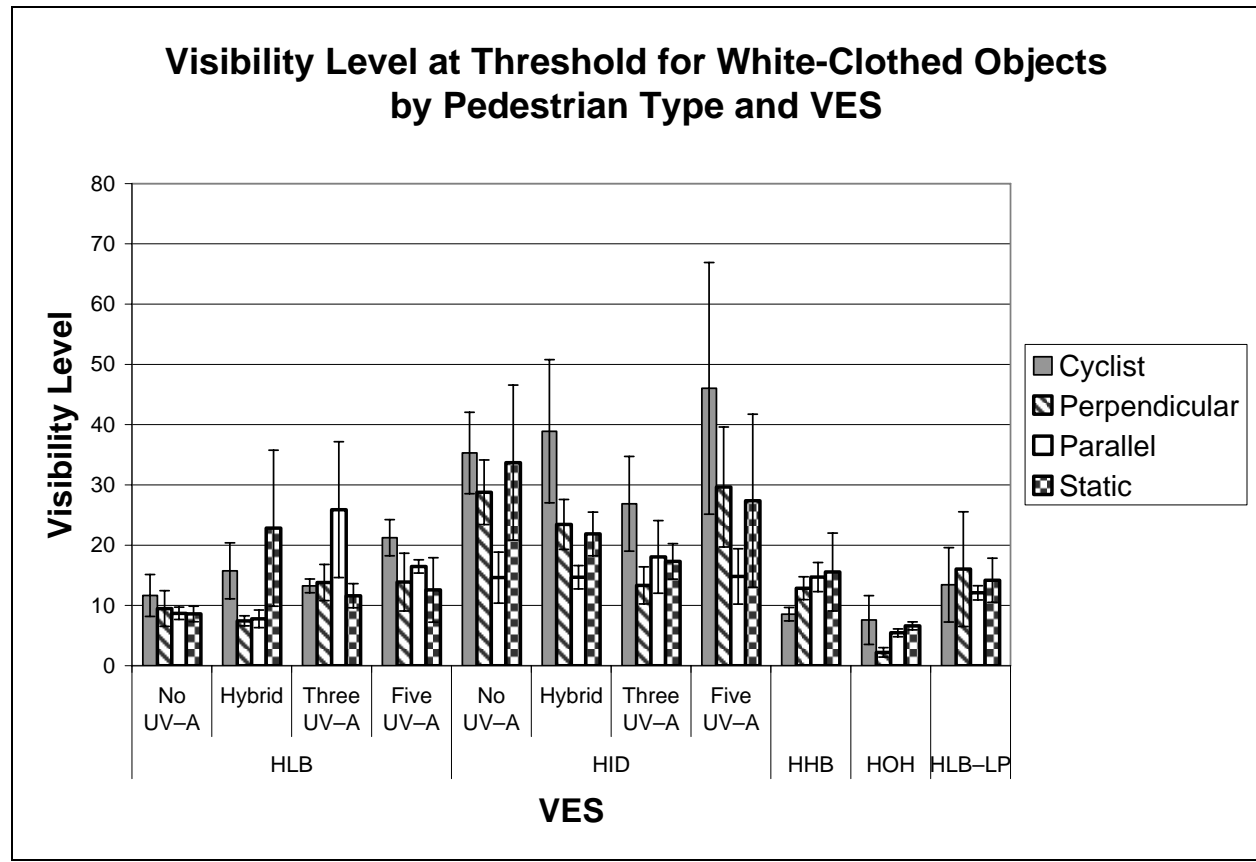


Figure 66. Bar graph. Threshold visibility level for white-clothed pedestrian objects.

A dosage factor was developed and calculated for the threshold values. This dosage factor evaluates the size of the object and the luminance from the object area, and it is defined as the

product of the object luminance and the object size in steradians. According to Gibbons, Andersen, and Hankey, the dosage factor has shown some value in accounting for the object size at the threshold point.⁽⁴⁾ The dosage factor for the black-clothed objects is shown in figure 67 and for the white-clothed objects in figure 68. The first item to note is that the range of values for both the black-clothed and the white-clothed objects is the same; however, there is not a single value that is evident as the required threshold. There seem to be differences between the threshold levels by VES, particularly for the white-clothed static pedestrian; however, the comparison of the HLB-based VESs to the HHB, HOH, and HLB–LP VESs shows a generally consistent threshold value.

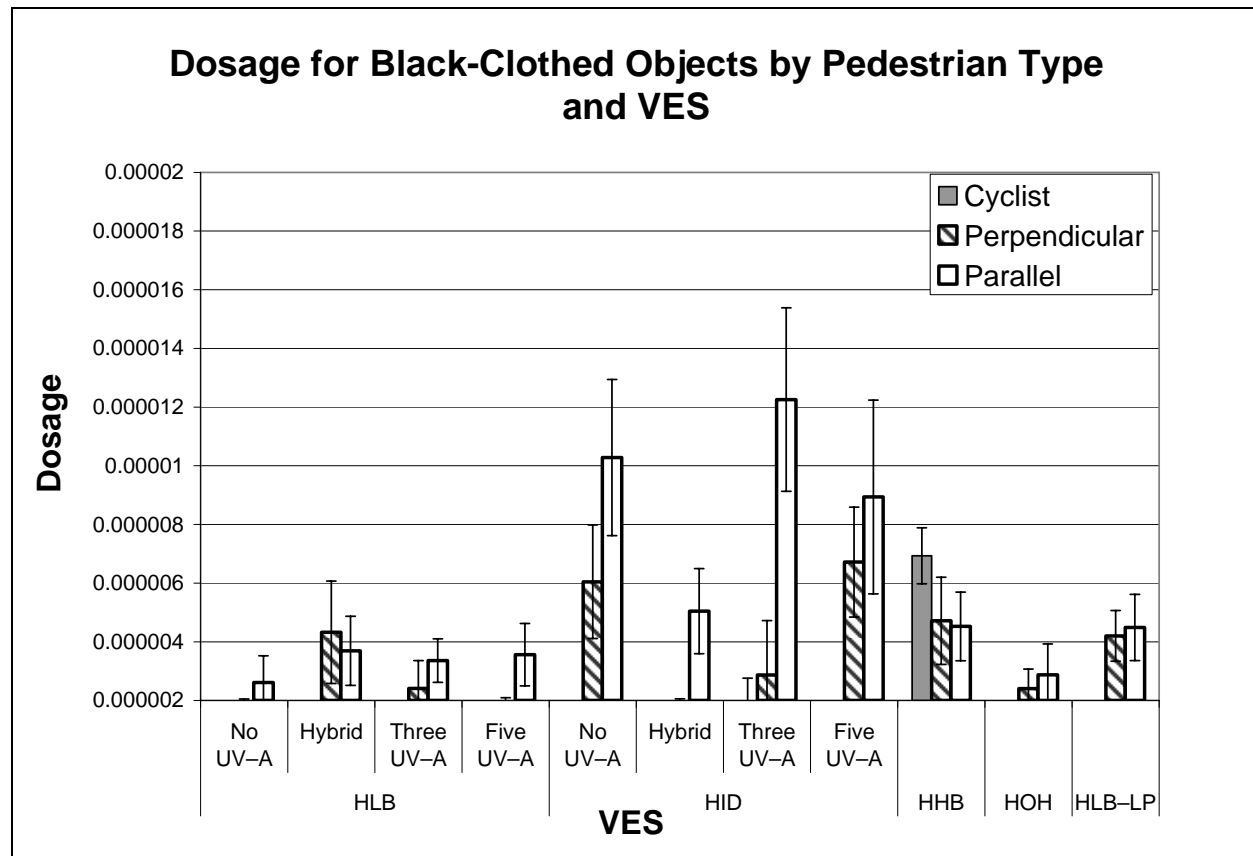


Figure 67. Bar graph. Threshold dosage factor for black-clothed pedestrian objects.

Dosage for White-Clothed Objects by Pedestrian Type and VES

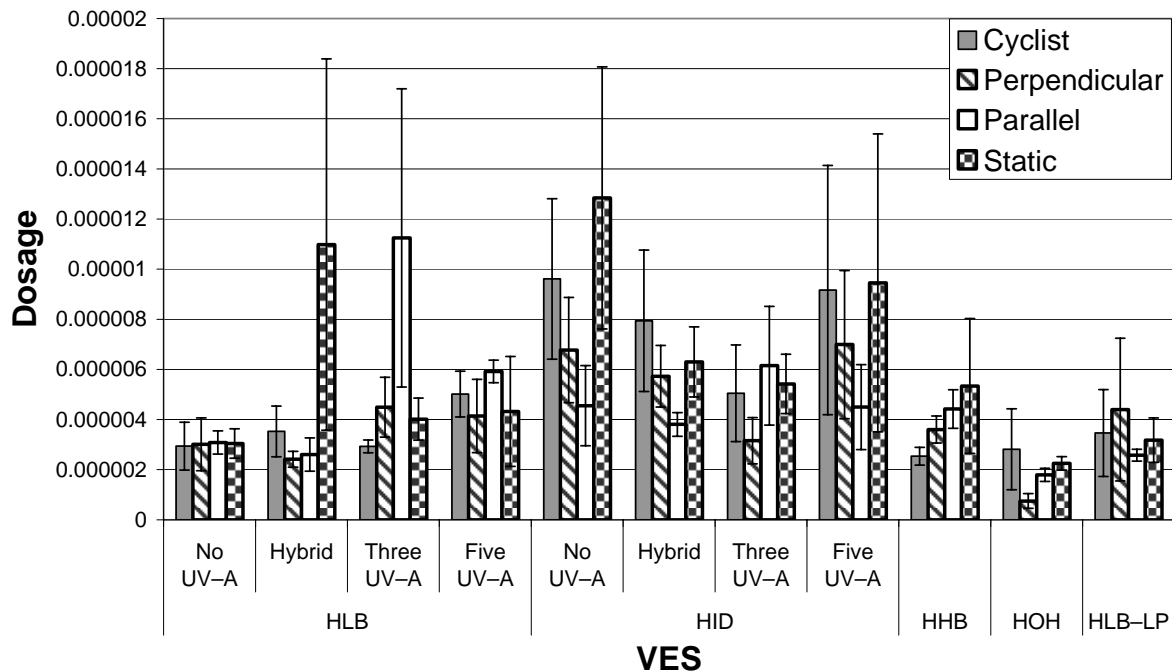


Figure 68. Bar graph. Threshold dosage factor for white-clothed pedestrian objects.

In the assessment of the threshold requirements for the detection and recognition of the objects, the metrics of the Weber contrast ratio and VL as well as a dosage factor seem to provide some insight, but they do not provide a single threshold value for all of the objects and VESs. The Weber ratio provides some equivalent results, and it is the most closely correlated to the visibility distance results, but it does not account for the object size. The VL provides some insight into what attracts the eye of the participant, but it is not comparable between white-clothed and dark-clothed pedestrians. The dosage factor provides both an equivalent basis for comparison between objects and some comparable results, but it has evident differences as well.

One of the issues not considered in this analysis is that of movement. During the ENV visual performance studies, the cyclist and perpendicular and parallel pedestrians were all in motion, either walking or riding a bicycle. The cyclist and the perpendicular pedestrian moved across the roadway, and the parallel pedestrian moved along the shoulder. The sensitivity of the eye to motion and the direction of the motion may have influenced the object visibility. Similarly, the

changes of the background as the object moved and the changes in the contrast with motion both would have influenced the visibility. This motion is a factor not accounted for in any of the metrics, and it may explain some of the evident differences.

CHAPTER 5—EFFECT OF ADVERSE WEATHER

Adverse weather conditions affect the observer by reducing the transmittance of the atmosphere. For example, when light shines through a rainstorm, the raindrops both absorb and scatter the light, thereby reducing the illuminance on an object. During the ENV visual performance experiments, the performance of the VESs in adverse weather conditions was tested for rain, snow, and fog conditions. The results of these investigations are documented in Volumes IV, V, and VI of this report series.

The characterization of the objects in adverse weather conditions was considered as part of this investigation. To account for the effect of the weather conditions on the photometric measures, the transmittance of the atmosphere must be accounted for. From the transmittance, a factor is then used to scale the measured illuminance and luminance values used in the analysis. The method used for calculating the transmittance of the rain, snow, and fog used during the visual performance experiments varies by the weather type. The effect on the photometric characteristics of each of these conditions is considered individually along with their relationship to the visual performance study data.

RAIN

The rain condition was simulated on the Smart Road using the all-weather testing capabilities at the facility. The capabilities consist of 75 weather-making towers located along the side of the road. The system is operated from a pumping station where the pressure and the rain rate can be controlled to achieve the rain condition desired for the experiment. The rain rate for the object characterization was matched to that of the rain condition experiment.

As mentioned, to investigate the effect of the rain on the object visibility, the transmittance of light through the rain was measured. The transmittance was calculated using ratios of both the luminance and the illuminance under clear and rain conditions, which are shown in figure 69 and figure 70. In these equations, τ is the atmospheric transmittance, L is object luminance, and E is illuminance on an object. The transmittance of the atmosphere in the rain was then used to scale the object luminance and the background luminance to achieve the resulting contrast and VL in the rain event. It should be noted that the rain transmittance was only measured at one distance

(200 ft). In a typical analysis, transmittance would be measured at more than one distance; however, due to difficulties with rain consistency during the characterization process, this was not possible. The 200-ft distance was chosen as it represented close to the mean of the visibility distances found in the other ENV studies (ENV Volume IV).

$$\tau_{Illuminance} = \frac{E_{Weather}}{E_{Clear}}$$

Figure 69. Equation. Transmittance of illuminance based on the ratio of the clear measurements.

$$\tau_{Luminance} = \frac{L_{Weather}}{L_{Clear}}$$

Figure 70. Equation. Transmittance of luminance based on the ratio of the clear measurements.

In the rain event at station 4, measurements were made 61.0 m (200 ft) from the white-clothed parallel pedestrian and the white-clothed perpendicular pedestrian for the HID, three UV-A + HID, five UV-A + HID, HLB, and hybrid UV-A + HLB VESs. The illuminance, object luminance, and background luminance were all evaluated from this location, and then used to calculate the atmospheric transmittance. This calculation was made for each measurement type. The results are shown in figure 71.

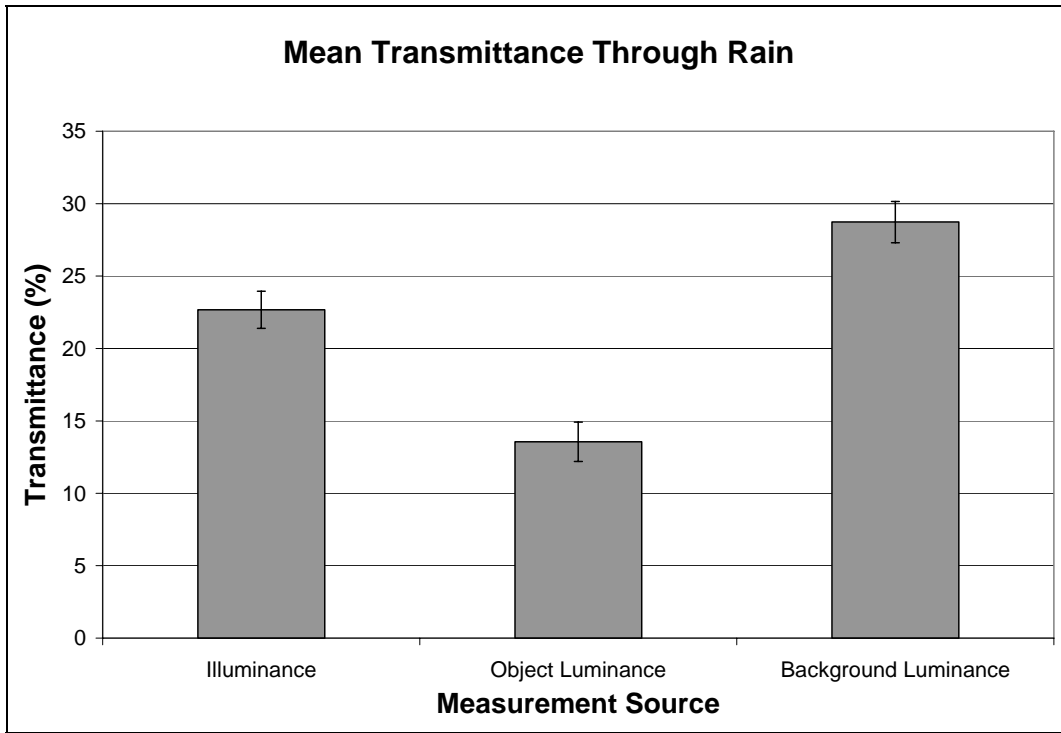


Figure 71. Bar graph. Transmittance of the atmosphere for the illuminance, object luminance, and background luminance in the rain.

It was expected that the transmittance calculated from the illuminance, the object luminance, and the background luminance would be the same; however, this was not the case. It should be remembered that the illuminance measurement was made at the object, meaning that the measured light traveled through the rain only once, whereas the object luminance is effectively attenuated twice as the light travels from the headlamps through the rain to the object and then back through the rain to the photometer. This would result in the effective transmittance being less for the object luminance than the illuminance. For the background luminance, the light traveled through the rain twice, but the background luminance is also influenced by backscatter, which is the light that reflects off the rain. This may have influenced the measurement results. Similarly, the rain was limited to the roadway area, and the viewed background may have been in the roadway or off to the edges, meaning that the entire path of the light was not necessarily within the rain event, and the attenuation from rain did not completely affect the measurement.

These values were used to scale the photometric measurements for comparison to the visual performance results.

SNOW

The same formulas for the transmittance of the atmosphere that were used for the rain are applicable to the snow conditions. Snow for the investigation was created using the same weather-making system as was used to make the rain, but the ambient temperature was such that the liquid crystallized. For the object characterization measurements, a snow condition was established on the roadway. The original measurement plan was the same as that of the rain; however, it was found that the luminance measurements could not be made reliably because the snow-making action caused the snow to blow. It was then decided that the transmittance of the light through the snow could only be calculated using the measurements of illuminance.

The illuminance measurements were made through the snow for the HID and the HLB VESs at 15.2 m (50 ft), 30.5 m (100 ft), 45.7 m (150 ft), 70.0 m (200 ft), 76.2 m (250 ft), and 91.4 m (300 ft). Multiple distances were used to evaluate the effect of a longer light path through the snow. The illuminance results for the clear and the snow conditions are shown in figure 72. An interesting and unexpected result was the increase in the illuminance value on the object at 15.2 m (50 ft) in the snow condition as compared to the clear condition. This could be caused by light scattering as it passes through the snow. Some of this scatter will be backscatter, which reflects back at the driver, and some will be forward scatter, which scatters onto the object. It is believed the forward scatter causes the observed increase in the illuminance. The effects of the forward scatter and the backscatter were not accounted for in the snow condition experiment, and therefore, cannot be accounted for here.

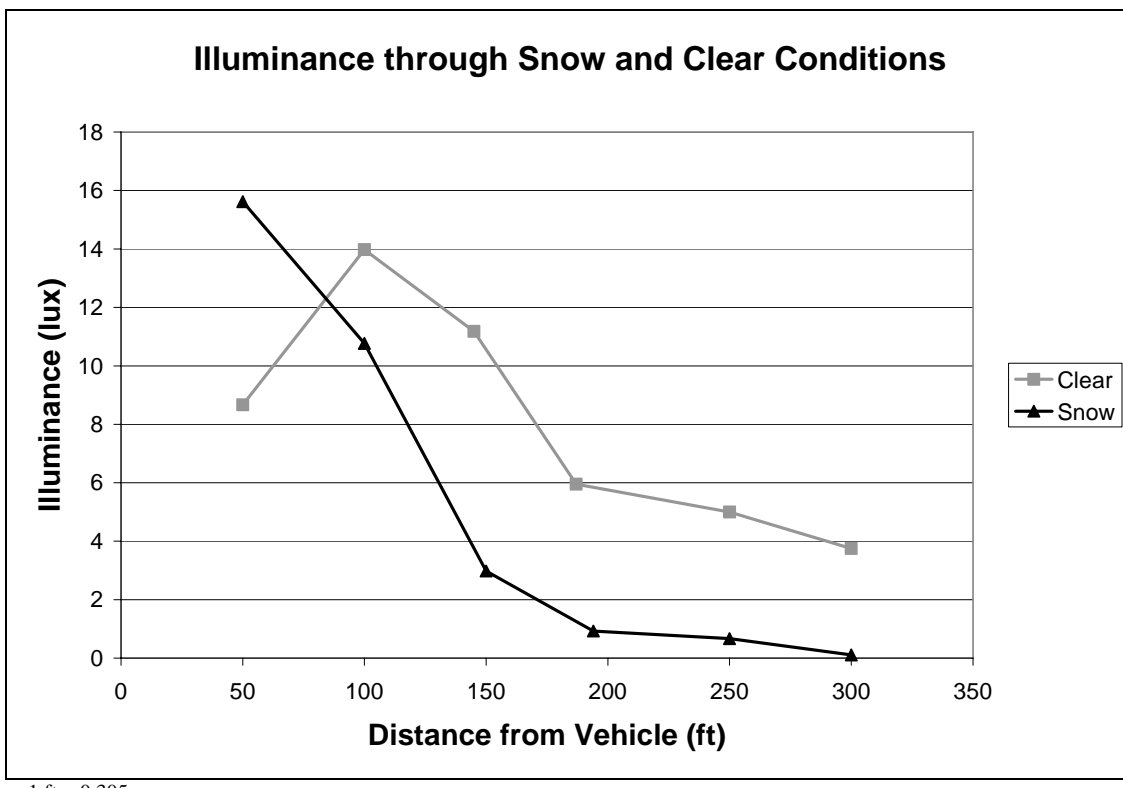


Figure 72. Line graph. Illuminance for both clear and snow conditions.

The transmittance was calculated for the snow condition for all of the distances with the exception of the 15.2-m (50-ft) distance, and the results are shown in figure 73. As expected, the attenuation of the light increases the farther the measurement is from the vehicle headlamps. An interesting comparison is that of the 45.7-m (150-ft) measurement to the 91.4-m (300-ft) measurement. The transmittance in the snow at 45.7 m (150 ft) is approximately 26 percent and approximately 5 percent at 91.4 m (300 ft). These values are similar to the values at 70.0 m (200 ft) for the illuminance and the object luminance factors in the rain condition, respectively, and further reinforce the hypothesis that the lower value of transmittance for object luminance is due to the impact of the path length through which the light must pass.

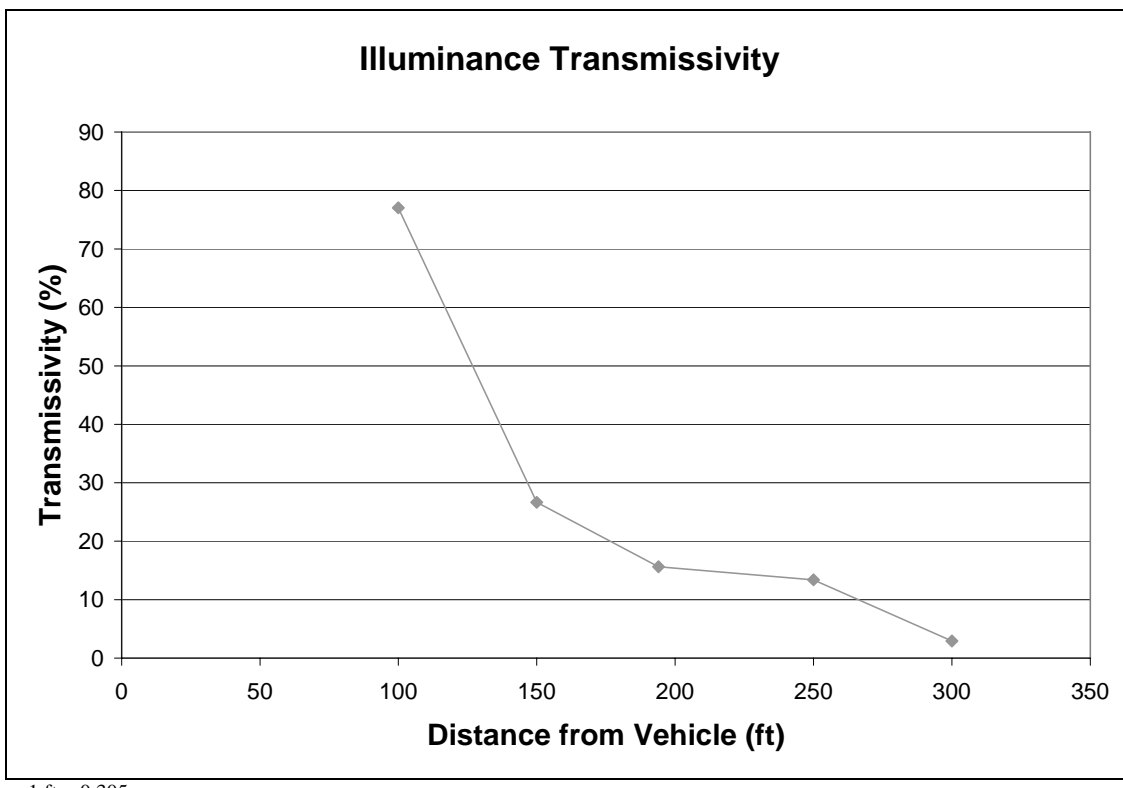


Figure 73. Line graph. Transmittance of the atmosphere for the illuminance through snow.

As with the rain condition, the calculated values of transmittance through snow were used to scale the photometric measurements for comparison to the visual performance results in the snow condition experiments.

FOG

For the ENV studies, fog was manufactured on the Smart Road using the weather-making system. In this configuration, the water was mixed with compressed air in an atomizing nozzle mounted over the center of the roadway. This atomized moisture was then directed to the roadway as fog. The thickness of the fog could be controlled by adjusting the ratio of water to air pressure supplied to the atomizing nozzle.

In fog, light is scattered as a result of the collision of the photons with the water droplets that make up the fog bank. Because of the complexity of this function, a mathematical model of the transmittance was developed to account for the effect of this weather condition. During the fog

condition experiments, an illuminance meter was used to measure the backscatter from the vehicle headlamps as a measure of the fog density. These values were then calibrated during the development of the mathematical model. Following is a description of the model development.

When an incident beam of light strikes a particle, the photons, which are much smaller than the particle, are scattered in all directions (figure 74).

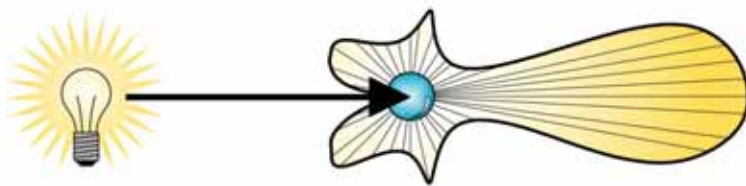


Figure 74. Diagram. Possible reaction of light after collision with a water particle in a fog bank.

The exact nature of the scatter pattern depends on many things: the size of the particle, the number of particles, and the polarization of the incident light among others.

A model of this scattering behavior is based on a process called Mie scattering, named after the investigator who developed the foundation of the descriptive model. Mie scattering requires that the scattering particle be larger than the wavelength of the light that is striking it. For a fog bank, the particle sizes range from 0.1 micrometers (μm) to approximately $15 \mu\text{m}$.⁽⁵⁾ In the case of visible light, the wavelength is in the range of 360 to 800 nanometers (nm), which is much smaller than a typical particle in a fog bank, meaning that the Mie scattering model is valid in the fog scenario.

The nature of the scattering is defined by the angular scattering coefficient $\beta(\theta)$. The symbol θ represents the angle of observation, measured from the incident ray. By convention, $\theta = 0^\circ$ is in the direction of the incident beam, and $\theta = 180^\circ$ opposes the beam as backscatter. The intensity of the light in the given direction is defined by the equation shown in figure 75, where E_{incident} is the incident illuminance on the scattering particle.

$$I(\theta) = \beta(\theta)E_{incident}$$

Figure 75. Equation. Intensity of light based on the scattering coefficient and incident illuminance.

The derivation of $\beta(\theta)$ is based on two complex functions (i_1, i_2), which have particle size, number of particles, observation angle, and index of refraction as parameters. Each of the complex functions represents the nature of perpendicular and parallel polarization. For a headlamp situation, some assumptions can be made that simplify the calculation. The first is that polarization is not an issue because the light source is incoherent (contains many different polarizations and wavelengths). Second, the observation angles for the objects in the roadway environment do not change significantly.

With these simplifications, the total scattering coefficient can be used to quantify the fog characteristic. The total scattering coefficient represents the amount of luminous flux scattered or attenuated from the incident beam. That is to say, as photons are either scattered or absorbed by the particles in the atmosphere, they are removed from the total flux in the incident light beam. To calculate the total scattering coefficient, the incident beam can be broken into very small lamina as shown in figure 76.

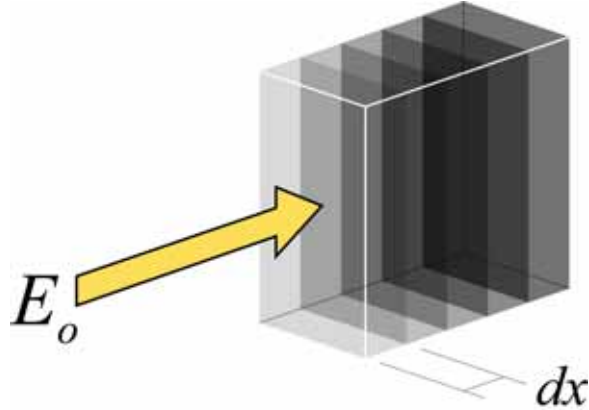


Figure 76. Diagram. Depiction of the incident beam broken into small lamina.

The change in luminous intensity for each lamina can be calculated as shown in figure 77.

$$\frac{dE}{E_o} = -\beta \cdot dx$$

Figure 77. Equation. Differential change in illuminance for each portion of a light beam.

Here, the E value is the illuminance incident on the lamina, dx is length of the lamina, and β represents the total scattering per unit length. To find the total attenuation for the beam at distance x , the equation in figure 77 must be integrated, yielding the equation in figure 78. This is known as Bouguer's law of attenuation.

$$E_x = E_0 e^{(-\beta x)}$$

Figure 78. Equation. Total attenuation according to Bouguer's law.

The visibility of an object is based on the contrast of the object to its background. Because contrast is proportional to the luminance of the target, the contrast can be substituted for the illuminance to represent the reduction in contrast of an object in the fog condition as shown in figure 79.

$$C_x = C_0 e^{(-\beta x)}$$

Figure 79. Equation. Reduction caused by the fog attenuation.

Two assumptions are made during this contrast equation development: that the luminance of the background does not change because of the fog and that the fog is not so significant that it represents the background. In reality though, the light scattered from the fog bank does become the background luminance for the object.

Calibration Procedure

During the calibration procedure, a series of different fog densities were used to generate a scattering field. These densities were developed using varying water pressures at the rain tower base. Each of the VES vehicles in the test was placed in the fog bank, and then a measurement was made of the backscatter from the fog as well as the illuminance provided by the headlamps at distances of 30.48 m (100 ft), 60.96 m (200 ft), and 91.44 m (300 ft). A final measurement was made of the headlamp illuminance and the backscatter in a clear condition without fog. It should be remembered that the measurement of ambient illuminance at the approximate position of the driver's eye was used as the measurement of backscatter. Table 13 summarizes the measurement matrix used during the calibration procedure.

Table 13. Fog modeling calibration measurement.

Distance	100 ft, 200 ft, 300 ft
Fog Condition	Clear, water pressure set at 25 psi, 40 psi, 70 psi, 110 psi, 150 psi
VESSs	HLB (SUV 1 and SUV 2), HID, HLB-LP

SUV = sport utility vehicle

psi = pounds per square inch

1 ft = 0.305 m

1 psi = 6.89 kilopascals (kPa)

Using Bouguer's law, the scattering coefficient was calculated. In this case, the illuminance in the clear condition at each distance was used as E_o . Figure 80 shows the results of the β variable.

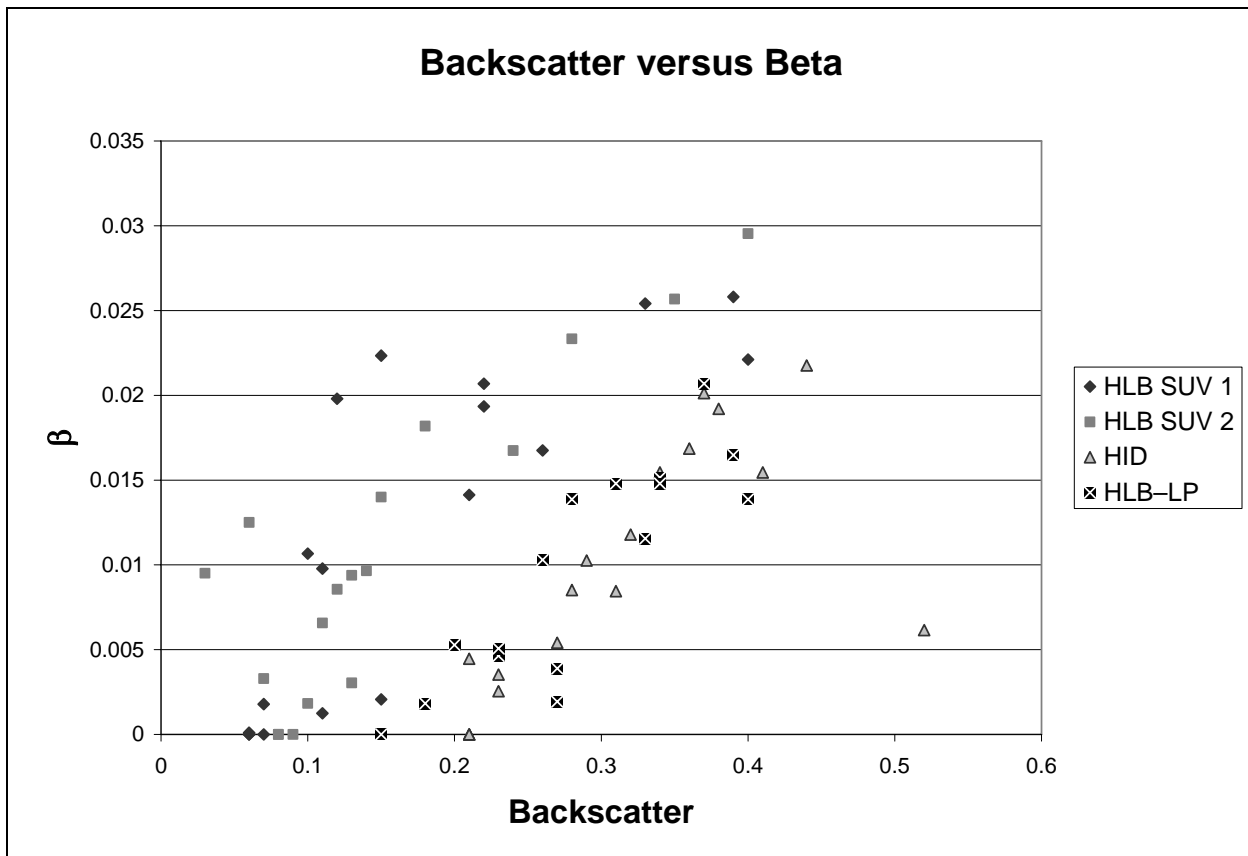


Figure 80. Scatter plot. Measured backscatter versus the $\beta(\theta)$ function.

The extinction ratio, which is the ratio of the clear illuminance to the fog illuminance, was also calculated for each of the vehicles and fog conditions. The results for this calculation are shown in figure 81.

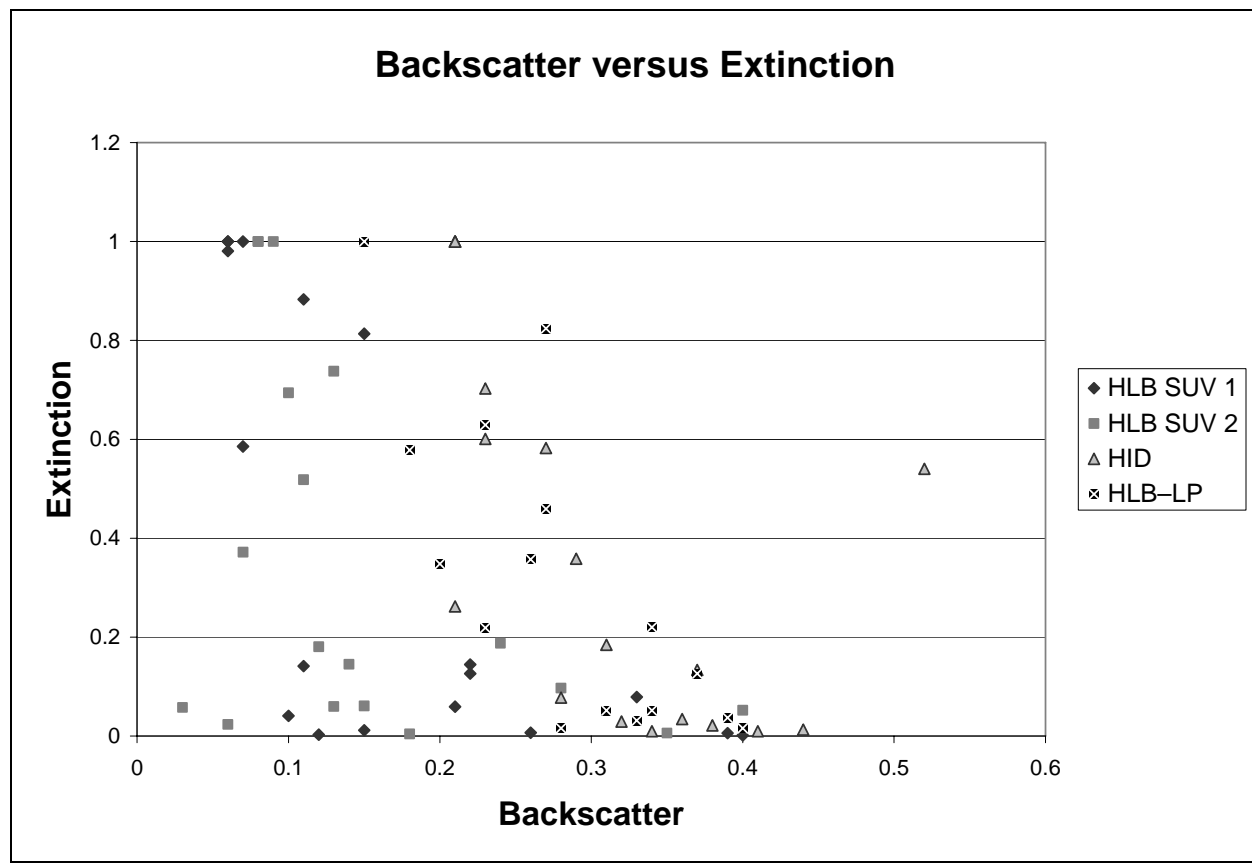


Figure 81. Scatter plot. Measured backscatter versus the extinction factor.

Based on these results, a mathematical model was established between the backscatter measurement and the fog conditions.

Mathematical Model

The difficulty with Bouguer's law is that distance is intrinsically part of the calculation. During the ENV experimentation, visibility distance is the measured value. This means that a relationship exists in the data between the model and the results. In an effort to investigate this relationship, a model of both the total scattering and the extinction ratio was developed. It should be noted that the removal of distance from the equation results in a much more variable equation with a lesser degree of correlation.

The models were developed in two stages. The first stage adjusted all of the vehicle-specific data by the base backscatter illuminance value, obtained from the measured backscatter in the clear condition mentioned as E_0 earlier. This value is shown for each of the vehicles in table 14.

Table 14. Backscatter measurements in the clear condition.

Vehicle	Base Backscatter Value
HLB (SUV 1 and SUV 2)	0.06
HID	0.21
HLB-LP	0.15

After adjusting the backscatter model, a single mathematical relation for each of the two variables was developed using a nonlinear regression methodology. The resulting relationships are shown in figure 82 and figure 83. The factor a in the equations is related to the base backscatter value as above.

$$\beta = 0.0324(1 - e^{(-3.92(Bsc-a))})$$

Figure 82. Equation. $\beta(\theta)$ function based on the adjusted backscatter.

$$Ex = e^{(-16.35(Bsc-a))}$$

Figure 83. Equation. Extinction factor based on the adjusted backscatter.

Each of these models was then used to calculate a metric for the fog density based on the backscatter measurement from each vehicle (figure 84 and figure 85).

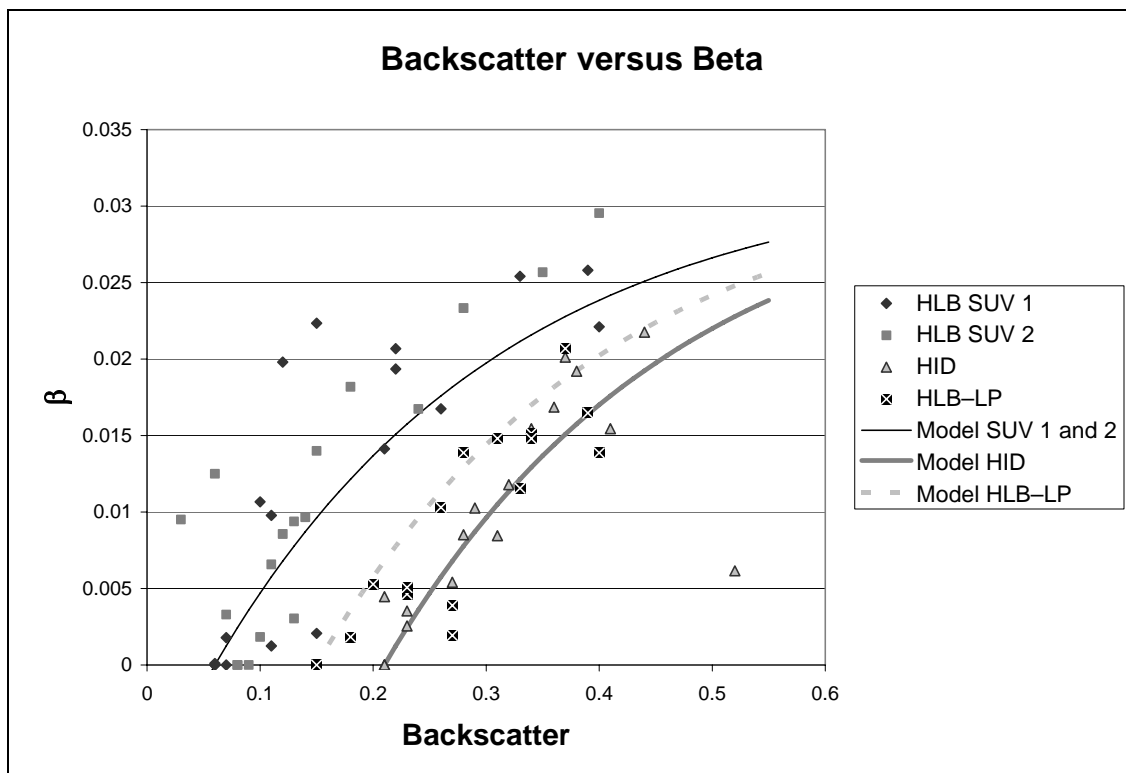


Figure 84. Scatter plot. Backscatter versus β by model.

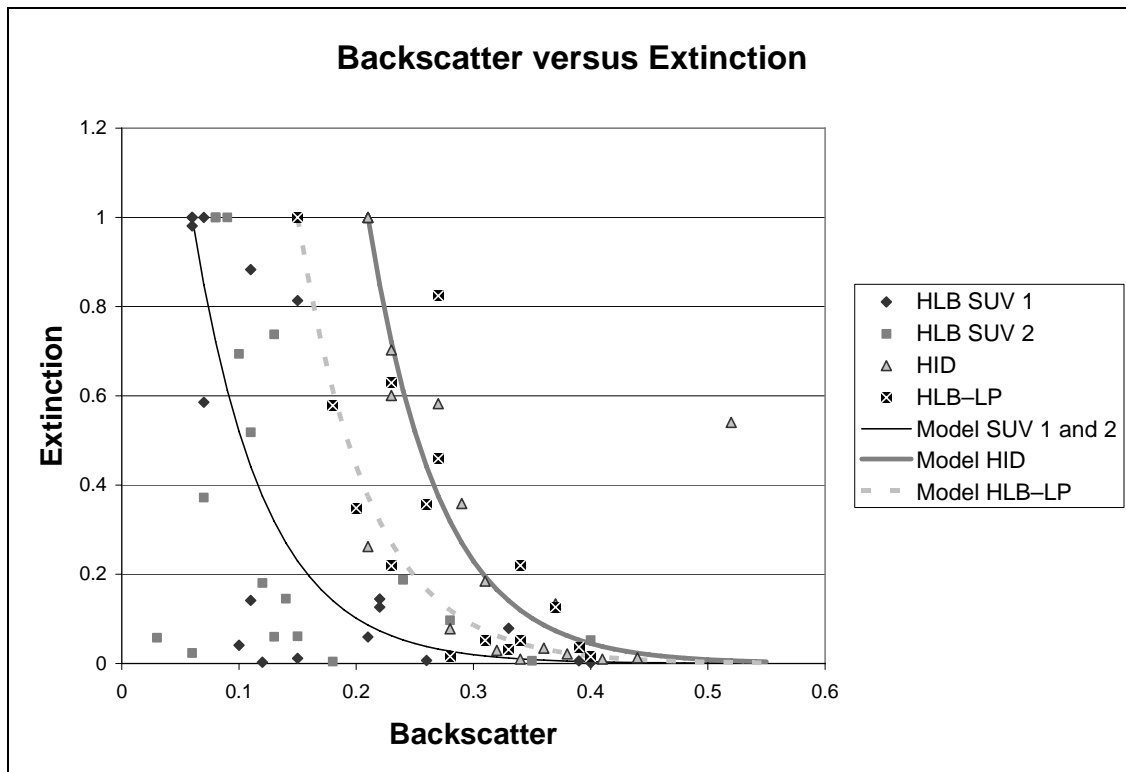


Figure 85. Scatter plot. Backscatter versus extinction with model.

These mathematical models were used with the measured backscatter illuminance measurements to estimate the atmospheric transmittance, and thus, the photometric condition of the objects during the fog condition experiment.

VISUAL PERFORMANCE EXPERIMENT CORRELATION

Similar analyses to those performed for the clear condition were performed for the rain, snow, and fog conditions. The correlation of the metrics discussed and the performance of the participants was investigated along with the threshold values for each of the metrics involved.

Correlation Analysis

The correlation analysis for each of the weather conditions are shown in table 15. The dosage factor has also been included in this analysis. In these results it can be seen that there are very similar correlations for the conditions of rain and snow as compared to the clear condition; however, the correlation of the fog condition results for VL to the participant data is less significant.

Table 15. Correlation results between participant detection distance and photometric metrics for all weather conditions.

	All Conditions	Clear	Fog	Rain	Snow
Object Luminance	0.381	0.596	0.406	0.660	0.595
ΔL	0.385	0.603	0.402	0.662	0.593
Contrast	0.418	0.657	0.222	0.658	0.610
VL	0.380	0.621	0.062	0.604	0.582
Weber Ratio	0.414	0.674	0.307	0.665	0.641
Dosage	0.414	0.654	0.406	0.654	0.595

The results for the recognition distance are very similar, as seen in table 16. Here again the correlation to the fog condition is the lowest of all of the weather conditions, with the VL performing very poorly.

Table 16. Correlation results between participant recognition distance and photometric metrics for all weather conditions.

	All Conditions	Clear	Fog	Rain	Snow
Object Luminance	0.381	0.577	0.400	0.637	0.558
ΔL	0.384	0.583	0.395	0.639	0.557
Contrast	0.411	0.626	0.211	0.625	0.574
VL	0.380	0.601	0.064	0.581	0.554
Weber Ratio	0.420	0.659	0.295	0.656	0.623
Dosage	0.412	0.630	0.400	0.631	0.558

The likely reason why the correlation to the fog conditions is poor is that the changes in the background luminance were not fully accounted for. In the investigation, the luminance of the objects in the fog could not be measured; so instead, they were calculated based on a model of the light extinction. The transmittance model performs well and is well calibrated; however, it does not account for the changes in the visual background of the object. The fog extinguishes the background luminance, but because of scatter, the atmosphere is transformed into a luminous source and becomes the effective background of the object. The effect of this transition was not accounted for in the calculations, likely leading to the poor correlation performance of the photometric values. This problem would not be evident in the other conditions because the rain, while extinguishing the light, does not create a background. Similarly, the snow can become a scattered background, but it would not have the density of fog. It is likely that a complete luminance measurement in all conditions would further aid in this analysis; however, the transient nature of the weather conditions makes it difficult to provide reliable results.

Threshold Analysis

The threshold analysis was performed for all of the conditions. One of the limitations of this threshold analysis is that no data below the 70-m (200-ft) limit of the photometric measurements could be used. This limitation meant that very little data was available for the calculation for the snow and fog thresholds, so these conditions could not be included in the analysis; however, for the rain condition the threshold results could be considered. In the rain condition, both black-clothed and white-clothed objects were presented, but, as in the snow and fog conditions, very few of the black-clothed conditions met the minimum 70-m (200-ft) criterion, meaning that the threshold for only the white-clothed objects will be presented here.

Figure 86 shows the threshold results for the Weber ratio in the rain condition. This figure shows a very consistent result across all of the VES types and pedestrian locations. It is also interesting to note that the value of this ratio is higher in these conditions than in the clear condition.

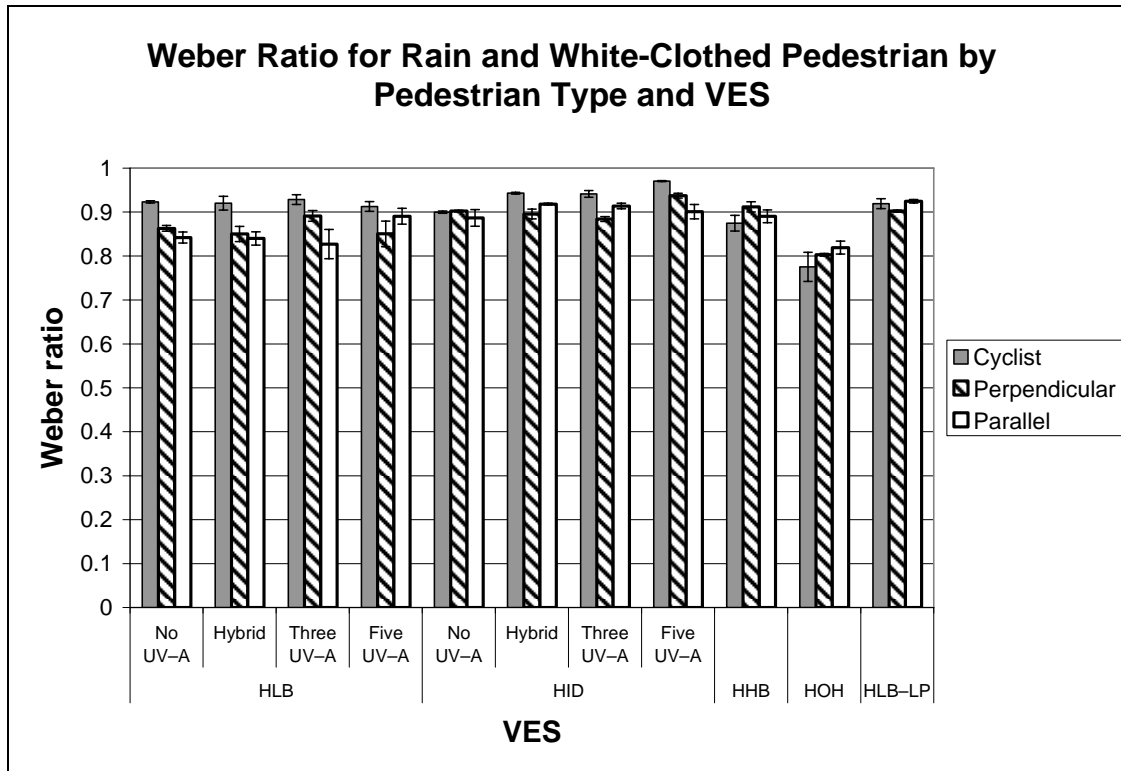


Figure 86. Bar graph. Threshold Weber ratio for white-clothed pedestrian objects in rain condition.

Figure 87 shows the threshold results for the VL in the rain condition. These results are less consistent than those for the Weber ratio; however, within the VES base-lamp type, there is some consistency. For example, all of the HLB-based VESs appear to result in a common level of threshold value. In figure 87, as with the Weber ratio, the VL is much higher than that for the clear condition. Where the VL ranged from 40 to 50 for the white-clothed pedestrians in the clear condition, this value is more likely 100 to 150 in the rain condition.

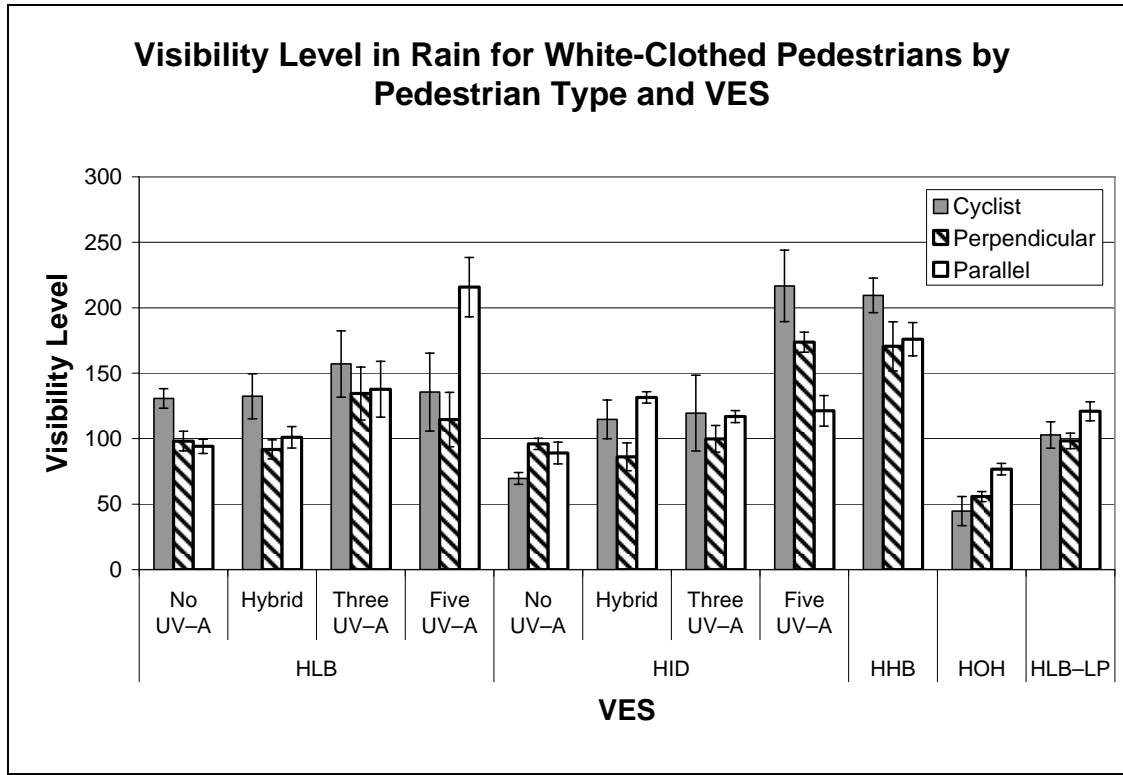


Figure 87. Bar graph. Threshold visibility level for white-clothed pedestrian objects in rain condition.

Finally, the threshold dosage for the rain condition is shown in figure 88. This value shows a very consistent result for all of the conditions, particularly within the VES base-lamp types. The HHB seems to require a higher dosage than the other VES types, which might be related to the different aiming location specified for the HHB as compared to the other VESs. As a final note, the dosage level is again higher than that for the clear condition objects.

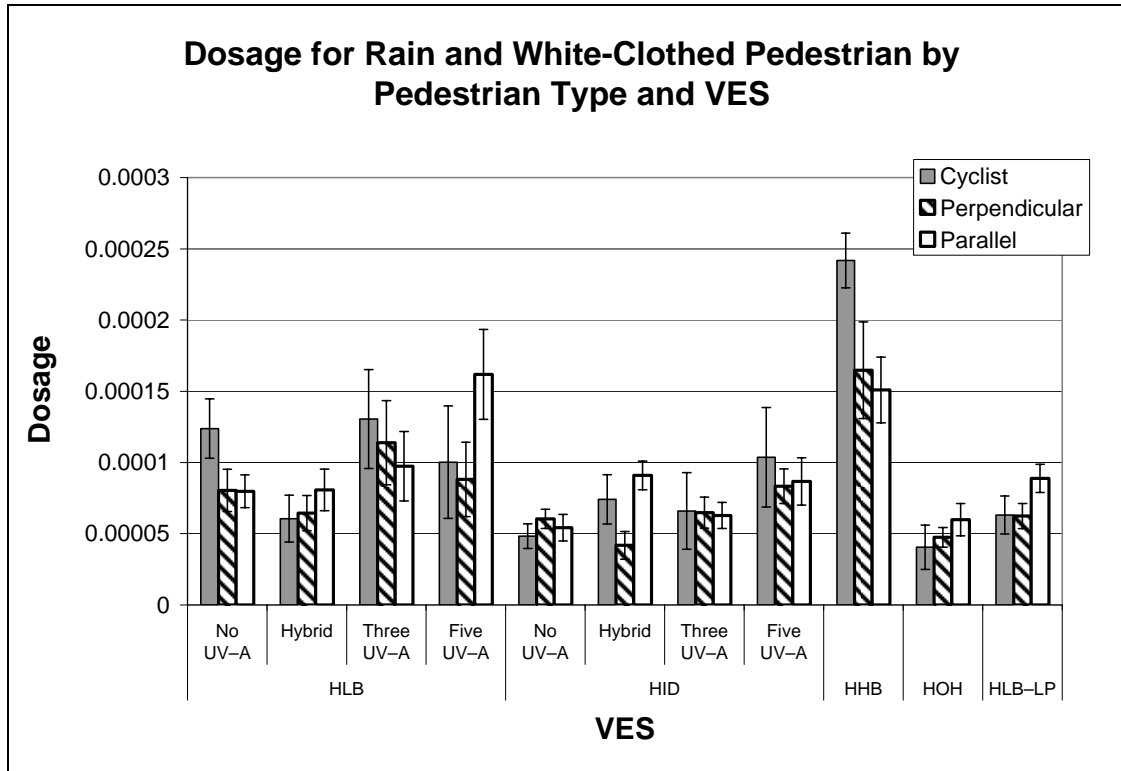


Figure 88. Bar graph. Threshold dosage for white-clothed pedestrian objects in rain condition.

Each of these metrics shows that a higher threshold value is required in the rain than in the clear condition at the point of detection. This can indicate that the distraction of the driver by the rain event, the attenuation of the light by the rain, and the additional workload of driving in rain require a higher level of lighting to achieve object detection. It should be noted that these calculations are limited because they are based on an attenuation calculation, not direct measurement, and that, as with the clear condition measurement, motion of the object is not taken into account.

REFERENCES

1. Adrian, W.K. (1989). "Visibility of Targets: Model for Calculation." *Lighting Research and Technology*, 21(4), 181–188.
2. Standard Practice Subcommittee of the IESNA Roadway Lighting Committee. (2000). American National Standard Practice for Roadway Lighting (ANSI/IESNA RP-8-00). New York, NY: Illuminating Engineering Society of North America.
3. Hood, D.C., & Finkelstein, M.A. (1986). "Sensitivity to Light." In K.R. Boff, L. Kaufman, & J.P. Thomas (Eds.), *Handbook of Perception and Human Performance: Vol. 1* (pp. 5–1 to 5–66). New York, NY: Wiley.
4. Gibbons, R., Andersen, C., & Hankey, J. (2005). *The Wet Night Visibility of Pavement Markings: A Static Experiment*. Presented at the 84th Annual Meeting of the Transportation Research Board, Washington, DC.
5. McCartney, E.J. (1976). *Optics of the Atmosphere: Scattering by Molecules and Particles*. New York, NY: John Wiley & Sons, Inc.

